AEDC-TR-67-79

THE INFLUENCE OF HALL EFFECT AND INITIAL VELOCITY PROFILE ON MHD FLOW IN THE ENTRANCE REGION OF A PARALLEL PLATE CHANNEL

William T. Snyder and Arsev H. Eraslan
The University of Tennessee Space Institute

April 1967

ARNOLD ENGINEERING DEVELOPMENT CENTER
AIR FORCE SYSTEMS COMMAND
ARNOLD AIR FORCE STATION, TENNESSEE

NOTICES

When U. S. Government drawings specifications, or other data are used for any purpose other than a definitely related Government procurement operation, the Government thereby incurs no responsibility nor any obligation whatsoever, and the fact that the Government may have formulated, furnished, or in any way supplied the said drawings, specifications, or other data, is not to be regarded by implication or otherwise, or in any manner licensing the holder or any other person or corporation, or conveying any rights or permission to manufacture, use, or sell any patented invention that may in any way be related thereto.

Qualified users may obtain copies of this report from the Defense Documentation Center.

References to named commercial products in this report are not to be considered in any sense as an endorsement of the product by the United States Air Force or the Government.

THE INFLUENCE OF HALL EFFECT AND INITIAL VELOCITY PROFILE ON MHD FLOW IN THE ENTRANCE REGION OF A PARALLEL PLATE CHANNEL

William T. Snyder and Arsev H. Eraslan
The University of Tennessee Space Institute

FOREWORD

The work reported herein was sponsored by Arnold Engineering Development Center (AEDC), Air Force Systems Command (AFSC), Arnold Air Force Station, Tennessee, under Program Element 62405334, Project 8950, Task 895001.

The results of research presented were obtained by the University of Tennessee Space Institute under Contract AF 40(600)-1113. The manuscript was submitted for publication on April 13, 1967.

The reproducibles used in the reproduction of this report were supplied by the authors.

The authors wish to acknowledge the contribution to this work by their graduate students, 1st Lt. Elmer E. Goins, Jr., 1st Lt. Jimmie Don Young, and Mr. Francesco A. Iannuzzi. The assistance of Dr. M. K. Newman in designing the experimental facility is gratefully acknowledged.

This technical report has been reviewed and is approved.

Ian F. Flemming
F/L, RCAF
Research Division
Directorate of Plans
and Technology

Edward R. Feicht
Colonel, USAF
Director of Plans and
Technology

ABSTRACT

A new method is presented for the analysis of MHD flow in the entrance region of a parallel plate channel including the Hall effect. The method involves a linearization of the inertia terms and the introduction of a stretched axial coordinate. A solution is obtained for the velocity distribution in an incompressible fluid which is valid from the duct inlet to the fully developed region. In practice, flows in which the Hall effect is significant will be compressible. Since the primary objective of the present analysis is to develop the analytical technique for extending the linearization scheme to MHD flows with Hall effect, the constant density assumption is justifiable as a first approximation. From this solution numerical results are obtained for the entrance length, pressure distribution, boundary layer thickness, and wall shear stress distribution in the entrance region for various values of the Hartmann number and the Hall parameter.

Two different methods of analysis of fully developed MHD channel flow with variable conductivity are presented. Calculated velocity profiles are presented by the two methods for several conductivity variations across the channel.

A new experimental MHD channel flow facility designed to use potassium chloride (KCl) as the working fluid is described. Experimental data for the inlet region pressure distribution in this facility without a magnetic field are presented, and a comparison between the experimental data and analytical prediction is made. The agreement between the experimentally measured entrance region pressure drop and the theoretical curve is considered as satisfactory verification of the theoretical model employed in the present investigation.

TABLE OF CONTENTS

ABSTRACT iii

NOMENCLATURE ix

I. INTRODUCTION 1

II. PREVIOUS WORK 2

III. THEORETICAL INVESTIGATION

3.1 Formulation of the Problem and Solution for Arbitrary Initial Profile 4

3.2 Velocity Solution for Uniform Initial Profile 9

3.3 Evaluation of $\epsilon(x)$ 12

3.4 The Entrance Length 15

3.5 Influence of $\omega\tau$ on Fully Developed Velocity Profile 16

3.6 Influence of $\omega\tau$ on Entrance Region Boundary Layer Thickness 16

3.7 Entrance Region Pressure Distribution 17

3.8 Entrance Region Wall Shear Stress Distribution 19

3.9 Influence of Initial Velocity Profile on Entrance Length 20

3.10 A Generalized Momentum Integral Analysis 22

3.11 The Influence of Variable Conductivity on MHD Channel Flow 29

IV. EXPERIMENTAL INVESTIGATION

4.1 Experimental Facility 42

4.2 Instrumentation 44

4.3 Experimental Results 46

V. SUMMARY 47

VI. REFERENCES 50

LIST OF ILLUSTRATIONS

Figure

1. a. MHD Flow Geometry
   b. Geometry for Generator and Accelerator Modes
2. Relationship between the Physical and Stretched Coordinate for Ha = 2
3. Relationship between the Physical and Stretched Coordinate for Ha = 6
4. Relationship between the Physical and Stretched Coordinate for Ha = 10
5. Entrance Length for Ha = 2, 4, 6
6. Entrance Length for Ha = 8, 10
7. Fully Developed Velocity Profiles for Ha = 2
8. Fully Developed Velocity Profiles for Ha = 6
9. Fully Developed Velocity Profiles for Ha = 10
10. Boundary Layer Development for Ha = 2
11. Boundary Layer Development for Ha = 6
12. Boundary Layer Development for Ha = 10
13. Entrance Region Pressure Correction for Ha = 2
14. Entrance Region Pressure Correction for Ha = 6
15. Entrance Region Pressure Correction for Ha = 10
16. Asymptotic Values of K
17. Entrance Region Wall Shear Stress Distribution for Ha = 2
18. Entrance Region Wall Shear Stress Distribution for Ha = 6
19. Entrance Region Wall Shear Stress Distribution for Ha = 10
20. Entrance Length for $\omega\tau = 0$ and N = 2, 6, 10
21. Longitudinal Variation of Entrance Region Centerline Velocity

22. Velocity Profiles for Case I with M = 3, $\Phi_y^* = 0$ Using Fredholm Integral Equation Formulation

23. Velocity Profiles for Case II with M = 3, $\Phi_y^* = 0$ Using Fredholm Integral Equation Formulation

24. Velocity Profiles for Case II with M = 3, $Ha^* = 2$ Using Fredholm Integral Equation Formulation

25. Velocity Profiles for Case II with M = 3, $Ha^* = 4$ Using Fredholm Integral Equation Formulation

26. Velocity Profiles for Case II with M = 3, $Ha^* = 8$ Using Fredholm Integral Equation Formulation

27. Velocity Profiles for Case III with M = 3, $Ha^* = 2$ Using Fredholm Integral Equation Formulation

28. Velocity Profiles for Case III with M = 3, $Ha^* = 4$ Using Fredholm Integral Equation Formulation

29. Velocity Profiles for Case III with M = 3, $Ha^* = 8$ Using Fredholm Integral Equation Formulation

30. Short Circuit Velocity Profiles for Case IV by the B. G. Galerkin Method

31. Open Circuit Velocity Profiles for Case IV by the B. G. Galerkin Method

32. Schematic Drawing of MHD Flow Loop

33. MHD Flow Loop Test Section

34. Photograph of MHD Flow Loop and Test Section

35. Experimental Entrance Region Pressure Drop for Ha = 0

LIST OF TABLES

1. Eigenvalues of tan $\gamma_n = \gamma_n$

2. Effect of the Degree of the Polynomial Velocity Profile on the Entrance Length

3. Values of Open Circuit Φ_y for Case IV

NOMENCLATURE

a_n	Velocity profile coefficients, Eq. (78)
A_o	Constant, Eq. (30)
b	Ion slip parameter
b_n	Velocity profile coefficients, Eq. (114)
B_o	Constant, Eq. (31)
B_{in}	Definite integral, Eq. (109)
$\bar{B}$	Magnetic field vector
B_z	z-component of $\bar{B}$
C	Velocity profile coefficient, Eq. (85)
C_o	Constant, Eq. (26)
C_n	Coefficient, Eq. (18)
C_n^*	Velocity profile coefficient, Eq. (106)
D_o	Constant, Eq. (27)
E_o	Function, Eq. (28)
$\bar{E}$	Electric field vector
$\bar{E}'$	$\bar{E} + \bar{V} \times \bar{B}$
f	Fully developed friction factor, Eq. (60)
$f(\eta^*)$	Function, Eq. (101)
F_o	Function, Eq. (29)
$F(\lambda^*, \theta^*)$	Function, Eq. (96)
G_k	B. G. Galerkin approximating functions, Eq. (114)
h	Channel half height
H	Velocity head, Eq. (129)
Ha	$B_z h \left[\frac{\sigma}{\mu(1+\Omega^2)}\right]^{\frac{1}{2}}$
Hac	$(1 + i\Omega)^{\frac{1}{2}}$ Ha

Ha^*	$2B_z h \left[\frac{\sigma_o}{\mu}\right]^{\frac{1}{2}}$
i	$\sqrt{-1}$
I(k)	Definite integral, Eq. (120)
I(n,k)	Definite integral, Eq. (120)
I_n	Definite integral, Eq. (108)
I_y	Total electric current, Eq. (125)
$\bar{J}$	Electric current density
K	Pressure correction factor, Eq. (62)
$K(\eta^*,t)$	Kernel, Eq. (102)
M	Number of terms in Fredholm integral equation series solution, Eq. (106)
N	Degree of velocity profile polynomial, Eq. (78)
p	Pressure
r	$(1 + \Omega^2)^{\frac{1}{2}}$
Re	Reynolds number, $\frac{\rho \bar{U} h}{\mu}$
S	Number of terms in B. G. Galerkin series solution, Eq. (114)
u	x-component of velocity
$\bar{U}$	Average velocity, Eq. (9)
v	y-component of velocity
$\bar{V}$	Vector velocity
V_c	u + iv
w	z-component of velocity
x,y,z	Coordinate axes
α	$\frac{u}{\bar{U}}$
β	Stretched coordinate, Eq. (12)
γ_n	Eigenvalues, Eq. (16)

Γ	Conductivity profile, $\frac{\sigma}{\sigma_o}$
δ	$\frac{v}{\bar{U}}$
δ^*	Displacement thickness, Eq. (74)
Δ	Boundary layer thickness
ϵ	Scale factor, Eq. (12)
η	$\frac{z}{h}$
η^*	$\frac{z}{2h}$
θ	$\frac{V_c}{\bar{U}}$
θ^*	Momentum thickness, Eq. (75)
λ_n	$\gamma_n^2 + Ha^2$
λ^*	Shape factor, Eq. (84)
$\Lambda(x)$	Eq. (8)
μ	Viscosity
ν	Kinematic viscosity, $\frac{\mu}{\rho}$
ρ	Density
σ_o	Scalar conductivity
σ	$\frac{\sigma_o}{1 + b}$
τ	Shear stress
τ^*	Dimensionless shear stress, Eq. (64)
Φ_x	$\frac{E_x}{\bar{U}B_z}$
Φ_y	$\frac{E_y}{\bar{U}B_z}$

Φ_y^* $\quad -\dfrac{\sigma_o B_z E_y}{\dfrac{dP}{dx}}$

Ψ $\quad \Omega Ha^2$

$\omega\tau$ $\quad$ Hall parameter

Ω $\quad \dfrac{\omega\tau}{1 + b}$

SUBSCRIPTS

e Entrance region

f Fully developed region

F Fredholm integral equation theory

G B. G. Galerkin method theory

o Initial inlet profile

oc Open circuit

s Core flow outside the boundary layer

w Wall value

I
INTRODUCTION

In recent years, two promising areas of engineering applications of magnetohydrodynamics (MHD) have been defined, namely MHD power generation and MHD acceleration. A recent survey of the MHD channel flow literature by Pai (Ref. 1) indicates that most of the analytical studies performed to date are for the fully developed region, the region far downstream from the entrance to the channel. For an incompressible fully developed flow at constant area, flow conditions are independent of the spatial coordinate in the flow direction.

In practice, it is likely that a significant portion of the flow in MHD generator and accelerator channels will occur in the entrance region in which the flow undergoes an adjustment from a set of initial conditions to the fully developed state. In addition, the practical range of operation of MHD devices indicates that the Hall coefficient will be significant (Ref. 2).

In the analytical portion of the present investigation the MHD flow in the entrance region of a parallel plate channel with Hall effect present is analyzed. A linearization technique developed by Sparrow, Lin and Lundgren (Ref. 3) for non MHD flows is employed. The method was recently extended to MHD flows without the Hall effect by Snyder (Ref. 4).

In order to determine the validity of the analytical solution, experimental data are presented giving measured velocity profiles and pressure distributions in the entrance region of a parallel plate channel. The working fluid for the experiments was water. A comparison between analytical and experimental data is presented which verifies the validity of the analytical method.

II
PREVIOUS WORK

Relatively few studies of MHD entrance problems are available in the literature. One of the first efforts made to estimate the MHD entry length was by Shercliff (Ref. 5). He considered a linear transient problem in which a flow is initiated from rest in an infinitely long channel by imposing an initial condition of constant mass flow rate. There is a transient period in which the flow settles to a steady state flow with a constant pressure gradient. The time required for the flow to settle to a steady state condition is converted to an entry length by multiplying by the mean velocity. This method is not precise, as acknowledged by Shercliff himself, and even though the entry length may be given to the correct order of magnitude by this method, the details of the flow for the transient problem would not be expected to agree with the flow in the actual steady state entrance problem. Roidt and Cess (Ref. 6) analyzed the entrance problem by applying the boundary layer technique of Schlichting (Ref. 7). Since nonsimilar velocity profiles are obtained in the boundary layer portion of the flow, a series solution for the stream function is necessary. The labor involved in obtaining higher order terms in the series becomes excessive. Shohet, Osterle, and Young (Ref. 8) obtained a numerical solution to the entrance problem by writing the governing equations in finite difference form and solving them on a digital computer. The same problem was solved also by Hwang and Fan (Ref. 9) by direct numerical integration of the governing equations in finite difference form.

All of the above analyses used the simple Ohm's law in the form $\bar{J} = \sigma(\bar{E} + \bar{v} \times \bar{B})$, thus excluding the Hall effect. The analysis of Chekmarev (Ref. 10) appears to be the only one in the open literature in which an effort is made to include the Hall current. Chekmarev considered an approximate linearized version of the entrance problem which will be subsequently shown to be a special case of the present analysis. The principle interest of Chekmarev was in the formulation of the problem with no numerical results given.

In the present analysis, the postulation of a boundary layer model in the entrance region is not necessary. A solution for the velocity distribution is obtained which is continuous over the cross sectional area of the duct from inlet to the fully developed region. From the velocity

distribution the physical quantities of interest such as the entrance length, pressure distribution, wall shear stress distribution, and electric current distribution may be determined. Because of the presence of the Hall current, two components of the equation of motion must be retained to account for the Hall induced transverse velocity. Solutions for both the longitudinal and transverse velocity components are obtained.

III
THEORETICAL INVESTIGATION

3.1 FORMULATION OF THE PROBLEM AND SOLUTION FOR ARBITRARY INITIAL PROFILE

The geometry of the MHD parallel plate channel is shown in Fig. 1a. The relative orientations of the electromagnetic quantities in the (x-y) plane are shown in Fig. 1b for generator and accelerator modes of operation. A constant magnetic field B_z is applied in the z-direction and the channel is assumed to be infinite in the y-direction. The electric field E' relative to the moving fluid is related to the electric field $\bar{E}$ in the stationary system by the relation

$$\bar{E}' = \bar{E} + \bar{V} \times \bar{B} \tag{1}$$

The generalized Ohm's law including ion slip and Hall effect has been discussed by Cowling (Ref. 11) and may be written as

$$\bar{J} = \frac{\sigma_o}{1+b} \bar{E}' - \frac{\omega\tau}{(1+b)B} (\bar{J} \times \bar{B}) + \frac{b}{B^2(1+b)} (\bar{B} \cdot \bar{J})\bar{B} \tag{2}$$

The ion slip term, b, becomes significant only for $\omega\tau > 10$. If no component of $\bar{J}$ is parallel to $\bar{B}$, the term $\bar{J} \cdot \bar{B}$ vanishes. Assuming the magnetic Prandtl number to be small relative to unity implies that the induced magnetic field, B_x, is small compared to the externally applied field, B_z. With these assumptions, the x and y components of $\bar{J}$ may be obtained from Eq. (2) as

$$J_x = \frac{\sigma}{(1+\Omega^2)} [E'_x - \Omega E'_y] \tag{3}$$

$$J_y = \frac{\sigma}{(1+\Omega^2)} [\Omega E'_x + E'_y] \tag{4}$$

where $\sigma = \frac{\sigma_o}{1+b}$ $\Omega = \frac{\omega\tau}{1+b}$

The governing equations of motion in the x and y directions may be written as

$$\rho\left(u\frac{\partial u}{\partial x} + w\frac{\partial u}{\partial z}\right) = -\frac{\partial P}{\partial x} + \mu\frac{\partial^2 u}{\partial z^2} + J_y B_z \tag{5}$$

$$\rho\left(u\frac{\partial v}{\partial x} + w\frac{\partial v}{\partial z}\right) = -\frac{\partial P}{\partial y} + \mu\frac{\partial^2 v}{\partial z^2} - J_x B_z \tag{6}$$

The assumptions implied by Eq. (5) and Eq. (6) are as follows:

(1) $\frac{\partial}{\partial y} = 0$ except for $\frac{\partial P}{\partial y}$

(2) Terms involving $\frac{\partial}{\partial x}$ are negligible compared to $\frac{\partial}{\partial z}$

(3) The contribution to the body force by the induced field B_x is negligible

(4) The fluid density and viscosity are assumed constant.

Assumption (1) is a consequence of the infinite channel dimension in the y-direction. Assumption (2) is a standard boundary layer assumption and is valid except in the immediate vicinity of the channel entrance. Assumption (3) implies a small magnetic Reynolds number, a valid assumption for most laboratory conditions of MHD flows. Assumption (4) is made for simplicity because the primary objective of the present analysis is to evaluate the effect of the Hall current on the entrance region flow development. A constant property assumption is reasonable as a first approximation to study the qualitative features of the flow although the quantitative results would certainly be influenced by variable properties.

It is convenient to combine Eq. (5) and Eq. (6) into a single equation by introducing complex notation. Multiplying Eq. (6) by $i = \sqrt{-1}$, adding the result to Eq. (5), and substituting for the current components from Eq. (3) and Eq. (4) gives

$$\rho\left(u\frac{\partial V_c}{\partial x} + w\frac{\partial V_c}{\partial z}\right) = -\left(\frac{\partial P}{\partial x} + i\frac{\partial P}{\partial y}\right) + \mu\frac{\partial^2 V_c}{\partial z^2}$$

$$+ \frac{\sigma B_z}{1+\Omega^2}\left[E_x(\Omega - i) + E_y(1+i\Omega) - B_z V_c(1+i\Omega)\right] \qquad (7)$$

where $V_c = u + iv$ is the complex velocity.

In (Ref. 4), the MHD entrance problem without Hall effect is analyzed by extending the linearization technique of Sparrow, Lin and Lundgren (Ref. 3) to the MHD case. Eq. (7) has the same form as the equation of motion in the absence of Hall effect and thus the same linearization technique will be used. Following the procedure of (Ref. 4), Eq. (7) is linearized to the form

$$\epsilon(x)\bar{U}\frac{\partial V_c}{\partial x} = \Lambda(x) + \nu\frac{\partial^2 V_c}{\partial z^2}$$

$$+ \frac{\sigma B_z}{\rho(1+\Omega^2)}\left[E_x(\Omega - i) + E_y(1+i\Omega) - B_z V_c(1+i\Omega)\right] \qquad (8)$$

where $\bar{U}$ is the mean velocity defined as

$$\bar{U} = \frac{1}{h}\int_0^h V_c\,dz = \frac{1}{h}\int_0^h u\,dz \qquad (9)$$

The mean value of the complex velocity V_c is equal to the mean value of the x-component of velocity u because of the physical restraint of no net mass flow in the y-direction, i.e. $\int_0^h v\,dz = 0$. Thus $\bar{U}$ is a real quantity. As in (Ref. 4), $\epsilon(x)$ is a weighting function and $\Lambda(x)$ includes the complex pressure gradient $\partial P/\partial x + i \cdot \partial P/\partial y$ plus the residual of the inertia terms after linearization. Integrating Eq. (8) over the upper half of the channel cross section determines $\Lambda(x)$. Performing the integration and utilizing Eq. (9) gives

$$0 = h\Lambda(x) + \nu \left.\frac{\partial V_c}{\partial z}\right|_{z=h}$$

$$+ \frac{\sigma h B_z}{\rho(1+\Omega^2)} \left[E_x(\Omega - i) + E_y(1+i\Omega) - B_z\bar{U}(1+i\Omega)\right] \qquad (10)$$

Substituting for $\Lambda(x)$ from Eq. (10) into Eq. (8) gives

$$\epsilon\bar{U} \frac{\partial V_c}{\partial x} = -\frac{\nu}{h} \left.\frac{\partial V_c}{\partial z}\right|_{z=h}$$

$$+ \nu \frac{\partial^2 V_c}{\partial z^2} + \frac{\sigma B_z^2(1+i\Omega)}{\rho(1+\Omega^2)} (\bar{U} - V_c) \qquad (11)$$

It is convenient to introduce dimensionless quantities

$$\alpha = \frac{u}{\bar{U}} \qquad \delta = \frac{v}{\bar{U}} \qquad \theta = \frac{V_c}{\bar{U}} \qquad \eta = \frac{z}{h} \qquad R_e = \frac{\rho\bar{U}h}{\mu}$$

$$\text{Ha}^2 = \frac{\sigma B_z^2 h^2}{\mu(1+\Omega^2)} \qquad \text{Hac}^2 = (1+i\Omega)\text{Ha}^2 \qquad d\beta = \frac{dx}{\epsilon R_e h} \qquad (12)$$

The dimensionless form of Eq. (11) becomes

$$\frac{\partial\theta}{\partial\beta} = \frac{\partial^2\theta}{\partial\eta^2} - \left.\frac{\partial\theta}{\partial\eta}\right|_{\eta=1} + \text{Hac}^2(1 - \theta) \qquad (13)$$

with boundary conditions,

$$\theta(\eta=1) = 0 \qquad \frac{\partial\theta}{\partial\eta}(\eta=0) = 0 \qquad \theta(\beta=0) = \theta_o(\eta) \qquad (14)$$

Eq. (13) and associated boundary conditions given by Eq. (14) are identical to Eq. (9) and Eq. (10) of (Ref. 4) and thus will have the same form of solution.

The solution to Eq. (13) satisfying the boundary conditions of Eq. (14) is

$$\theta = \frac{Hac(\cosh Hac\eta - \cosh Hac)}{\sinh Hac - Hac \cosh Hac}$$

$$+ \sum_{n=1}^{\infty} C_n e^{-(\gamma_n^2+Hac^2)\beta} (\cos \gamma_n\eta - \cos \gamma_n) \qquad (15)$$

where the γ_n are real eigenvalues and are the roots of the transcendental equation

$$\gamma_n = \tan \gamma_n \qquad n = 1, 2, \ldots \qquad (16)$$

The γ_n are the same eigenvalues that occurred in (Ref. 3) and (Ref. 4), and the first twenty-five eigenvalues were tabulated in those references. During the course of the present investigation, a computer program was written to evaluate the γ_n since more than twenty-five terms were found to be necessary to obtain convergence under certain conditions. After these calculations were performed, a reference by Reisman (Ref. 12) was found in which the first hundred values are tabulated. The values of γ_n are tabulated in Table 1. For large n, the γ_n obey the recurrence relation,

$$\lim_{n \to \infty} (\gamma_{n+1} - \gamma_n) = \pi \qquad (17)$$

The constants C_n are complex and depend on the initial velocity profile $\theta_o(\eta)$. The functions $f_n(\eta) = \cos\gamma_n\eta - \cos\gamma_n$ form an orthogonal set over the interval $0 \leq \eta \leq 1$ which allows determination of the C_n with the result

$$C_n = \frac{2}{(\gamma_n^2 + Hac^2)\cos\gamma_n}$$

(Equation continued)

$$+ \frac{2}{\sin^2\gamma_n} \int_0^1 \theta_o(\eta)(\cos\gamma_n\eta - \cos\gamma_n)d\eta \qquad (18)$$

The first term of Eq. (15) represents the fully developed velocity profile in complex form. It is seen to be identical to the fully developed Hartmann profile in terms of the complex Hartmann number Hac. That the fully developed velocity profile with Hall effect present could be put in the form of the Hartmann profile with a complex Hartmann number was first pointed out by Yen (Ref. 13).

It should be emphasized at this point that Eq. (15) must be separated into real and imaginary parts to be physically meaningful. Even though the form of the complex solution is identical to that contained in (Ref. 4), this apparent simplicity of the complex solution is deceptive because the separation of Eq. (15) into real and imaginary parts is a rather tedious exercise im complex algebra. This separation is done in the next section for the case of uniform initial velocity profile.

3.2 VELOCITY SOLUTION FOR UNIFORM INITIAL PROFILE

For a uniform initial velocity profile, $\theta_o(\eta) = 1$ and Eq. (18) becomes

$$C_n = \frac{2}{(\gamma_n^2 + Hac^2)\cos\gamma_n} \qquad (19)$$

The real part of Eq. (15) gives the dimensionless longitudinal velocity component $\alpha = u/\bar{U}$ and the complex part gives the transverse velocity $\delta = v/\bar{U}$. Because of the lengthy expressions involved, it is convenient to list the fully developed and the entrance region portions of the velocity profile separately. The first term of Eq. (15) is the fully developed profile and the series term is the entrance region profile. Thus the dimensionless velocity components will be written

$$\alpha = \frac{u}{\bar{U}} = \alpha_f + \alpha_e \qquad (20)$$

$$\delta = \frac{v}{\bar{U}} = \delta_f + \delta_e \qquad (21)$$

where subscripts f and e refer to the fully developed and entrance portions respectively. After a considerable amount of complex algebra manipulations, the real and imaginary parts of Eq. (15) may be written as

$$\alpha_f = \frac{C_o E_o(\eta) + D_o F_o(\eta)}{C_o^2 + D_o^2} \tag{22}$$

$$\delta_f = \frac{D_o E_o(\eta) - C_o F_o(\eta)}{C_o^2 + D_o^2} \tag{23}$$

$$\alpha_e = 2 \sum_{n=1}^{\infty} \frac{e^{-\lambda_n \beta}[\cos\gamma_n \eta - \cos\gamma_n][\lambda_n \cos\Psi\beta - \Psi \sin\Psi\beta]}{[\lambda_n^2 + \Psi^2]\cos\gamma_n} \tag{24}$$

$$\delta_e = -2 \sum_{n=1}^{\infty} \frac{e^{-\lambda_n \beta}[\cos\gamma_n \eta - \cos\gamma_n][\lambda_n \sin\Psi\beta - \Psi \cos\Psi\beta]}{[\lambda_n^2 + \Psi^2]\cos\gamma_n} \tag{25}$$

$$C_o = \sinh A_o \cos B_o - A_o \cosh A_o \cos B_o + B_o \sinh A_o \sin B_o \tag{26}$$

$$D_o = \cosh A_o \sin B_o - A_o \sinh A_o \sin B_o - B_o \cosh A_o \cos B_o \tag{27}$$

$$E_o(\eta) = A_o(\cosh A_o \eta \cos B_o \eta - \cosh A_o \cos B_o) - B_o(\sinh A_o \eta \sin B_o \eta - \sinh A_o \sin B_o) \tag{28}$$

$$F_o(\eta) = B_o(\cosh A_o\eta \cos B_o\eta - \cosh A_o \cos B_o)$$

$$+ A_o(\sinh A_o\eta \sin B_o\eta$$

$$- \sinh A_o \sin B_o) \tag{29}$$

$$A_o = Ha\sqrt{\frac{r + 1}{2}} \tag{30}$$

$$B_o = - Ha\sqrt{\frac{r - 1}{2}} \tag{31}$$

$$r = \sqrt{1 + \Omega^2} \tag{32}$$

$$Hac = A_o - iB_o \tag{33}$$

$$\lambda_n = \gamma_n^2 + Ha^2 \tag{34}$$

$$\Psi = \Omega Ha^2 \tag{35}$$

The longitudinal and transverse velocity components, given by Eq. (22) through Eq. (25) may be used to calculate physical quantities of interest in the entrance region. Before these calculations are presented the limiting case of $\omega\tau = 0$ will be considered first. From the definitions $\Omega = \omega\tau/(1 + b)$ and $\Psi = \Omega Ha^2$, it is clear that $\Psi = 0$ for $\omega\tau = 0$. From the definitions contained in Eq. (26) through Eq. (35), the following expressions apply for $\omega\tau = 0$.

$$\Omega = 0 \tag{36}$$

$$r = 1 \tag{37}$$

$$B_o = 0 \tag{38}$$

$$A_o = Ha \tag{39}$$

$$C_o = \sinh Ha - Ha \cosh Ha \tag{40}$$

$$D_o = 0 \tag{41}$$

$$E_o(\eta) = Ha(\cosh Ha\eta - \cosh Ha) \tag{42}$$

$$F_o(\eta) = 0 \tag{43}$$

$$Hac = Ha \tag{44}$$

Substituting Eq. (36) through Eq. (44) into Eq. (22) through Eq. (25) gives

$$\alpha = \frac{Ha(\cosh Ha\eta - \cosh Ha)}{\sinh Ha - Ha \cosh Ha} + 2 \sum_{n=1}^{\infty} \frac{e^{-(\gamma_n^2 + Ha^2)\beta} (\cos \gamma_n\eta - \cos \gamma_n)}{(\gamma_n^2 + Ha^2)\cos \gamma_n} \tag{45}$$

$$\delta = 0 \tag{46}$$

Eq. (45) is identical to Eq. (18) of (Ref. 4). Eq. (46) confirms the anticipated result that the transverse velocity vanishes for $\omega\tau = 0$.

3.3 EVALUATION OF $\epsilon(x)$

The velocity solution given by Eq. (22) through Eq. (25) is in terms of the stretched axial coordinate β. The physical coordinate x is related to the stretched coordinate β from Eq. (12) by the relation

$$\frac{1}{R_e}\,\frac{x}{h} = \int_0^{\beta} \epsilon d\beta \tag{47}$$

Therefore a knowledge of the variation of ϵ with β is required in order to transform from the β to x variable.

In (Ref. 4), the procedure used to evaluate ϵ was based on the assumption that the pressure gradient calculated from the equation of motion is equal to the pressure gradient obtained from a mechanical energy equation. This procedure will be used in the present analysis. To facilitate the operations which are to follow, it is convenient to write the inertia term of Eq. (5) in the form

$$u\,\frac{\partial u}{\partial x} + w\,\frac{\partial u}{\partial z} = \frac{\partial uu}{\partial x} + \frac{\partial uw}{\partial z} \tag{48}$$

Eq. (48) is the result of combining the continuity equation with the inertia term. Combining Eq. (5) with Eq. (4) and Eq. (48) gives

$$\rho\left(\frac{\partial uu}{\partial x} + \frac{\partial uw}{\partial z}\right) = -\frac{\partial P}{\partial x} + \mu\,\frac{\partial^2 u}{\partial z^2}$$

$$+ \frac{\sigma B_z}{1 + \Omega^2}\left[\Omega(E_x + vB_z) + (E_y - uB_z)\right] \tag{49}$$

Integrating Eq. (49) over the half width of the channel from z = 0 to z = h gives

$$-\frac{1}{\rho}\,\frac{\partial P}{\partial x} = \frac{1}{h}\,\frac{\partial}{\partial x}\int_0^h u^2 dz - \frac{\nu}{h}\,\frac{\partial u}{\partial z}\bigg|_{z=h}$$

$$- \frac{\sigma B_z{}^2 \bar{U}}{\rho(1 + \Omega^2)}\left[\Omega\Phi_x + (\Phi_y - 1)\right] \tag{50}$$

where

$$\Phi_x = \frac{E_x}{\bar{U}B_z} \qquad \Phi_y = \frac{E_y}{\bar{U}B_z} \tag{51}$$

A mechanical energy equation may be obtained by multiplying Eq. (5) by u with the result

$$\frac{1}{2}\frac{\partial uu^2}{\partial x} + \frac{1}{2}\frac{\partial wu^2}{\partial z} = -\frac{u}{\rho}\frac{\partial P}{\partial x} + \nu u\frac{\partial^2 u}{\partial z^2}$$

$$+ \frac{\sigma B_z}{\rho(1+\Omega^2)}[\Omega(uE_x + uvB_z) + (uE_y - u^2B_z)] \qquad (52)$$

Integrating Eq. (52) gives

$$-\frac{1}{\rho}\frac{\partial P}{\partial x} = \frac{1}{h\bar{U}}\frac{\partial}{\partial x}\int_0^h \frac{u^3}{2}\,dz + \frac{\nu}{h\bar{U}}\int_0^h (\frac{\partial u}{\partial z})^2 dz$$

$$-\frac{\sigma B_z{}^2\bar{U}}{\rho(1+\Omega^2)}[\Omega(\Phi_x + \frac{1}{h\bar{U}^2}\int_0^h uv\,dz)$$

$$+ (\Phi_y - \frac{1}{h\bar{U}^2}\int_0^h u^2 dz)] \qquad (53)$$

Equating the pressure gradient expression from Eq. (50) and Eq. (53) and introducing dimensionless quantities gives the following expression for ϵ.

$$\epsilon(Ha,\Omega,\beta) = \frac{\frac{\partial}{\partial\beta}\int_0^1 (\alpha^2 - \frac{\alpha^3}{2})d\eta}{\int_0^1 (\frac{\partial\alpha}{\partial\eta})^2 d\eta + \frac{\partial\alpha}{\partial\eta}\Big|_{\eta=1} + Ha^2[\int_0^1 (\alpha^2-1)d\eta - \Omega\int_0^1 \alpha\delta d\eta]} \qquad (54)$$

The right side of Eq. (54) is a known function of β, Ha, and Ω from Eq. (22) through Eq. (25). The physical coordinate x is then given by Eq. (47).

Eq. (54) shows that ϵ, the weighting function, is a

function of β as well as the electromagnetic parameters Ha and Ω. The integrals appearing in Eq. (54) were evaluated numerically. The relation between the physical coordinate x and the stretched coordinate β was determined from Eq. (47) which involves a numerical integration of ϵ with respect to β. The results are shown in Figs. 2, 3, and 4. Shown also for comparison are the curves for $\epsilon = 1$, an assumption made by Chekmarev (Ref. 10). The assumption $\epsilon = 1$ is seen to be a poor one as Ha increases at $\omega\tau = 0$. For $\omega\tau = 10$, the $\epsilon = 1$ curve is approached more closely. Basing the entrance length determination on the assumption $\epsilon = 1$ results in a longer entrance length prediction than that based on a variable ϵ given by Eq. (54).

3.4 THE ENTRANCE LENGTH

For incompressible, constant area flow, a fully developed velocity profile is approached which is independent of the axial coordinate. Because the fully developed profile is approached asymptotically, the definition of the entrance length is arbitrary. The customary definition of the entrance length is the distance required for the centerline velocity to become a specified fraction of the fully developed centerline velocity. The difference between the fully developed centerline velocity and the centerline velocity at any position β may be written from Eq. (24) as

$$\alpha_f(\eta=0)-\alpha(\eta=0) = 2\sum_{n=1}^{\infty} \frac{e^{-\lambda_n\beta}(\cos\gamma_n-1)(\lambda_n\cos\Psi\beta - \Psi\sin\Psi\beta)}{(\lambda_n^2 + \Psi^2)\cos\gamma_n} \quad (55)$$

The entrance length will be defined as that distance at which $\alpha_f(\eta = 0) - \alpha(\eta = 0) = 0.05$. This definition corresponds to the location at which the centerline velocity is 95% of the fully developed centerline value. Entrance length values are shown in Fig. 5 for Hartmann number values of Ha = 2, 4, 6 and in Fig. 6 for values Ha = 8, 10. For a given value of Ha, the entrance length is seen to increase with increasing values of $\omega\tau$. For the smaller values of Ha, the entrance length values appear to be approaching an asymptotic limit as $\omega\tau$ increases. The asymptotic limit is not so obvious for the larger values Ha = 8 and Ha = 10 since $\omega\tau = 10$ was the largest value used in the calculations. However, an examination of the complete equation of motion given by Eq. (7) shows that in the limit as $\omega\tau \to \infty$ with $\bar{B}$ and $\bar{E}$ held constant, the electromagnetic body force term vanishes. Thus as $\omega\tau \to \infty$,

the entrance region flow approaches the non MHD entrance region as a limit. Additional justification of this conclusion is provided by an examination of the influence of $\omega\tau$ on the fully developed velocity profiles.

3.5 INFLUENCE OF $\omega\tau$ ON FULLY DEVELOPED VELOCITY PROFILE

Fully developed velocity profiles are shown in Figs. 7, 8, 9 for Ha values of 2, 6, 10 and $\omega\tau$ values of 0 and 10. Shown also for comparison is the profile for fully developed flow in the absense of a magnetic field, the well known parabolic distribution given by the relation

$$\frac{u}{\bar{U}} = \frac{3}{2}\left[1 - \left(\frac{z}{h}\right)^2\right] \tag{56}$$

As $\omega\tau$ increases, the curves approach the parabolic distribution. Thus the parameters Ha and $\omega\tau$ distort the velocity profiles in opposite trends. Increasing Ha tends to flatten the profile in the center of the channel, resulting in an increased shear stress at the wall, whereas increasing $\omega\tau$ causes the profile to become more nearly parabolic in shape, resulting in a decrease in the wall shear stress. This trend in the fully developed region suggests that in the entrance region, the boundary layer thickness should increase as $\omega\tau$ increases.

3.6 INFLUENCE OF $\omega\tau$ ON ENTRANCE REGION BOUNDARY LAYER THICKNESS

The definition of the boundary layer thickness in either external or internal flows is arbitrary because of the non-uniqueness of the boundary layer thickness. In internal flows, a frequently used definition is the distance from the wall at which the velocity becomes a specified fraction of the centerline velocity. In the present analysis, the boundary layer thickness will be defined as the distance from the wall at which the local velocity is 90% of the centerline velocity. This definition, although arbitrary, will serve the purpose of illustrating the influence of $\omega\tau$ on the boundary layer thickness.

The entrance region boundary layer thickness is shown plotted in Figs. 10, 11, 12 for Ha values of 2, 6, 10 and $\omega\tau$ values of 0 and 10. The curves are terminated at the end of the entrance region that was previously defined as the position at which the centerline velocity is 95% of the fully developed centerline value. The boundary layer

thickness so defined is seen to increase as $\omega\tau$ increases, a result qualitatively compatible with the observed effect of $\omega\tau$ on the fully developed velocity profiles.

3.7 ENTRANCE REGION PRESSURE DISTRIBUTION

The pressure distribution in the entrance region may be obtained by integrating either Eq. (50) or Eq. (53) from the entrance, $x = 0$, to any position x. Because of the simpler form of Eq. (50), it will be used to determine the pressure distribution. To emphasize the entrance region effect on the pressure distribution, it is convenient to separate the pressure drop into a fully developed portion and an entrance region portion. This separation can be accomplished by using the identity

$$\left.\frac{\partial u}{\partial z}\right|_{z=h} = \left.\frac{\partial u_f}{\partial z}\right|_{z=h} + \left.\frac{\partial (u - u_f)}{\partial z}\right|_{z=h} \tag{57}$$

where u_f is the fully developed velocity. Substituting Eq. (57) into (50) and integrating from $x = 0$ to $x = x$ gives

$$\frac{P_o - P}{\rho} = \frac{1}{h}\int_0^h u^2 dz - \bar{U}^2 - \frac{\nu}{h}\int_0^x \left.\frac{\partial u_f}{\partial z}\right|_{z=h} dx$$

$$- \frac{\nu}{h}\int_0^x \left.\frac{\partial (u - u_f)}{\partial z}\right|_{z=h} dx - \frac{\sigma B_z^2 \bar{U} x}{\rho(1 + \Omega^2)} [\Omega\Phi_x + (\Phi_y - 1)] \tag{58}$$

Writing Eq. (58) in dimensionless form gives

$$\frac{P_o - P}{\frac{1}{2}\rho\bar{U}^2} = -\frac{2}{Re}\left(\frac{x}{h}\right)\left(\left.\frac{\partial \alpha_f}{\partial \eta}\right|_{\eta=1} + Ha[\Omega\Phi_x + (\Phi_y - 1)]\right)$$

$$+ 2\left(\int_0^1 \alpha^2 d\eta - 1 - \int_0^\beta \epsilon \left.\frac{\partial (\alpha - \alpha_f)}{\partial \eta}\right|_{\eta=1} d\beta\right) \tag{59}$$

The first bracketed term of Eq. (59) is the pressure drop resulting from the fully developed flow and the second bracketed term is an entrance region correction term. Rewriting Eq. (59) in terms of a fully developed friction factor and an entrance region correction term gives

$$\frac{P_o - P}{\frac{1}{2}\rho\bar{U}^2} = f \frac{1}{Re} \left(\frac{x}{h}\right) + K \tag{60}$$

where

$$f = -2\left(\left.\frac{\partial\alpha}{\partial\eta}\right|_{\eta=1} + Ha^2[\Omega\Phi_x + (\Phi_y - 1)]\right) \tag{61}$$

$$K = 2\left(\int_0^1 \alpha^2 d\eta - 1 - \int_0^\beta \epsilon \left.\frac{\partial(\alpha - \alpha_f)}{\partial\eta}\right|_{\eta=1} d\beta\right) \tag{62}$$

The fully developed friction factor, f, is a function of both components of the electric field Φ_x and Φ_y. The entrance region pressure correction, K, is independent of the electric field, however. It is interesting to observe that the Hall current induced transverse velocity component, δ, does not appear in the longitudinal pressure distribution. It would appear in the transverse pressure distribution, however, since the transverse velocity induces a transverse pressure distribution.

The entrance region pressure correction is shown in Figs. 13, 14, 15 for Ha values of 2, 6, 10 and $\omega\tau$ values of 0 and 10. An examination of the curves shows that for a fixed value of Ha, K increases with increasing $\omega\tau$. The influence of $\omega\tau$ becomes more pronounced as Ha increases. For a fixed value of $\omega\tau$, K decreases with increasing Ha. The curves are terminated at the end of the entrance region.

For the fully developed region, the pressure gradient becomes constant and is given by the fully developed friction factor defined by Eq. (61). Thus it is clear that the value of K should asymptotically approach a constant value in the limit as $x \to \infty$. This conclusion is also evident from the definition of K given by Eq. (62). The asymptotic values of K are shown on Figs. 13, 14, 15.

Since the curves were terminated at the arbitrarily defined entrance length, i.e. the position at which the centerline velocity becomes 95% of the fully developed centerline velocity, the asymptotic value is not reached by the curves. The total pressure in the entrance region should be based on the asymptotic value of K. The variation of the asymptotic value of K with $\omega\tau$ is shown in Fig. 16 for Ha values of 2, 6, 10.

3.8 ENTRANCE REGION WALL SHEAR STRESS DISTRIBUTION

The shear stress at the wall is given by the expression

$$\tau_w = -\mu \left.\frac{\partial u}{\partial z}\right|_{z=h} = -\frac{\mu\bar{U}}{h}\left.\frac{\partial \alpha}{\partial \eta}\right|_{\eta=1} \tag{63}$$

The negative sign is used to make τ_w a positive quantity since the velocity gradient at the wall is negative. Defining a dimensionless shear stress as

$$\tau^* = \frac{\tau}{\left(\frac{\mu\bar{U}}{h}\right)} \tag{64}$$

and evaluating the velocity gradient from Eq. (20), (22), and (24) gives

$$\tau_w^* = \frac{[\sinh A_o \cos B_o][C_o(B_o^2 - A_o^2) - 2A_oB_oD_o]}{C_o^2 + D_o^2}$$

$$+ \frac{[\cosh A_o \sin B_o][D_o(B_o^2 - A_o^2) + 2A_oB_oC_o]}{C_o^2 + D_o^2}$$

$$+ 2\sum_{n=1}^{\infty} \frac{e^{-\lambda_n\beta}\gamma_n^2[\lambda_n \cos \Psi\beta - \Psi \sin \Psi\beta]}{[\lambda_n^2 + \Psi^2]} \tag{65}$$

The first two terms in Eq. (65) give the wall shear stress in the fully developed region and the summation represents the contribution due to the entrance region.

The variation of the wall shear stress in the entrance region is shown in Figs. 17, 18, and 19. The results are plotted as a ratio of local wall shear stress to the fully developed value. Since the initial velocity profile at the channel entrance was assumed to be uniform, a discontinuity in the velocity distribution at the wall occurs, resulting in an infinite value of shear stress at the inlet. This is not a physically meaningful result but is a consequence of the assumption of an initial uniform profile, a physically impossible condition for a viscous fluid.

3.9 INFLUENCE OF INITIAL VELOCITY PROFILE ON ENTRANCE LENGTH

The solution for the entrance region velocity profile is given by Eq. (15) with the constants C_n given by Eq. (18). The $\theta_o(\eta)$ appearing in Eq. (18) is the initial velocity profile at the channel entrance. The results presented so far have been for uniform initial profile, i.e. $\theta_o = 1$. In an actual MHD channel, the initial profile would not be uniform.

In order to assess the influence of the initial velocity profile on flow development in the entrance region, a family of initial profiles was assumed described by the relation

$$\theta_o(\eta) = \alpha_o(\eta) = \frac{N + 1}{N} [1 - \eta^N] \tag{66}$$

where N is a constant. This profile is seen to satisfy the relation

$$\int_0^1 \theta_o(\eta) d\eta = 1 \tag{67}$$

which is required by the definition of mean velocity and the condition of no net mass flow in the transverse direction. This family of initial profiles was chosen because it allows representation of the laminar fully developed non-MHD flow as well as flows with steeper velocity gradients near the wall than the laminar fully developed gradient. Thus a

turbulent type profile could be approximated by taking N sufficiently large. The uniform initial profile is also included as a limiting case in the limit $N \to \infty$.

Numerical results were obtained for the three values N = 2, 6, 10 with $\omega\tau = 0$. This latter condition implies that the transverse velocity component vanishes and thus $\theta = \alpha$. The entrance length variation with N and Ha is shown in Fig. 20. For N = 2, corresponding to a parabolic initial velocity profile, the variation of entrance length with Ha is seen to begin at 0 for Ha = 0, reach a maximum value at Ha = 4, and approach asymptotically a value independent of Ha for Ha > 10. This qualitative feature of a maximum value of entrance length occurring is present only for the case N = 2 and can be explained as follows. For a non-MHD flow, N = 2 corresponds to the fully developed laminar profile. Thus for Ha = 0, N = 2, the inlet flow is already fully developed, giving an entrance length of zero. As N increases, the entrance length variation with Ha is seen to approach the curve corresponding to a uniform initial profile.

A measure of the influence of the initial velocity profile on the entrance region flow development can be obtained by comparing the wall shear stress of the initial profile with the fully developed wall shear stress for a given value of Hartmann number. From Eq. (66) the dimensionless shear stress at the wall is given by

$$\tau^*_{wo} = N + 1 \tag{68}$$

The fully developed MHD wall shear stress for $\omega\tau = 0$ is given by

$$\tau^*_w = \frac{Ha^2}{Ha \coth Ha - 1} \tag{69}$$

For large Ha, the difference between Eq. (69) and Eq. (68) may be written

$$\tau^*_w - \tau^*_{wo} = Ha - N \tag{70}$$

Eq. (70) shows that for large values of Ha, the fully developed wall shear stress and the initial wall shear

stress become equal when Ha = N. This conclusion is illustrated in Fig. 21 in which the entrance region centerline velocity is plotted for N = 2, 6, 10 and Ha = 2, 6, 10. From the curves it is clear that when Ha = N, there is very little change in the centerline velocity. Since the primary mechanism involved in adjusting an initial velocity profile to a fully developed profile is the diffusion of vorticity generated at the wall into the central portion of the flow, if the inlet wall shear stress is equal to the fully developed wall shear stress, there will be no significant adjustment of vorticity necessary and hence no velocity entrance length. This conclusion would not be valid for a compressible flow with variable properties, however.

3.10 A GENERALIZED MOMENTUM INTEGRAL ANALYSIS

The previous analysis of the MHD entrance region problem did not use a boundary layer - core flow model. Instead the equation of motion was linearized in such a way that a solution for the velocity profile was obtained which is continuous from the entrance of the channel to the fully developed region. If a boundary layer - core flow model is used, two techniques are available, (1) the momentum integral method and (2) a non similar series expansion.

Several investigations of the MHD entrance region problem based on the momentum integral method have appeared in the literature in recent years. Moffatt (Ref. 14) was the first investigator to apply the momentum integral method to the study of MHD boundary layer formation over a flat plate. He assumed a parabolic velocity distribution in the boundary layer.

Maciulaitis and Loeffler (Ref. 15) applied the momentum integral method and got a closed form solution by assuming the velocity distribution to have a parabolic variation and the centerline velocity to vary down the channel.

Tan (Ref. 16) also found a closed form solution by using the momentum integral method and assuming a Hartmann-like velocity distribution previously used by Moffatt (Ref. 14) who had solved the problem numerically.

Dhanak (Ref. 17) applied the classical Karman-Pohlhausen method to the entrance region and solved the resulting equation by an iterative scheme.

Although several authors have applied momentum integral methods to MHD entrance flow, using simple parabolic,

Hartmann-like or Karman-Pohlhausen velocity distributions, these works, rather than establish the validity of the momentum integral method, have created controversy as to whether or not one can validly apply such a method to MHD flows. Hugelman and Haworth (Ref. 18) reasoned that the classical Karman-Pohlhausen method does not take into account enough boundary conditions. They suggested using a fifth-degree polynomial. Heywood and Moffatt (Ref. 19) state that integral method results are too much dependent upon the velocity profile assumed and that Dhanak's solution, in particular, did not proceed far enough downstream to show clearly the effect of the magnetic field.

One of the most severe limitations of the classical momentum integral method in which fourth-degree polynomial profiles are assumed is that the solution cannot be obtained over the entire range from entrance to the fully developed region. This is a limitation for an MHD entrance region flow as well.

In the present investigation the momentum integral method has been generalized to include a polynomial velocity profile of arbitrary degree. It is found that increasing the degree of the assumed polynomial velocity profile permits a solution which is continuous from the entrance region to the fully developed region.

The method will be developed for the case $\omega\tau = 0$ which means that only the x-component of the equation of motion is needed. Eq. (5) with $\omega\tau = 0$ becomes

$$\rho\left(u\frac{\partial u}{\partial x} + w\frac{\partial u}{\partial z}\right) = -\frac{\partial P}{\partial x} + \mu\frac{\partial^2 u}{\partial z^2} + \sigma B_z(E_y - uB_z) \tag{71}$$

with the continuity equation given by

$$\frac{\partial u}{\partial x} + \frac{\partial w}{\partial z} = 0 \tag{72}$$

Eq. (71) is integrated over the boundary layer thickness Δ to obtain the momentum integral equation in the form

$$\frac{d\theta^*}{dx} = \frac{\tau_w}{\rho U_s^2} + \frac{2\theta^*\sigma B_z^2}{\rho U_s} - \frac{\theta^*}{U_s}\left(2 + \frac{\delta^*}{\theta^*}\right)\left(\frac{dU_s}{dx} + \frac{\sigma B_z^2}{\rho}\right) \tag{73}$$

where δ^* and θ^* are the displacement thickness and momentum thickness respectively, defined as

$$\delta^* = \int_0^{\Delta} \left(1 - \frac{u}{u_s}\right) dz \tag{74}$$

$$\theta^* = \int_0^{\Delta} \frac{u}{u_s} \left(1 - \frac{u}{u_s}\right) dz \tag{75}$$

The velocity u_s is the uniform core velocity outside the boundary layer. A relationship between δ^*, u_s, and $\bar{U}$, the average velocity may be obtained from a mass balance given by the expression

$$\bar{U}h = \int_0^{\Delta} u\,dz + \int_{\Delta}^{h} u_s\,dz \tag{76}$$

Adding and subtracting the term $\int_0^{\Delta} u_s\,dz$ to the right side of Eq. (76) and rearranging gives

$$\frac{\delta^*}{h} = 1 - \frac{\bar{U}}{u_s} \tag{77}$$

To solve Eq. (73) requires an assumed velocity profile. The conventionally used profile, following the classic work of von Karman and Pohlhausen, is a polynomial of degree four. The fourth-degree polynomial profile has certain limitations, however, the most serious being that a solution cannot be obtained which is valid from the entrance region to the fully developed region. At a certain distance downstream from the entrance, a velocity overshoot occurs in the boundary layer, that is the local boundary layer velocity becomes larger than the local free stream velocity. Although such an overshoot is possible in a compressible, variable property fluid, there appears to be no physical mechanism which would allow a velocity overshoot in an incompressible, constant property fluid. Thus the momentum integral solution is considered to be valid only to the position at which boundary layer overshoot occurs.

In the present investigation, the momentum integral method is generalized to allow a polynomial velocity profile of arbitrary degree. It is shown that for a given Hartmann number, taking a polynomial profile of sufficiently high degree will always allow a solution which is valid over the entire entrance region.

Consider a boundary layer profile expressed as a polynomial of degree N of the form

$$\frac{u}{u_s} = \sum_{n=1}^{N} a_n \eta^{*n} \tag{78}$$

where

$$\eta^* = \frac{z}{\Delta}$$

The coefficients a_n will be functions of x and N boundary conditions are required to determine the N values of a_n. In the present analysis, three boundary conditions are applied at the wall, $\eta^* = 0$, and the remaining N - 3 are applied at the outer edge of the boundary layer, $\eta^* = 1$. In particular the boundary conditions become

at $\eta^* = 0$ $\qquad u = 0 \qquad v = 0$

$$\nu \frac{\partial^2 u}{\partial z^2} = \frac{1}{\rho}\frac{\partial P}{\partial x} - \frac{\sigma B_z E_y}{\rho} = -u_s\left(\frac{du_s}{dx} + \frac{\sigma B_z^2}{\rho}\right) \tag{79}$$

at $\eta^* = 1$ $\qquad u = u_s$

$$\frac{\partial u}{\partial z} = \frac{\partial^2 u}{\partial z^2} = \ldots \frac{\partial^m u}{\partial z^m} = 0 \qquad m = N - 3 \tag{80}$$

The first two conditions of Eq. (79) are the velocity non slip conditions and the third condition is the equation of motion evaluated at the wall. The first condition of

Eq. (80) requires the boundary layer velocity to match the free stream velocity at the outer edge of the boundary layer and the remaining conditions require the first N - 3 derivatives of the velocity profile to vanish at the outer edge.

Substituting the boundary conditions from Eqs. (79) and (80) into Eq. (78) gives

$$a_2 = -\frac{\lambda^*}{2} \tag{81}$$

$$\sum_{n=1}^{N} a_n = 1 \tag{82}$$

$$\sum_{n=1}^{N-(m-1)} [(n+m-1)(n+m-2)\ldots n]a_{n+m-1} = 0 \quad m=1,2,\ldots N-3 \tag{83}$$

where

$$\lambda^* = \frac{\nabla^2}{\nu}\left(\frac{du_s}{dx} + \frac{\sigma B_z^2}{\rho}\right) \tag{84}$$

The parameter λ^* defined by Eq. (84) is the boundary layer shape factor and it is clear that each of the a_n coefficients will be a function of λ^* and thus a function of x.

Eqs. (81) through (83) are a set of N equations for the N unknown a_n coefficients. For large N, the direct solution of the equations in explicit form is not feasible. By starting with a different form for the polynomial velocity profile, however, it is possible to obtain an exact recurrence relation for all the a_n in terms of λ^*, valid for arbitrary degree N.

For this purpose, consider the function

$$\frac{u}{u_s} = (1 - \eta^*)^{N-1}(C\eta^* - 1) + 1 \tag{85}$$

where C is a coefficient to be determined. It is clear that Eq. (85) is a polynomial of degree N and that the outer edge condition $u/u_s(\eta^* = 1) = 1$ is automatically satisfied. The non slip condition at $\eta^* = 0$ is also automatically satisfied. It may be shown by differentiation that the N - 3 outer edge conditions given by Eq. (80) are also automatically satisfied. The remaining boundary condition is the second condition of Eq. (79) which can be used to determine C with the result

$$C = \frac{\lambda^* - (N - 1)(N - 2)}{2(N - 1)} \tag{86}$$

Substituting Eq. (86) into (85) gives

$$\frac{u}{u_s} = (1 - \eta^*)^{N-1}\left[\frac{\lambda^* - (N-1)(N-2)}{2(N - 1)}\,\eta^* - 1\right] + 1 \tag{87}$$

as an equivalent form of the Nth degree polynomial profile which satisfies all the required boundary conditions. Expanding the term $(1 - \eta^*)^{N-1}$ by the binomial theorem then gives a polynomial of degree N. Equating the coefficients of successive powers of η^* from Eqs. (78) and (87) gives exact recurrence relations for the a_n with the result

$$a_n = (-1)^{n+1}\left[\binom{N-1}{n-1}\,\frac{\lambda^* - (N-1)(N-2)}{2(N - 1)} - \binom{N-1}{N}\right] \tag{88}$$

for n = 1, 2, 3 ...N-1 and

$$a_N = (-1)^{N+1}\left[\frac{\lambda^* - (N-1)(N-2)}{2(N - 1)}\right] \tag{89}$$

where

$$\binom{N-1}{n-1} = \frac{(N-1)!\;\; n}{n!\;\; (N-n)!}$$

$$\binom{N-1}{n} = \frac{(N-1)!\;\; (N-n)}{n!\;\; (N - n)!}$$

The wall shear stress, τ_w, appearing in Eq. (73) can now be explicitly related to λ^* and N with the result

$$\tau_w = \mu \left.\frac{\partial u}{\partial z}\right|_{z=0} = \frac{\mu u_s}{\Delta}\left(\frac{\lambda^*}{2(N-1)} + \frac{N}{2}\right) \tag{90}$$

Physically meaningful boundary layer results can be obtained for λ^* values in a well defined range. For sufficiently small values of λ^*, separation occurs whereas for large values of λ^*, velocity overshoot in the boundary layer occurs. The condition for boundary layer separation at the wall is

$$\left.\frac{\partial u}{\partial z}\right|_{z=0} = 0$$

which gives

$$\lambda^*_{min} = -N(N-1) \tag{91}$$

Velocity overshoot occurs in the boundary layer if $\frac{\partial u}{\partial z} = 0$ at some intermediate value of z between 0 and Δ. Applying this condition gives

$$\lambda^*_{max} = N(N-1) \tag{92}$$

Thus the physically allowable range for λ^* becomes

$$-N(N-1) \leq \lambda^* \leq N(N-1) \tag{93}$$

where the negative lower limit corresponds to separation and the positive upper limit corresponds to velocity overshoot.

With the expressions for a_n now known in explicit form, the displacement and momentum thicknesses may be evaluated from Eqs. (74) and (75) with the result

$$\frac{\delta^*}{\Delta} = \frac{3N(N-1) - \lambda^*}{2N(N^2-1)} \tag{94}$$

$$\frac{\theta^*}{\Delta} = \frac{(N-1)}{N(2N-1)} - \frac{(N-2)C}{N(N+1)(2N-1)} - \frac{C^2}{N(2N+1)(2N-1)} \tag{95}$$

where

$$C = \frac{\lambda^* - (N-1)(N-2)}{2(N-1)}$$

Combining Eqs. (73), (77), (94) and (95) leads to a single differential equation involving λ^* and θ^* which can be written in the form

$$\frac{d\lambda^*}{d\theta^*} = F(\lambda^*, \theta^*) \tag{96}$$

The derivation of Eq. (96) is quite lengthy and will not be presented here. Eq. (96) is non linear and must be integrated numerically. Once the numerical relationship between λ^* and θ^* is established, one may then obtain numerically the variations of θ^*, λ^*, δ^*, τ_w, u_s, and P with x. Of particular interest here is the variation of u_s, the free stream velocity, which gives a measure of the entrance length. The influence of the degree of the polynomial, N, on the entrance length is shown in Table 2. The entrance length is defined as the distance at which the centerline velocity becomes 95% of the fully developed centerline velocity. From the table it is clear that increasing N from 4 to 60 does not have a strong effect on the calculated entrance length. The influence of N is more significant for smaller values of Ha, and for Ha = 1, the difference in the calculated entrance lengths for N = 4 and N = 60 is 8%. The entrance length decreases slightly as N increases.

3.11 THE INFLUENCE OF VARIABLE CONDUCTIVITY ON MHD CHANNEL FLOW

The analysis presented thus far has been based on the assumption of constant fluid properties, including the electrical conductivity. The electrical conductivity is a strong function of temperature, however, and any flow with large temperature variations will have a spatially non uniform conductivity.

The direct solution of variable conductivity MHD flows requires the simultaneous solution of the energy equation

and the equation of motion. An iterative procedure is normally used in which a tentative solution to the equation of motion is obtained using an assumed spatial variation of the conductivity. Using this solution in the energy equation then gives a first order solution for the temperature profile. From the temperature profile and a prescribed temperature-conductivity variation, a corrected conductivity profile can be obtained. Using the corrected conductivity profile in the equation of motion allows the procedure to be repeated as many times as desired.

The effectiveness of the iteration procedure depends on the difficulty involved in solving the equation of motion with a spatial variation in conductivity. Exact solutions can be obtained for only a limited number of conductivity variations for fully developed, incompressible flow. Kieffer (Ref. 20) obtained exact solutions for three cases of conductivity variation, namely a linear variation, a parabolic variation, and a step function variation. These solutions appear to be the only closed form solutions in the literature for variable conductivity channel flow.

In the present investigation, two techniques of analysis of variable conductivity channel flows are presented. Both of these methods are capable of handling an arbitrary spatial variation of conductivity in the z-direction. The two methods employed are the use of Fredholm integral equation theory and the B. G. Galerkin method. The analysis is restricted to the fully developed flow region.

The Application of Fredholm Integral Equation Theory to Variable Conductivity MHD Channel Flows

The equation of motion for fully developed flow in the absence of Hall current may be written from Eq. (5) as

$$0 = - \frac{dp}{dx} + \mu \frac{d^2u}{dz^2} + \sigma B_z (E_y - uB_z) \tag{97}$$

The origin z = 0 as shown in Fig. 1a is located at the centerline of the channel. For the present analysis it is more convenient to locate the origin at the lower surface. Also, non dimensionalizing the velocity in terms of the pressure gradient is convenient. Thus the following dimensionless quantities are defined.

$$\alpha_F = - \frac{u}{\frac{(2h)^2}{\mu} \frac{dp}{dx}}$$

$$\Gamma = \frac{\sigma}{\sigma_o} \qquad Ha^{*2} = \frac{(2h)^2 \sigma_o B_z^2}{\mu}$$

$$\Phi_y^* = - \frac{\sigma_o B_z E_y}{\frac{dp}{dx}} \qquad \eta^* = \frac{z}{2h} \tag{98}$$

where σ_o is a constant reference value of conductivity. The notation α_F indicates the velocity profile obtained by using the Fredholm integral equation theory. The dimensionless form of Eq. (97) becomes

$$\frac{d^2\alpha_F}{d\eta^{*2}} - Ha^{*2}\Gamma(\eta^*)\alpha_F + \Phi_y^*\Gamma(\eta^*) + 1 = 0 \tag{99}$$

Eq. (99) can be converted to an integral equation by integrating the equation twice, subject to the boundary conditions $\alpha_F(\eta^* = 0) = 0$ and $\alpha_F(\eta^* = 1) = 0$. The resulting integral equation may be written

$$\alpha_F(\eta^*) = f(\eta^*) + Ha^{*2} \int_0^1 K(\eta^*, t)\alpha^*(t)dt \tag{100}$$

where

$$f(\eta^*) = \int_0^{\eta^*} (t - \eta^*)[\Phi_y^*\Gamma(t) + 1]dt + \eta^* \int_0^1 (1 - t)[\Phi_y^*\Gamma(t) + 1]dt \tag{101}$$

$$K(\eta^*, t) = t(\eta^* - 1)\Gamma(t) \qquad 0 \le t \le \eta^*$$

$$K(\eta^*, t) = \eta^*(t - 1)\Gamma(t) \qquad \eta^* \le t \le 1 \tag{102}$$

Eq. (100) is a Fredholm integral equation with kernel $K(\eta^*,t)$ defined by Eq. (102). To arrive at the standard form of the Fredholm integral equation, it is necessary to define the kernel differently in different regions of the interval as shown by Eq. (102). The kernel is continuous, however, over the entire interval.

The fact that the kernel vanishes at the end points of the interval t = 0 and t = 1 suggests a sine series expansion of the form

$$K(\eta^*,t) = \sum_{n=1}^{\infty} a_n(\eta^*)\sin(n\pi t)dt \tag{103}$$

The functions $a_n(\eta^*)$ may be evaluated using the orthogonality of the sine function with the result

$$a_n(\eta^*) = 2\int_0^1 K(\eta^*,t)\sin(n\pi t)dt \tag{104}$$

Substituting the definition of the kernel from Eq. (102) into Eq. (104) gives

$$a_n(\eta^*) = 2\left[\int_0^{\eta^*} t(\eta^* - 1)\Gamma(t)\sin(n\pi t)dt + \int_{\eta^*}^1 \eta^*(t - 1)\Gamma(t)\sin(n\pi t)dt\right] \tag{105}$$

For a degenerate kernel consisting of a finite number of terms, an exact solution to the Fredholm integral equations may be obtained. A degenerate kernel is defined as a kernel in which each term consists of a product of two functions, each function depending on only one of the variables in the kernel. $K(\eta^*,t)$ as given by Eq. (103) is seen to be degenerate, and if the Fourier series is truncated after a finite number of terms, an exact solution to the integral equation can be found. In the present analysis the series given by Eq. (103) is truncated after

M terms. This results in an integral equation which is an approximation to the original integral equation. However, an exact solution to the approximate integral equation can be obtained.

The solution details for the Fredholm integral equation are described in Lovitt (Ref. 21) and only the results will be presented here. With the kernel of Eq. (103) truncated after M terms, the solution to Eq. (100) is

$$\alpha_F(\eta^*) = f(\eta^*) + Ha^{*2} \sum_{n=1}^{M} C_n^* a_n(\eta^*) \tag{106}$$

The C_n^* coefficients are the solutions to the set of linear algebraic equations

$$C_n^* - Ha^{*2} \sum_{i=1}^{M} B_{in} C_i = I_n \qquad n = 1,2,\ldots M \tag{107}$$

$$I_n = \frac{1 + (-1)^{n+1}}{n^3\pi^3} + \frac{\Phi_y^*}{n^2\pi^2} \int_0^1 \Gamma(t)\sin(n\pi t)dt \tag{108}$$

$$B_{in} = -\frac{2}{n^2\pi^2} \int_0^1 \Gamma(t)\sin(i\pi t)\sin(n\pi t)dt \tag{109}$$

Prescribing a conductivity profile $\Gamma(t)$ permits evaluation of the terms I_n and B_{in}. It should be noted that $\Gamma(t)$ appears only within integrals in the above expressions and thus a conductivity profile in tabular form could also be handled.

Numerical results were obtained for three cases of conductivity profile, uniform, linear, and parabolic. The assumed conductivity variations for the three cases are

Case I $\qquad \Gamma(\eta^*) = 1$

Case II $\Gamma(\eta^*) = 2\eta^* \qquad 0 \leq \eta^* \leq 0.5$

$\Gamma(\eta^*) = 2(1 - \eta^*) \qquad 0.5 \leq \eta^* \leq 1.0$

Case III $\Gamma(\eta^*) = 4(\eta^* - \eta^{*2})$

In cases II and III, the reference conductivity σ_o has been taken as the centerline value. These profiles were chosen because exact solutions to the differential equation of motion can be obtained with which to compare the approximate results of the present analysis.

Velocity profiles for the three cases of conductivity variation are shown in Figs. 22 through 29. Each of these curves is based on a truncation of the kernel expansion given by Eq. (103) after three terms, i.e. M = 3. Shown also are the results from an exact solution of the differential equation. The agreement between the exact solution to the differential equation and the solution to the integral equation using a kernel series truncated after three terms is excellent.

To investigate the effect of the number of terms retained in the kernel expansion, M was varied from 3 to 20 with several intermediate values. In all cases, the discrepancy between the 3 and 20 term solutions never exceeded 3% and in most cases was less than 1%.

The application of the Fredholm integral equation theory to variable conductivity MHD channel flows appears to be a powerful technique for obtaining an accurate approximation to the fully developed velocity profile for an arbitrary spatial variation of conductivity. Since the conductivity profile $\Gamma(\eta^*)$ always appears in an integral, tabulated conductivity data could also be used, requiring only that the integrals be evaluated numerically.

The Application of the B. G. Galerkin Method to Variable Conductivity MHD Channel Flows

Another method suitable for analyzing variable conductivity channel flows is the B. G. Galerkin method. The B. G. Galerkin method is discussed extensively in (Ref. 22) and only the essentials of the method as it applies to the present problem will be discussed here. It is convenient to non dimensionalize Eq. (97) in a manner slightly different from that used in the application of the Fredholm integral

equation theory. The following dimensionless quantities are defined.

$$\alpha_G = - \frac{u}{\frac{h^2}{\mu}\frac{dP}{dx}} \qquad \Gamma = \frac{\sigma}{\sigma_o}$$

$$Ha^2 = \frac{h^2 \sigma_o B_z^2}{\mu}$$

$$\Phi_y^* = - \frac{\sigma_o B_z E_y}{\frac{dP}{dx}} \qquad \eta = \frac{z}{h} \tag{111}$$

The origin z = 0 will once again be taken at the centerline of the channel. Since the B. G. Galerkin method is most amenable to two point boundary conditions, it is convenient to obtain the solution over the entire channel instead of the half channel. Thus the range of η will be $-1 \leq \eta \leq 1$. The dimensionless form of Eq. (97) becomes

$$\frac{d^2\alpha_G}{d\eta^2} - Ha^2\Gamma(\eta)\alpha_G = - [\Phi_y^*\Gamma(\eta) + 1] \tag{112}$$

with boundary conditions $\alpha_G(\eta = -1) = 0$ and $\alpha_G(\eta = 1) = 0$.

The essential idea of the B. G. Galerkin method is to construct an approximate solution to Eq. (112) as a sum of functions each of which satisfies the boundary conditions. Let $G_k(\eta)$ be a set of continuous functions which satisfy the boundary conditions

$$G_k(\eta = -1) = G_k(\eta = 1) = 0 \qquad k = 1,2,...S \tag{113}$$

An approximate solution to Eq. (112) can be constructed from a linear combination of the $G_k(\eta)$ functions as

$$\alpha_G = \sum_{n=0}^{S} b_n G_n(\eta) \tag{114}$$

From Eq. (113) it is clear that the boundary conditions of Eq. (112) are satisfied by the solution given by Eq. (114). It remains to determine the coefficients b_n such that the differential equation is satisfied. Substituting Eq. (114) into Eq. (112) gives

$$\sum_{n=0}^{S} b_n G_n'' - Ha^2 \Gamma \sum_{n=0}^{S} b_n G_n = -[\Phi_y^* \Gamma + 1] \tag{115}$$

Multiplying Eq. (115) by each function of the set and integrating over the range of η gives

$$\sum_{n=0}^{S} b_n \int_{-1}^{1} G_k G_n'' d\eta - Ha^2 \sum_{n=0}^{S} b_n \int_{-1}^{1} \Gamma G_k G_n d\eta$$

$$= -\Phi_y^* \int_{-1}^{1} \Gamma G_k d\eta - \int_{-1}^{1} G_k d\eta \qquad k=0,1,2,\ldots S \tag{116}$$

Once a set of approximating functions $G_n(\eta)$ is chosen, the definite integrals in Eq. (116) can be evaluated. Eq. (116) represents a set of S + 1 linear equations for the S + 1 unknown coefficients b_n. With the b_n determined, the approximate solution to the differential equation is completed.

For the case of fully developed MHD channel flow, a set of approximating functions which satisfy the boundary conditions may be taken as

$$G_n = (1 - \eta^2)\eta^n \qquad n=0,1,2\ldots S \tag{117}$$

The approximate velocity profile for this set of functions becomes

$$\alpha_G = \sum_{n=0}^{S} b_n(1 - \eta^2)\eta^n \tag{118}$$

Substituting Eq. (117) into Eq. (116) and performing the integrations gives the following system of linear equations for the b_n's.

$$b_o\left(\frac{[1 - (-1)^{k+1}]}{(k+1)(k+3)} + \frac{Ha^2}{4} I(0,k)\right) +$$

$$b_1\left(\frac{[1 + (-1)^{k+1}]}{(k+2)(k+4)} + \frac{Ha^2}{4} I(1,k)\right) +$$

$$\sum_{n=2}^{S} b_n\left([1 + (-1)^{n+k}]\left(\frac{n(k+1) + k(n+1) - 1}{(n+k-1)(n+k+1)(n+k+3)} - \frac{Ha^2}{4} I(n,k)\right)\right)$$

$$= \frac{1}{2}\frac{[1 - (-1)^{k+1}]}{(k+1)(k+3)} - \frac{\Phi_y^*}{4} I(k) \qquad k=0,1,2...S \tag{119}$$

where the integrals I(n,k) and I(k) are given by

$$I(n,k) = \int_{-1}^{1} \Gamma(\eta)(\eta^2 - 1)^2 \eta^{n+k} d\eta$$

$$I(k) = \int_{-1}^{1} \Gamma(\eta)(\eta^2 - 1)\eta^k d\eta \tag{120}$$

For any given $\Gamma(\eta)$ conductivity profile the integrals of Eqs. (120) can be evaluated either analytically or numerically and the linear set of equations given by Eq. (119) solved for the unknown constants b_n.

Velocity profiles for Cases I and III were also obtained by the B. G. Galerkin method using a set of 20 approximating functions as defined by Eq. (117) with S = 19. The agreement between this approximate solution and the exact solution to the differential equation was excellent. For Case I, the maximum difference between the exact and approximate solutions was 0.003% whereas for Case II, the maximum difference was less than 1%.

In addition another non uniform conductivity profile was investigated by the B. G. Galerkin method. Because of the strong dependence of conductivity on temperature, in the vicinity of a highly cooled wall the conductivity may drop to essentially zero. A profile which exhibits a zero conductivity layer on each wall is given by the expression

$$\text{Case IV} \qquad \begin{aligned} \Gamma(\eta) &= 0 \qquad -1 \leq \eta \leq \xi \\ \Gamma(\eta) &= 1 \qquad -\xi \leq \eta \leq \xi \\ \Gamma(\eta) &= 0 \qquad \xi \leq \eta \leq 1 \end{aligned} \tag{121}$$

The profile given by Eq. (121) is discontinuous with a central portion of uniform conductivity of thickness 2ξ and zero conductivity layers of thickness ξ on each B wall.

Numerical results were obtained for Case IV for $\xi = 0.5$ which corresponds to a zero conductivity layer of thickness one quarter of the channel height. The resulting velocity profiles are shown in Figs. 30 and 31 for short circuit and open circuit conditions and for Hartmann numbers Ha = 6 and 10. Shown also for comparison are the profiles corresponding to uniform conductivity.

The profiles shown in Fig. 30 are for the short circuit case, i.e. $E_y = 0 = \Phi_y^*$. A large velocity overshoot occurs in which the maximum velocity is not on the centerline of the channel but occurs near the wall. The profiles shown in Fig. 31 are for the open circuit condition. The velocity overshoot does not occur for this loading condition, but the profiles are qualitatively quite different from the uniform conductivity profiles. In particular the shear stress at the wall is smaller for the non uniform conductivity case. Also the width of the central core of essentially uniform velocity is decreased due to the non uniform conductivity.

It should be noted that the velocities in Figs. 30 and 31 are normalized in terms of the pressure gradient instead of the mean velocity. This means that for a given value of Ha, the curves for uniform and non uniform conductivity correspond to different values of the mean velocity but the same value of the pressure gradient. The areas under the curves, which would give the mean velocity, are therefore different at the same value of Ha. A relation between the mean velocity and the pressure gradient is derived in the next section.

Operational Characteristics of the Channel

In analyzing variable conductivity channel flows, it is convenient from a mathematical viewpoint to non dimensionalize the velocity in terms of the pressure gradient instead of the mean velocity. This results in a loading parameter Φ_y^* defined by Eqs. (98) and (111) in terms of the pressure gradient. For uniform conductivity, the loading parameter is normally defined in terms of the mean velocity as $\Phi_y = E_y/\bar{U}B_z$. It is desirable to obtain a relation between Φ_y^* and Φ_y.

The mean velocity is defined as

$$\bar{U} = \frac{1}{2h}\int_{-h}^{h} u\,dz \tag{122}$$

which may be rewritten in terms of dimensionless quantities as

$$\bar{U} = -\frac{h^2}{2\mu}\frac{dP}{dx}\int_{-1}^{1} \alpha\,d\eta \tag{123}$$

Eq. (123) relates the mean velocity to the pressure gradient in terms of the integrated velocity profile, the velocity being non dimensionalized in terms of the pressure gradient. For specified values of E_y and B_z, the relation between Φ_y and Φ_y^* becomes

$$\Phi_y^* = \frac{Ha^2}{2}\Phi_y\int_{-1}^{1} \alpha\,d\eta \tag{124}$$

where Ha^2 is the Hartmann number defined by Eqs. (111).

The other physical quantities of interest are the open circuit values of Φ_y and Φ_y^*. For uniform conductivity, the open circuit value of Φ_y is 1 but will be different from 1 for non uniform conductivity. The open circuit condition can be established by considering the total current flowing in the y direction. The total y component of current per unit length of the channel in the x direction is

$$I_y = \int_{-h}^{h} J_y dz = h \int_{-1}^{1} \sigma(E_y - uB_z)d\eta \tag{125}$$

Writing Eq. (125) in terms of dimensionless quantities gives

$$I_y = - \frac{h}{B_z} \frac{dP}{dx} \int_{-1}^{1} \Gamma(\Phi_y^* - Ha^2\alpha)d\eta \tag{126}$$

The open circuit condition corresponds to $I_y = 0$. Solving for Φ_y^* with $I_y = 0$ gives

$$\Phi_y^*)_{oc} = \frac{Ha^2 \int_{-1}^{1} \Gamma\alpha d\eta}{\int_{-1}^{1} \Gamma d\eta} \tag{127}$$

A value of Φ_y^* must be assumed to obtain a solution for α by either the Fredholm integral equation method or the B. G. Galerkin method. Since the right side of Eq. (127) depends on the value of Φ_y^* assumed, the equation must be solved by trial and error for $\Phi_y^*)_{oc}$. That is, for a fixed value of Ha, the right side of Eq. (127) is evaluated for different assumed values of Φ_y^*. The particular value of Φ_y^* for which the right side of Eq. (127) equals Φ_y^* is the open circuit value $\Phi_y^*)_{oc}$. Combining Eqs. (126) and (127) gives

$$\Phi_y)_{oc} = 2 \frac{\int_{-1}^{1} \Gamma\alpha d\eta}{\int_{-1}^{1} \alpha d\eta \int_{-1}^{1} \Gamma d\eta} \tag{128}$$

It is clear from Eq. (128) that $\Phi_y)_{oc} = 1$ for $\Gamma = 1$, corresponding to uniform conductivity.

Values of $\Phi_y)_{oc}$ calculated from Eq. (128) are tabulated in Table 3 for several values of Ha for Case IV. The value of $\Phi_y)_{oc}$ is seen to decrease slightly with increasing Ha.

The relations contained in Eqs. (122) through (128) are valid for either the Fredholm integral equation theory or the B. G. Galerkin method of analyzing variable conductivity, fully developed, MHD channel flow.

IV
EXPERIMENTAL INVESTIGATION

4.1 EXPERIMENTAL FACILITY

There is very little experimental data available in the open literature for the entrance region of channels, even for non MHD flows. No experimental velocity profile data for MHD entrance region flows appear to be available. In order to obtain such data for determining the validity of the analytical results presented in previous sections, a new experimental MHD facility was designed and constructed as part of the present investigation. The design and fabrication of the facility was done by the Engineering Support Facility of ARO, Inc. The experiments were conducted by the Experimental Research Group, Technical Staff, OMD of ARO, Inc.

A schematic drawing of the flow loop is shown in Fig. 32. The loop is closed with a pump used for circulating the working fluid. The major components of the loop as shown in Fig. 32 consist of a test section, a downstream section joining the test section to the piping, flowmeters, a circulating pump, a pump bypass loop for flow control, a transition section from the piping to the plenum chamber, a plenum chamber, and appropriate valving for controlling the flow rate. The maximum capacity of the circulating pump is approximately 40 gpm which gives a maximum test section Reynolds number of 11,600. The channel and test section are designed for use with an electrolytic solution of potassium chloride (KCl) as the working fluid. The test section is made of plexiglass and the circulating piping is stainless steel. The system has venting ports and valves at several locations on the top side of the loop, particularly in the vicinity of abrupt cross sectional area changes, for removing entrapped gas from the system.

A cross sectional view of the test section in the x-z plane is shown in Fig. 33. The test section is rectangular and is constructed as a channel within a channel. The inner channel walls in the x-y plane, the so called B-walls since they are perpendicular to the magnetic field, are constructed with a sharp leading edge to provide a well defined inlet section with a reasonably flat initial velocity profile. The inner channel is provided with a total of 22 static pressure measuring stations one inch apart, the first static pressure station being located 2 inches from the inlet. At each pressure measuring station in the channel, the pressure

taps on opposite sides of the channel are interconnected with a common pressure line leading to the manometer.

The dimensions of the inside channel are 3/4 x 5 1/2 inches giving an aspect ratio of 7 1/3. This value of aspect ratio should be large enough to closely approximate a parallel plate geometry in the center portion of the channel. The two surfaces of the inner channel in the x-z plane are electrode surfaces. The electrodes are continuous platinum sheets 0.001 inch thick which are cemented to the channel walls. Electrical leads are attached to both electrode surfaces.

The pressure lines from the 22 static pressure measuring stations are individually separated from a common manifold by a needle valve. The pressure from any station can be communicated to the manifold by opening the appropriate valve, the remaining valves being closed. A pressure line from the manifold is communicated to one leg of a micro-manometer.

A pitot probe with traversing mechanism is installed for measuring velocity profiles. The tip of the probe is located at the last static pressure measuring station which is 23 inches from the entrance to the inner channel. The probe can be traversed across the channel in the z direction and can be positioned to an accuracy of 0.001 inch by means of a micrometer screw. The probe cannot be moved in the x-direction. By adjusting the flow rate and thereby the channel Reynolds number, the length of the entrance region can be varied. In this way the pitot tube can sense different portions of the entrance region flow by remaining at the same x-position.

The magnetic field is provided by an electromagnet with rectangular pole pieces. The pole pieces are 6 x 30 inches with several sets of different thickness available to vary the gap width. The maximum gap width obtainable is 2 inches. The magnet dimensions are such that the entire test section can be inserted in the air gap. The magnet is powered by D.C. electric welders. The maximum power rating of the magnet is 600 K.W. At maximum power, a field strength of 22,000 gauss can be produced in a 2 1/2 inch air gap. Magnetic field uniformity has been measured to indicate less than 5% non uniformity along the centerline of the magnet over the central 24 inches of pole piece length. The test section inlet is located 4 inches from the magnet so that the entire entrance region of the channel is in a magnetic field with less than 5% variation in the field strength uniformity.

A photograph of the test section, flow loop, and micromanometer is shown in Fig. 34. In the interest of clarity, the electromagnet is not shown.

4.2 INSTRUMENTATION

The principal measurements involved in the experiment are the fluid flow rate, the static pressure distribution in the channel, and the velocity profile across the 3/4 inch dimension of the inner channel in the z-direction, i.e. the velocity profile in a plane normal to the B-wall. The flow rate is measured by variable area flow meters, calibrated by the Instrumentation Branch of Engineering Support Facility of ARO, Inc. Two flow meters are used, one for low flow rates and the other for high flow rates. The pitot probe, located at the last static pressure station 23 inches from the channel inlet, is used to measure velocity profiles by communicating the probe pressure to one leg of a micromanometer and the channel wall static pressure to the other leg. In the vicinity of the channel wall, the velocity head to be measured is extremely small as will be demonstrated subsequently.

To maintain laminar flow in the channel, the Reynolds number must be kept sufficiently low. Using a liquid with the density of water as the working fluid, the relationship between the velocity head and the Reynolds number may be written as

$$H = \frac{\rho \bar{U}^2}{2} = 1.92 \times 10^{-8} (Re)^2 \text{ (inches of water)} \qquad (129)$$

The characteristic dimension used in the definition of the Reynolds number is the channel half height in the z-direction, h = 0.375 inches. Eq. (129) can be used to calculate the velocity head, i.e. difference between total and static pressure, to be measured. For example a value of Re = 5,000 gives H = 0.48 inch of water corresponding to the mean flow velocity in the channel. As the pitot probe approaches the channel wall, the velocity head decreases to zero at the wall. The minimum velocity measurable would be with the pitot probe touching the channel wall. The outside diameter of the pitot probe is 0.063 inch which means the closest position at which a velocity measurement can be made is 0.031 inch from the wall. For fully developed non MHD flow, the velocity head at this location in terms of the Reynolds number is

$$H_{min} = 1.11 \times 10^{-9} (Re)^2 \text{ (inches of water)} \qquad (130)$$

For Re = 5,000, H_{min} = 0.028 inch of water. Thus in the vicinity of the wall, extremely small pressure measurements are involved in determining the velocity head.

Initial efforts were made to measure the velocity head using a commercially available Hass micromanometer. This instrument is capable of measuring a pressure difference as small as 0.0001 inch of mercury. The Hass micromanometer is in principle a very sensitive U-tube manometer. Two glass cylinders containing the manometer fluid are interconnected through a tube. Applying a pressure differential to the free surfaces of the manometer fluid in each cylinder results in a deflection. The fluid level in each cylinder is determined by rods, sharpened to a needle point, actuated in the vertical direction by micrometer screws. When the needle points touch the liquid surface, a small dimple is formed on the surface which can be observed through a magnifying glass. With no pressure difference applied across the manometer, the micrometers are read for the rod positions at which the needle points touch the surfaces. When a pressure differential is applied, the liquid surfaces deflect and the deflections of the two surfaces are determined by the rod travel required for the needle points to touch the surfaces again.

Considerable difficulty was experienced in obtaining reproducible pressure measurements with the micromanometer. The difficulty was attributable to leaks in the manometer and connecting lines and to the extremely slow response time of the manometer. Generally four to five hours were required to obtain one data point due to the slow response of the manometer.

Several weeks time were devoted to attempting to solve the leak problem. After ascertaining that all valves and connections on the pressure lines were leak free, it was finally discovered that the tygon tubing was defective, being sufficiently porous to allow leaks to occur while waiting for the manometer to stabilize. Consequently, all tygon tubing was replaced by metal tubing.

Leaks were also detected at the "0" ring seals on the movable rods in the micromanometer. New "0" rings of smaller diameter were installed and the packing nuts were tightened as tight as possible and still permit movement of the rods. By retightening the packing nuts before each run, it was possible to obtain a limited number of pressure measurements.

Because of the severe problems experienced in using

the micromanometer system, an alternate method of pressure measurement was explored. A considerable effort was expended in attempting to use an electrokinetic pressure transducer. The theory of this device is discussed in (Ref. 23). The electrokinetic transducer has the advantage of an extremely fast response time. However, a severe drift problem was encountered in using the transducer which appeared insoluble without going into an extensive electronic circuitry development program. Consequently, no reproducible pressure measurements were obtained with the electrokinetic transducer. Because of its high sensitivity and fast response, however, the electrokinetic transducer shows some promise as a pressure sensor if the drift problem can be solved.

The use of a gas laser for measuring low velocities in liquids has received considerable attention in recent years. The laser velocimeter has virtually an instantaneous response to changes in flow velocity. Limitations of time and financial rescouces did not permit the exploration of the use of a gas laser in the present investigation. Because of the serious difficulties encountered with the micromanometer, however, it was concluded that the use of a micromanometer for measuring small velocities in liquids is not practical. The use of the gas laser should be considered in future experiments of the type described in this investigation.

4.3 EXPERIMENTAL RESULTS

During the course of the experimental investigation, it became apparent that velocity profiles could not be measured using the micromanometer because of the slow response and leak problem previously described. Consequently, the experimental effort was concentrated toward static pressure distribution measurements in the entrance region. A limited number of data points were obtained with no magnetic field using water as the working fluid. The experimental results are shown in Fig. 35.

A theoretical curve of entrance region pressure drop was calculated as a function of liquid flow rate from Eqs. (60) through (62) and is shown as the solid curve in Fig. 35. The agreement between the experimentally measured entrance region pressure drop and the theoretical curve is considered as satisfactory verification of the theoretical model employed in the present investigation.

V
SUMMARY

In this investigation an analysis of the influence of Hall current on flow development in the entrance region of a parallel plate MHD channel has been presented. Numerical results have been presented showing the influence of $\omega\tau$ on the entrance length, the entrance region boundary layer development, the entrance region pressure distribution, and the entrance region wall shear stress distribution. Constant electrical conductivity was assumed in this portion of the analysis. A new linearization scheme was developed for analyzing MHD entrance region flows which has features superior to a conventional boundary layer - core flow model of the entrance region. As an alternate method of analyzing the MHD entrance region flow, the von-Karman-Pohlhausen integral method was generalized to accommodate an assumed polynomial velocity profile of arbitrary degree. Closed form expressions for the velocity profile coefficients were obtained, and the range of values of the shape factor λ^* for which the integral method is valid was established as a function of the degree of the polynomial assumed.

In addition to the entrance region results, two methods of analyzing fully developed flows with arbitrary variation of conductivity were developed. These methods are the B. G. Galerkin method and the Fredholm integral equation method. Numerical results of calculated velocity profiles were presented for several conductivity profiles across the channel. Although limitations of time and financial resources did not allow these methods to be extended to the entrance region, it is felt that such an extension is possible.

A new MHD channel flow facility was designed and built for obtaining pressure distribution and velocity profile data in the entrance region of a parallel plate channel. The facility is designed to use potassium chloride (KCl) as the working fluid with a maximum magnetic field strength achievable of 22,000 gauss. Because of serious instrumentation problems encountered in measuring total velocity pressures, velocity profile data was not obtained. Only entrance region pressure distribution data was obtained.

This channel appears to be unique in that no other experimental facilities have been described in the open literature for obtaining MHD entrance region velocity profiles. The use of a gas laser velocimeter appears to be

promising, and a future experimental effort using a laser for measuring the velocity profiles would represent a significant contribution to a detailed understanding of MHD entrance region flows.

VI
REFERENCES

1. Pai, S. I. "A Critical Survey of Magnetofluiddynamics - Part II: Magnetohydrodynamic Channel Flows." O.A.R.U.-S.A.F. (ARL 63-175), May 1964.

2. Ring, L. E. "Optimization of MHD Crossed - Field Accelerators and Generators." Fifth Symposium on the Engineering Aspects of Magnetohydrodynamics, M.I.T.,1964.

3. Sparrow, E. M., Lin, S. H., Lundgren, T. S. "Flow Development in the Hydrodynamic Entrance Region of Tubes and Ducts." Phys. of Fluids 7:338, 1964.

4. Snyder, W. T. "Magnetohydrodynamic Flow in the Entrance Region of a Parallel-Plate Channel." AIAA J. 3:1833, 1965.

5. Shercliff, J. A. "Entry of Conducting and Non-Conducting Fluids in Pipes." Proc. Cambr. Phil. Soc. 52:573, 1956.

6. Roidt, M., Cess, R. D. "An Approximate Analysis of Laminar Magnetohydrodynamic Flow in the Entrance Region of a Flat Duct." Trans. ASME, Series E, 84:171, 1962.

7. Schlichting, H. "Laminare Kanaleinlaufstromung." ZAMP 14:368, 1934.

8. Shohet, J. L., Osterle, J. F., Young, F. J. "Velocity and Temperature Profiles for Laminar Magnetohydrodynamic Flow in the Entrance Region of a Plane Channel." Phys. of Fluids 5:545, 1962.

9. Hwang, C. L., Fan, L. T., "A Finite Difference Analysis of Laminar Magnetohydrodynamic Flow in the Entrance Region of a Flat Rectangular Duct." Appl. Sci. Res. Sect. B, 10:329, 1963.

10. Chekmarev, J. B. "The Influence of Anisotropy of Electrical Conductivity on the Development of Flow of a Viscous Fluid in the Initial Section of a Plane Channel." PMM 27: 1963.

11. Cowling, T. G. Magnetohydrodynamics. Interscience Publishers, Inc., New York, 1957.

12. Reisman, H., J. Aerosp. Sci. 29:158, 1962.

13. Yen, J. T. "Magnetoplasmadynamic Channel Flow and Energy Conversion with Hall Currents." Phys. of Fluids 7:723, 1964.

14. Moffatt, W. C. "Analysis of MHD Channel Entrance Flows Using the Momentum Integral Method." AIAA J. 2:1495, 1964.

15. Maciulaitis, A., Loeffler, A. L. "A Theoretical Investigation of MHD Channel Entrance Flows." AIAA J. 2:2100, 1964.

16. Tan, C. W. "Laminar MHD Channel Entrance Flows." AIAA J. 3:1369, 1965.

17. Dhanak, A. M. "Heat Transfer in Magnetohydrodynamic Flow in an Entrance Section." Trans. ASME, Series C, 87:231, 1965.

18. Hugelman, R. D., Haworth, D. R. "An MHD Boundary Layer Compatibility Condition." AIAA J. 3:1367, 1965.

19. Heywood, J. B., Moffatt, W. C. "Validity of Integral Methods in MHD Boundary Layer Analyses." AIAA J. 3:1565, 1965.

20. Kieffer, P. C. "Variable Conductivity Fully Developed MHD Channel Flow." M. S. Thesis, Air Force Institute of Technology, Wright-Patterson Air Force Base, Ohio, 1965.

21. Lovitt, W. V. Linear Integral Equations. Dover Publications, Inc., New York, 1950.

22. Kantorovich, L. V., Krylov, V. I. Approximate Methods of Higher Analysis. Interscience Publishers, Inc., New York, 1958.

23. Brugreen, D. "Electrokinetic Flow in Capillary Elements." ASD-TDR-63-243, 1963.

24. Goins, E. E., Jr. "The Influence of the Initial Velocity Profile on Magnetohydrodynamic Flow Development in the Entrance Region of a Parallel Plate Channel." M. S. Thesis, The University of Tennessee Space Institute, 1965.

25. Iannuzzi, F. A. "A Modified von-Karman - Pohlhausen Approximate Method Applied to Magnetohydrodynamic Channel." M. S. Thesis, The University of Tennessee Space Institute, 1966.

26. Young, J. D. "A Fredholm Integral Equation Solution for Variable Conductivity Magnetohydrodynamic Channel Flow." M. S. Thesis, The University of Tennessee Space Institute, 1965.

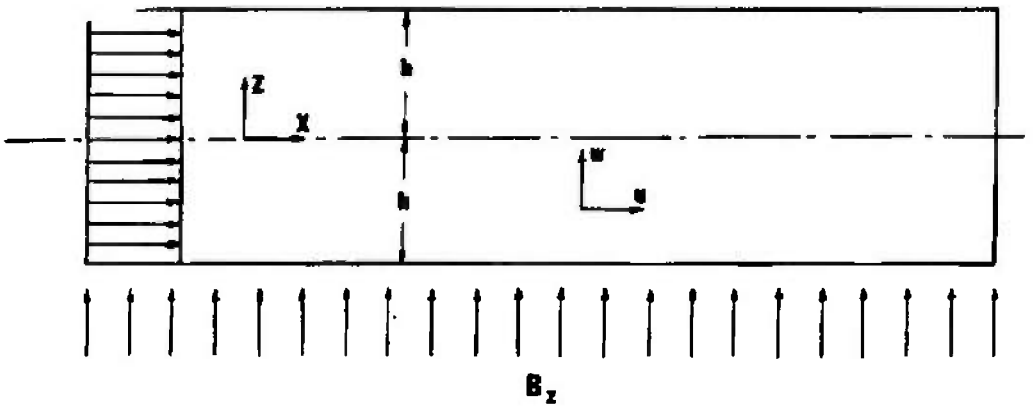

Fig. 1a MHD Flow Geometry

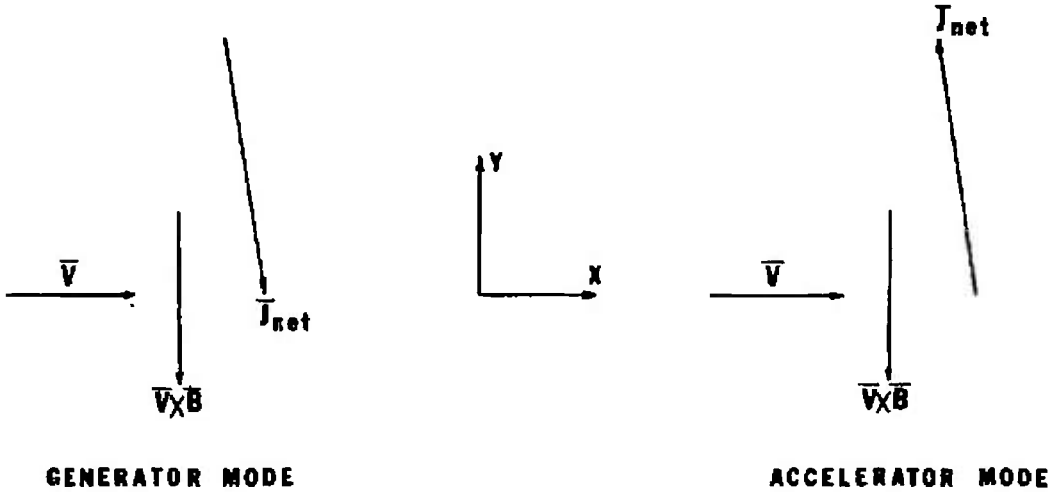

Fig. 1b Geometry for Generator and Accelerator Modes

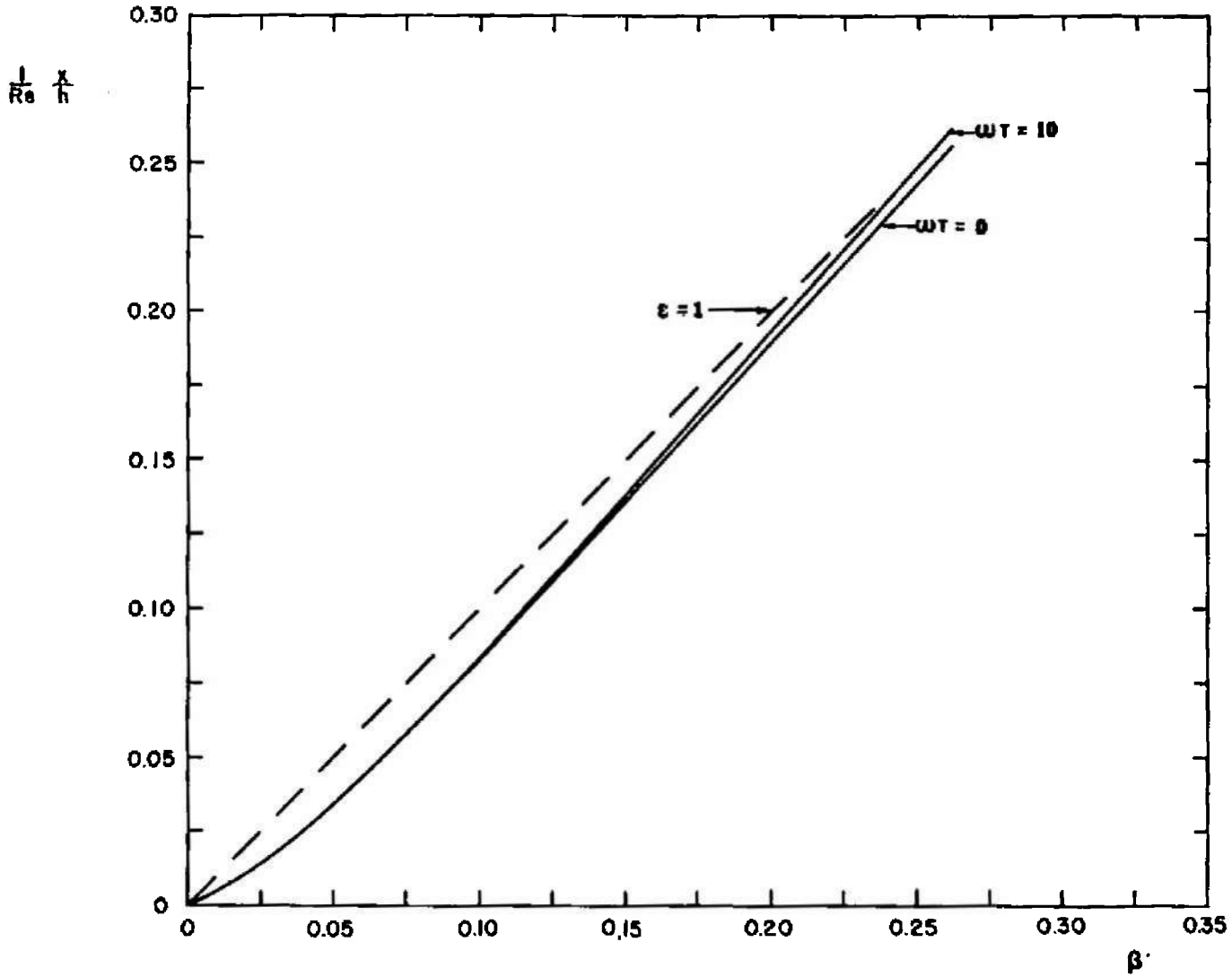

Fig. 2 Relationship between the Physical and Stretched Coordinate for Ha = 2

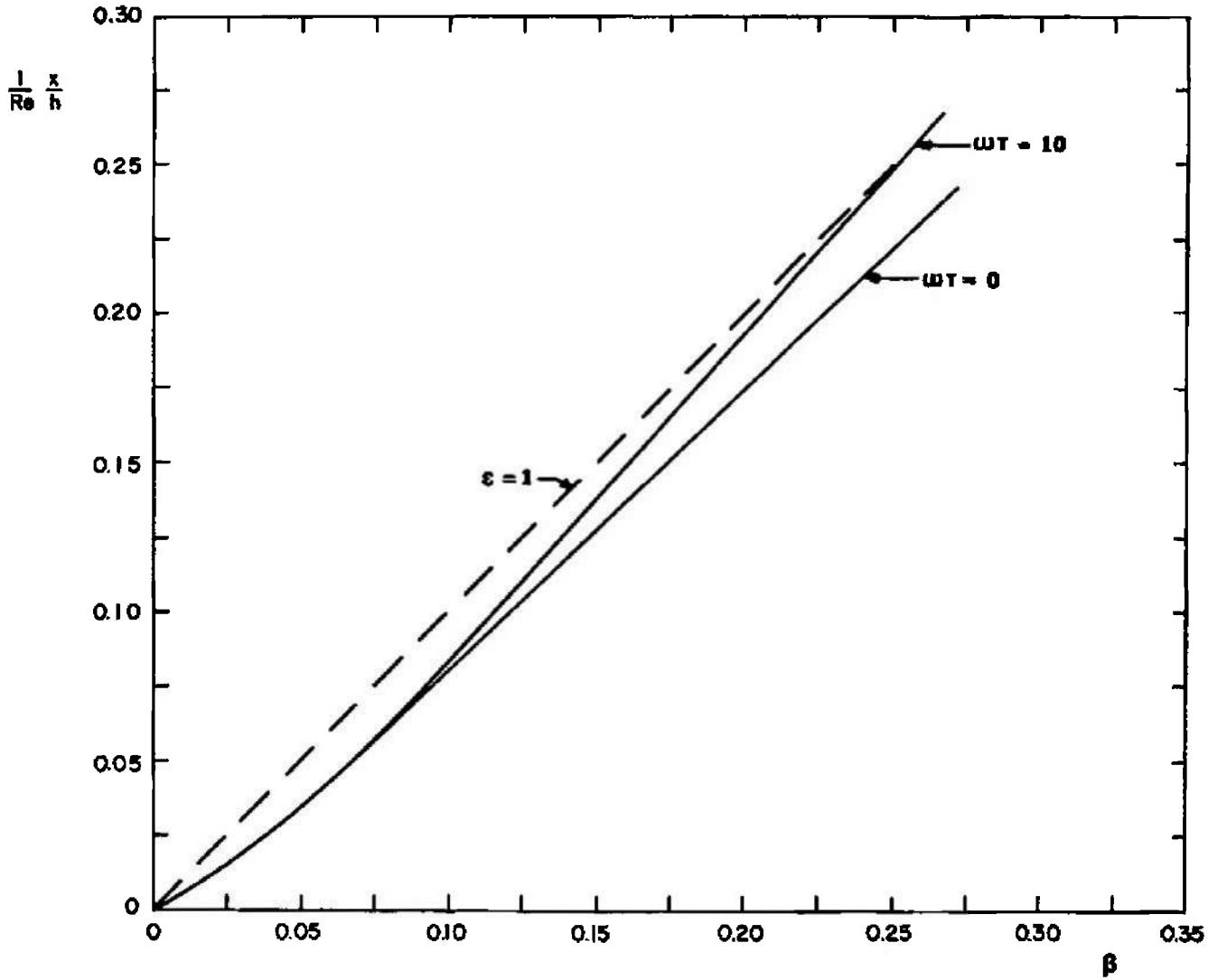

Fig. 3 Relationship between the Physical and Stretched Coordinate for Ha = 6

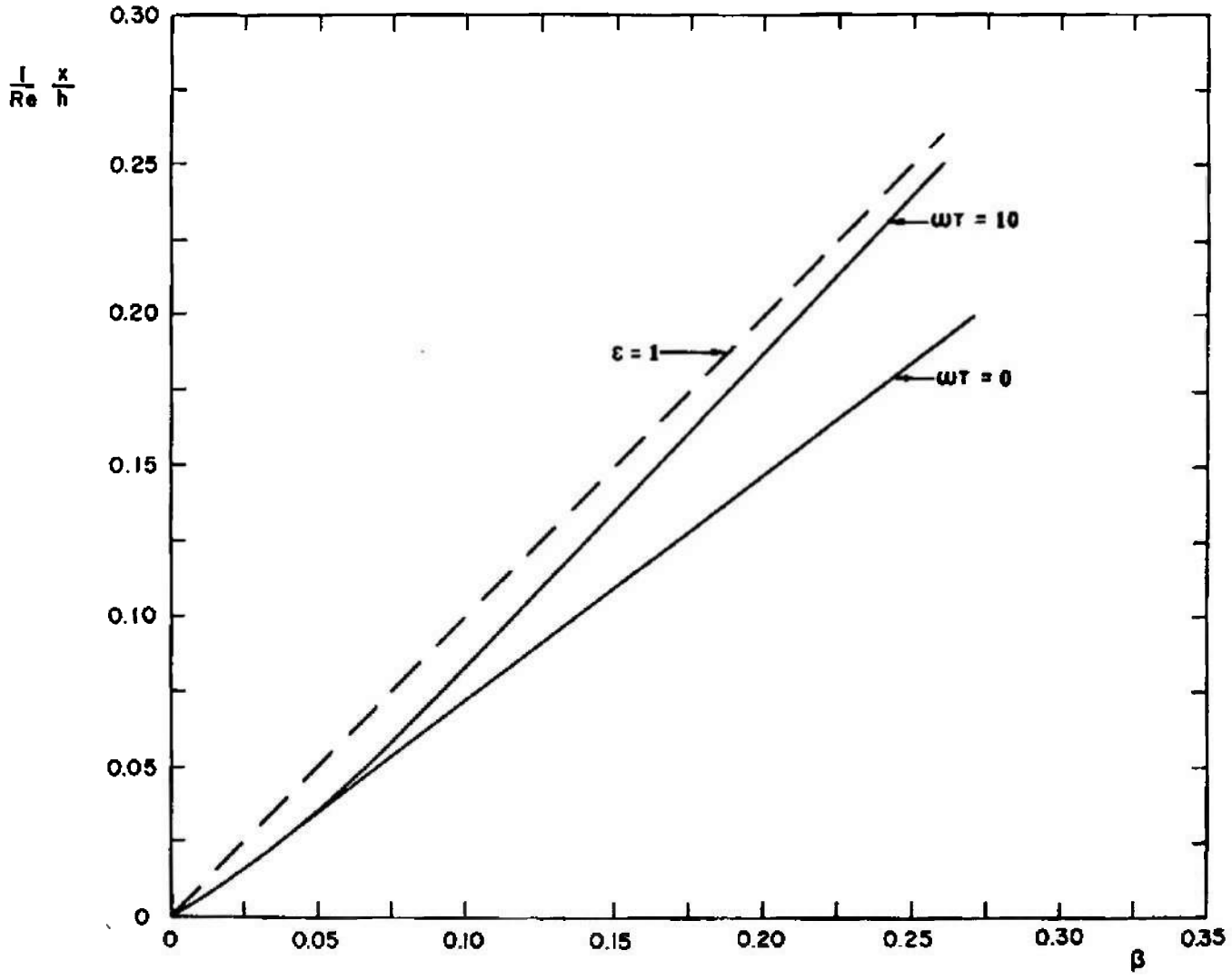

Fig. 4 Relationship between the Physical and Stretched Coordinate for Ha = 10

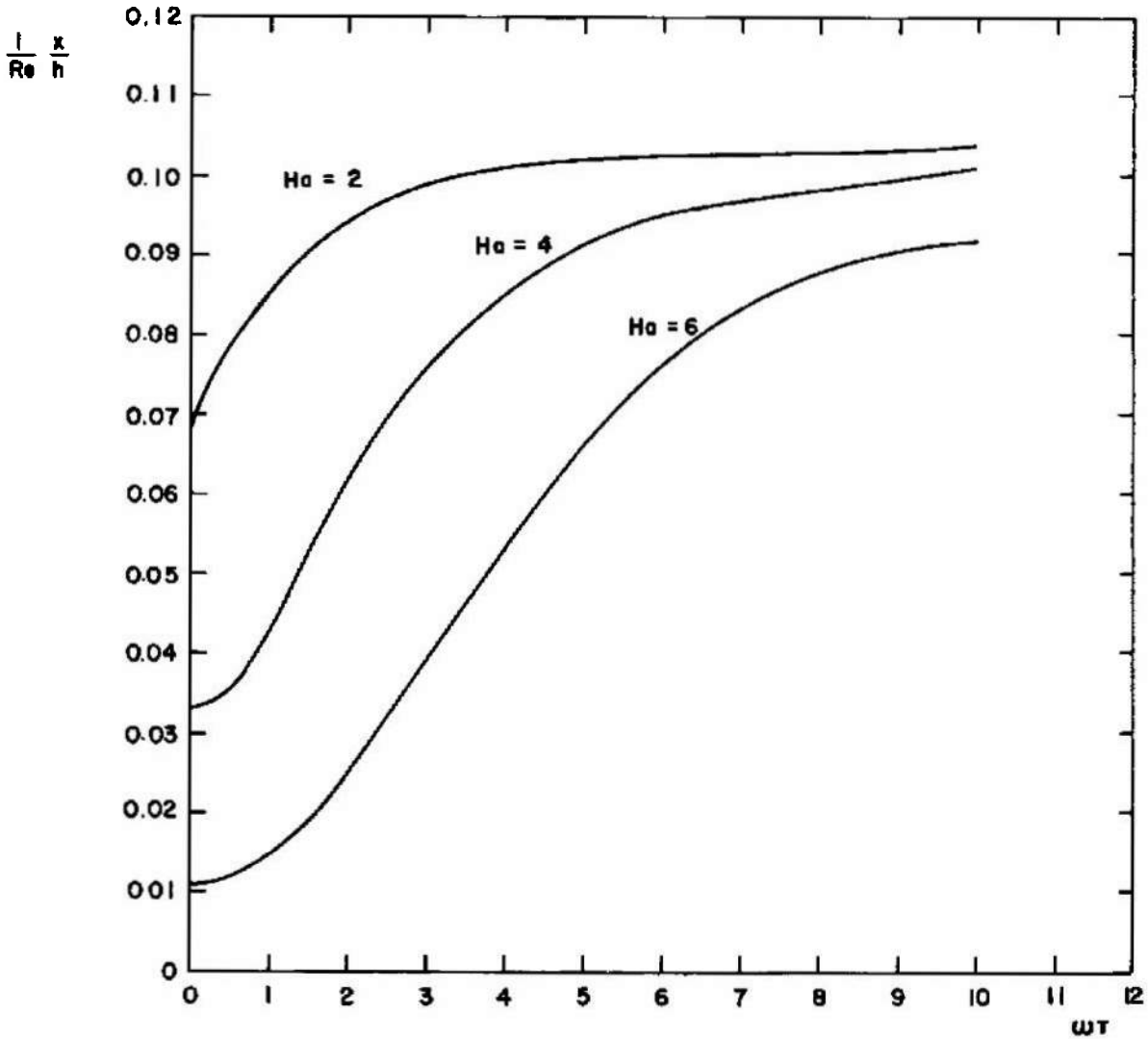

Fig. 5 Entrance Length for Ha = 2, 4, 6

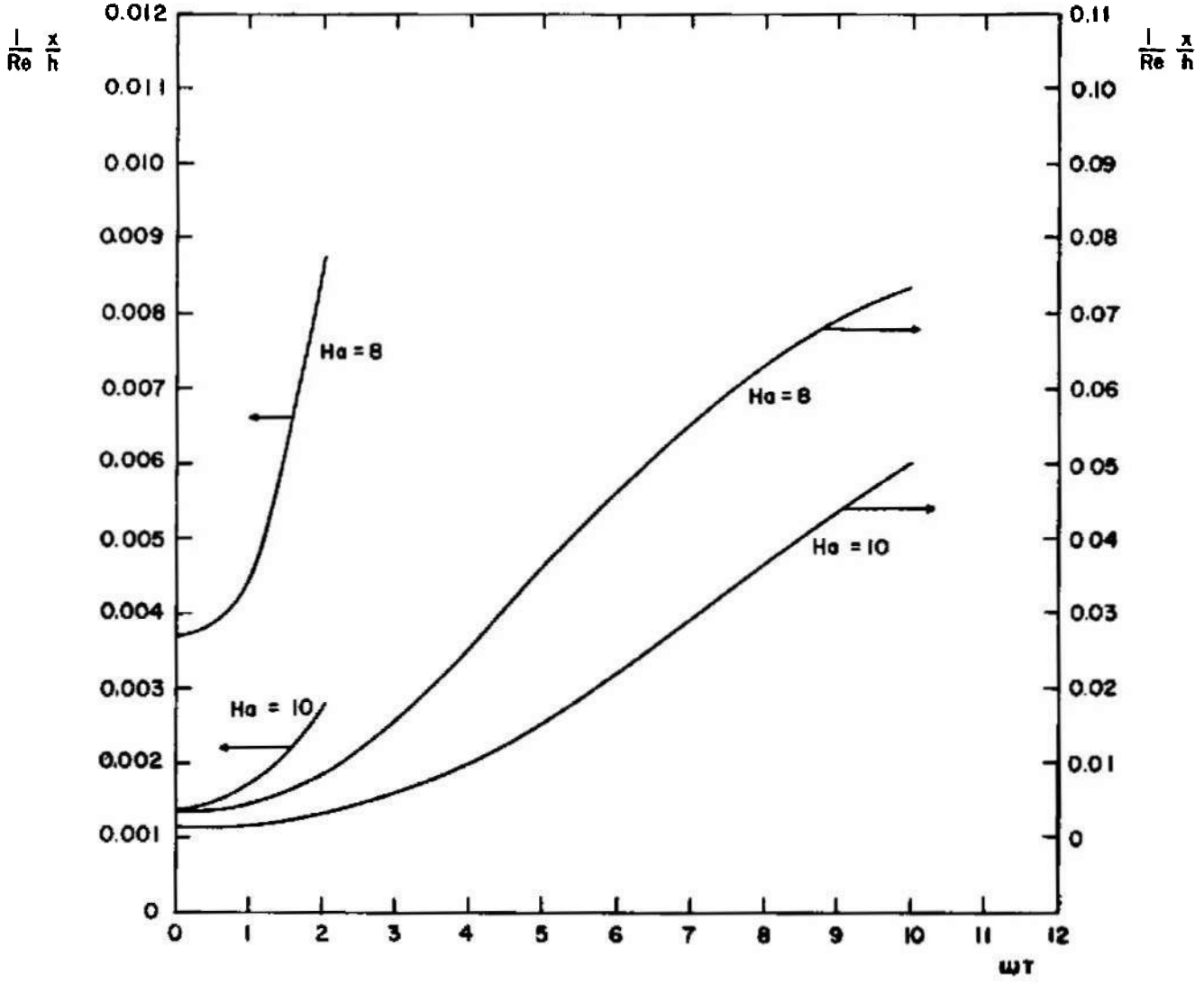

Fig. 6 Entrance Length for Ha = 8, 10

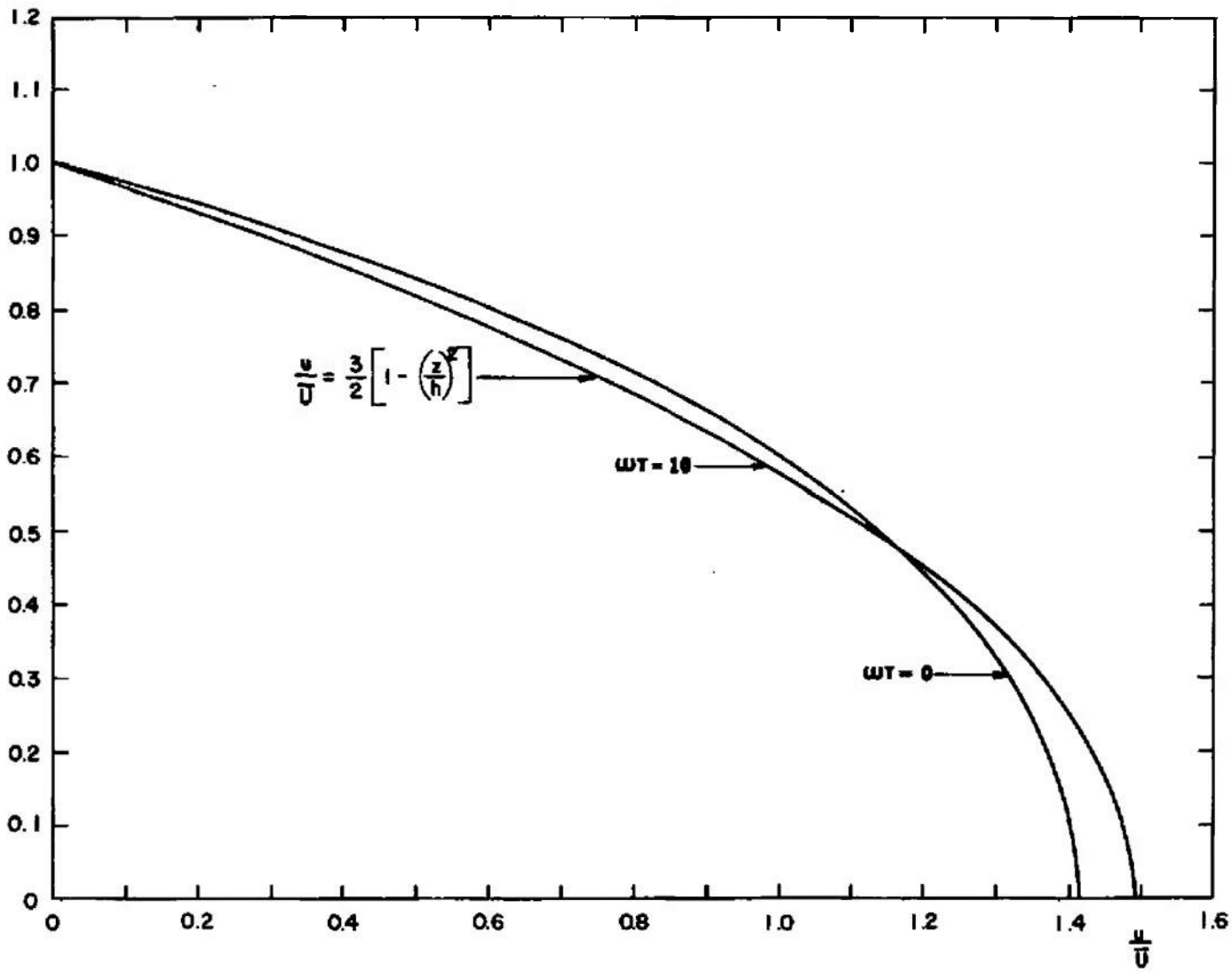

Fig. 7 Fully Developed Velocity Profiles for Ha = 2

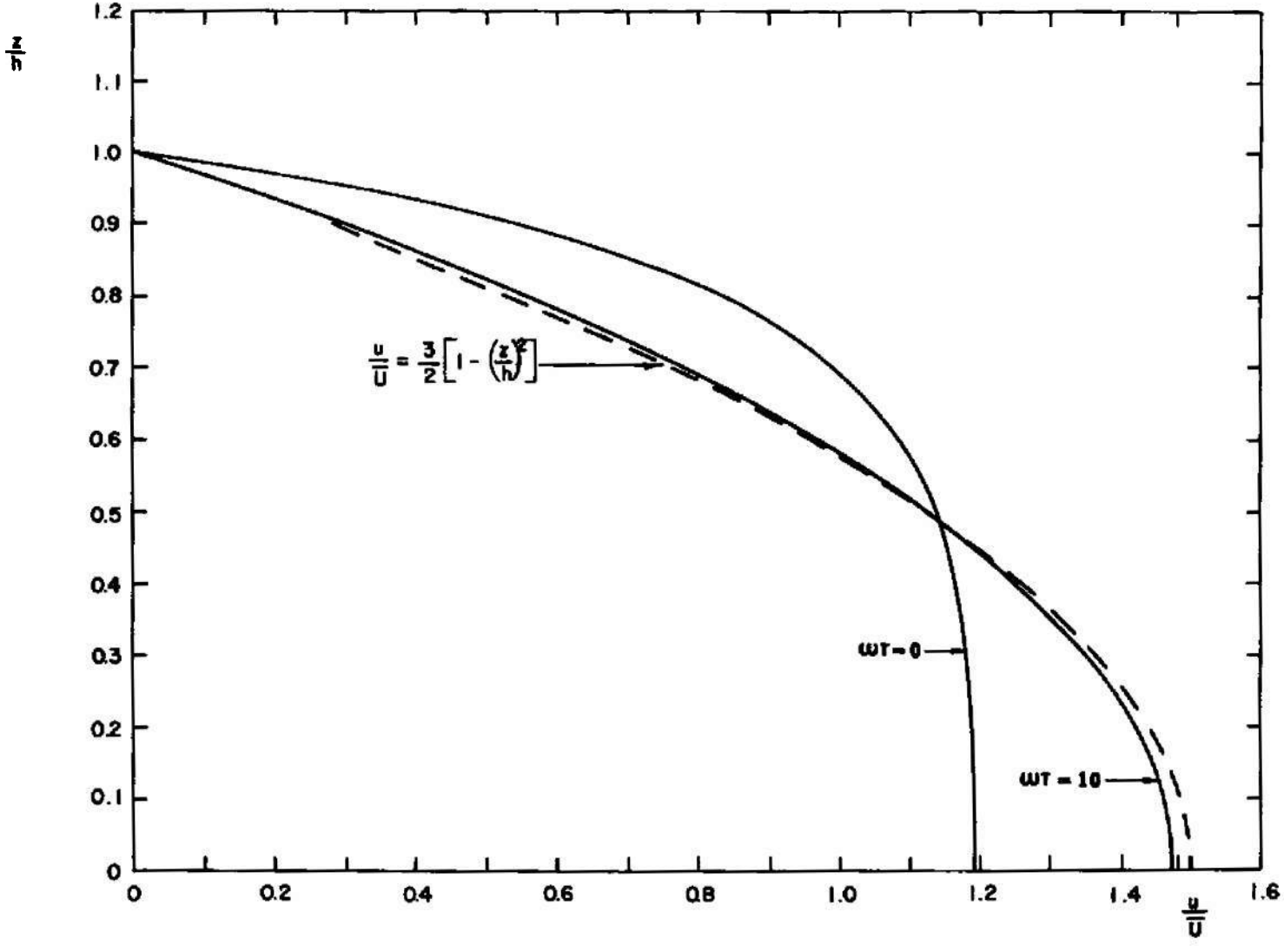

Fig. 8 Fully Developed Velocity Profiles for Ha = 6

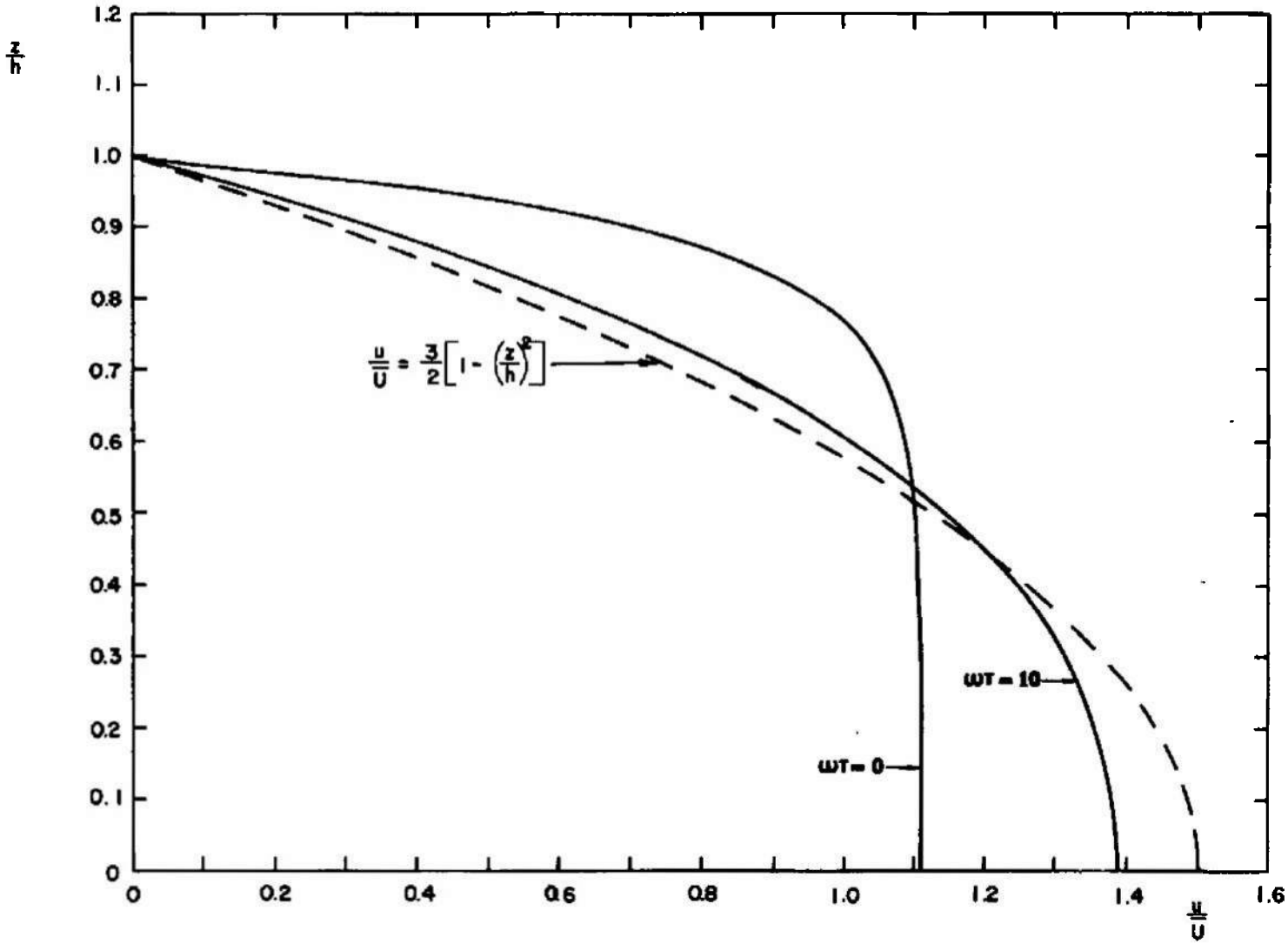

Fig. 9 Fully Developed Velocity Profiles for Ha = 10

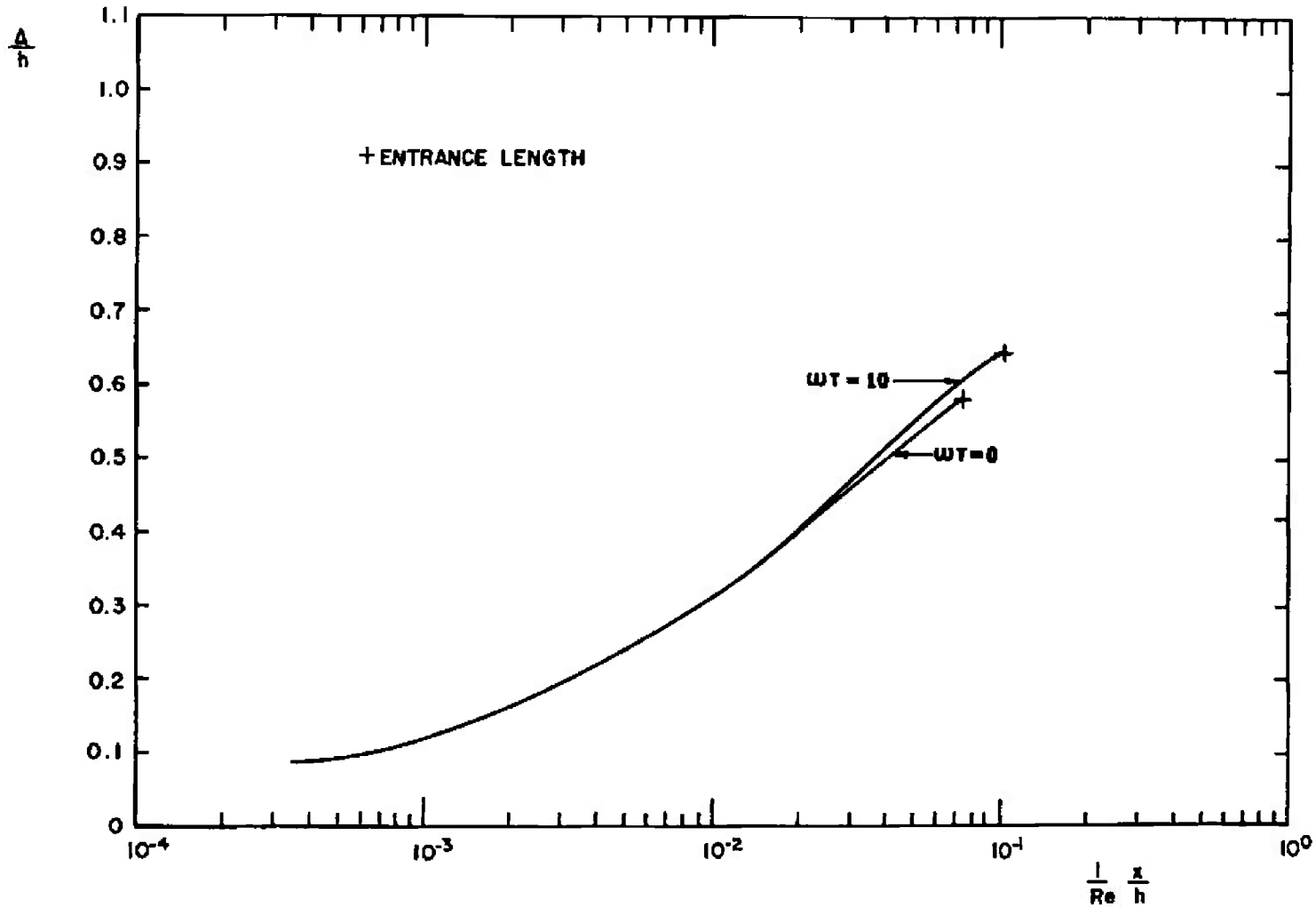

Fig. 10 Boundary Layer Development for Ha = 2

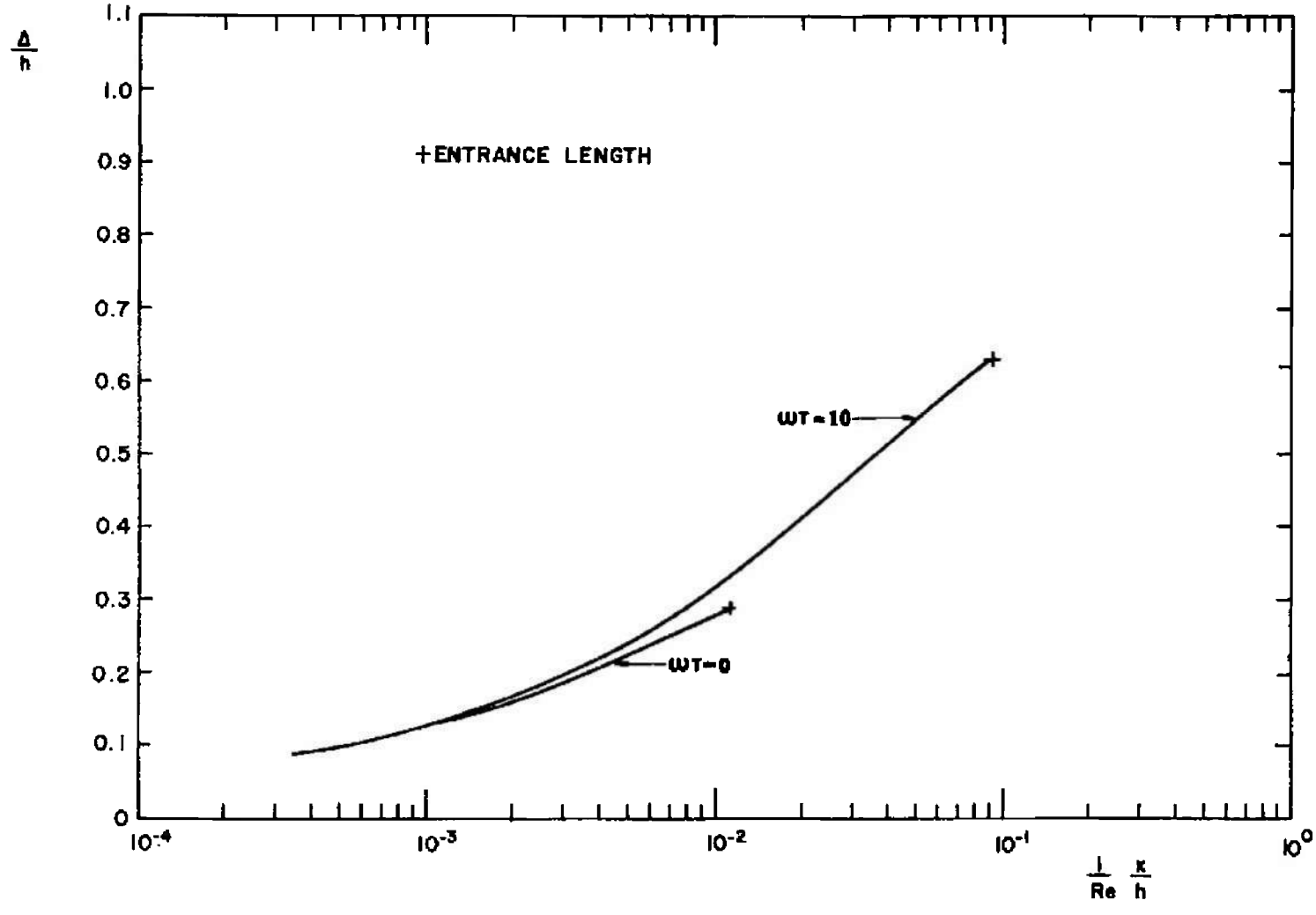

Fig. 11 Boundary Layer Development for Ha = 6

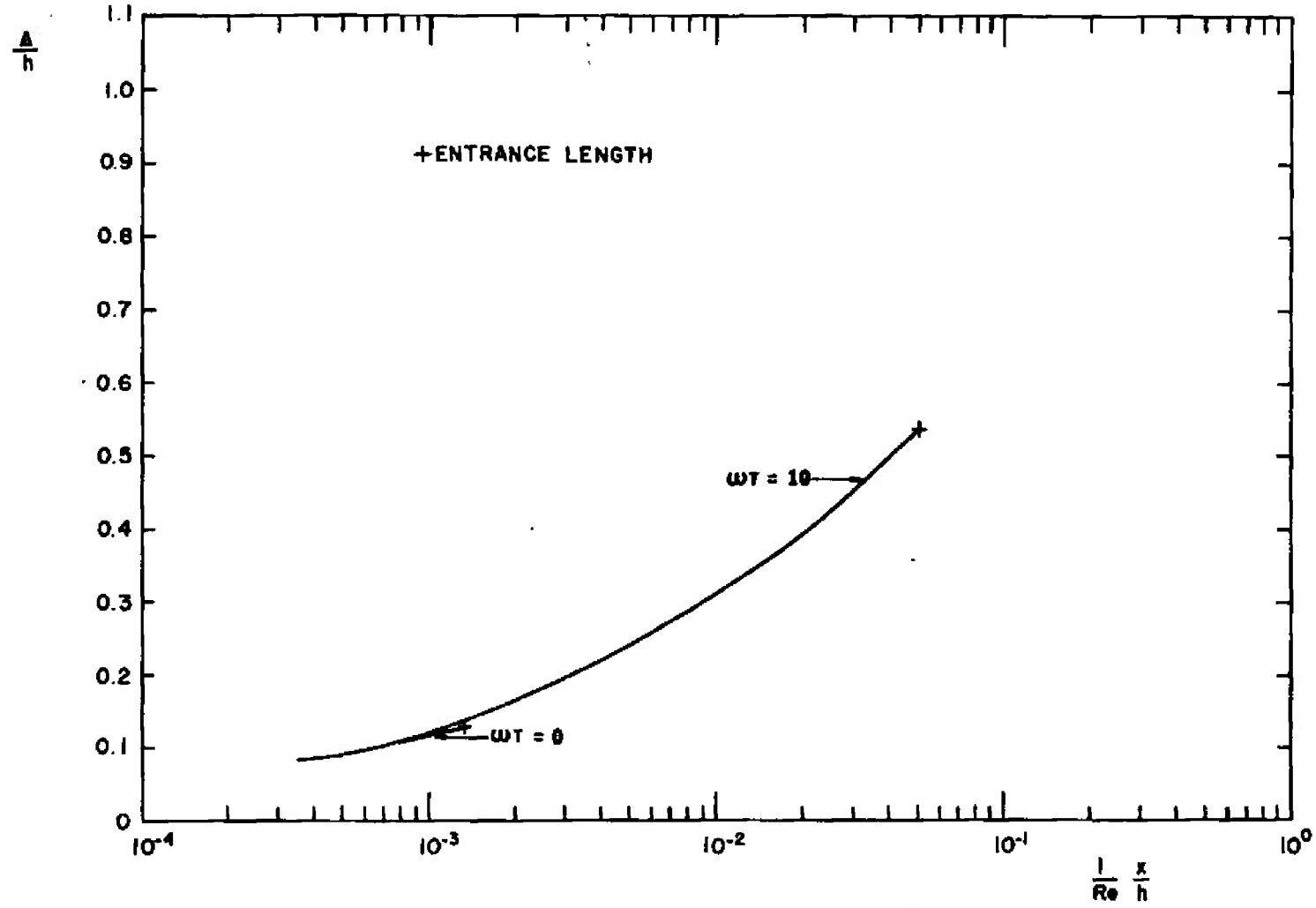

Fig. 12 Boundary Layer Development for Ha = 10

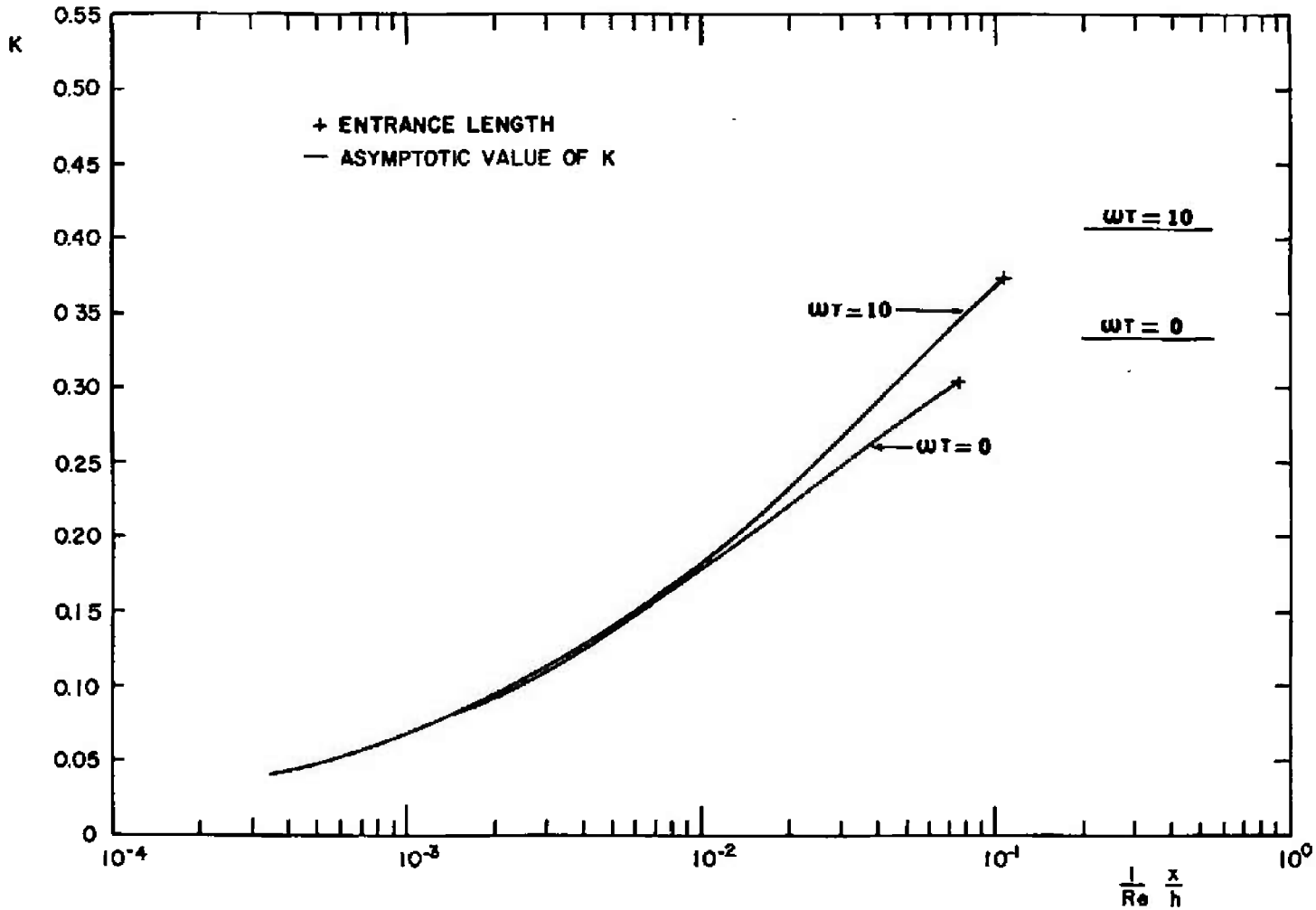

Fig. 13 Entrance Region Pressure Correction for Ha = 2

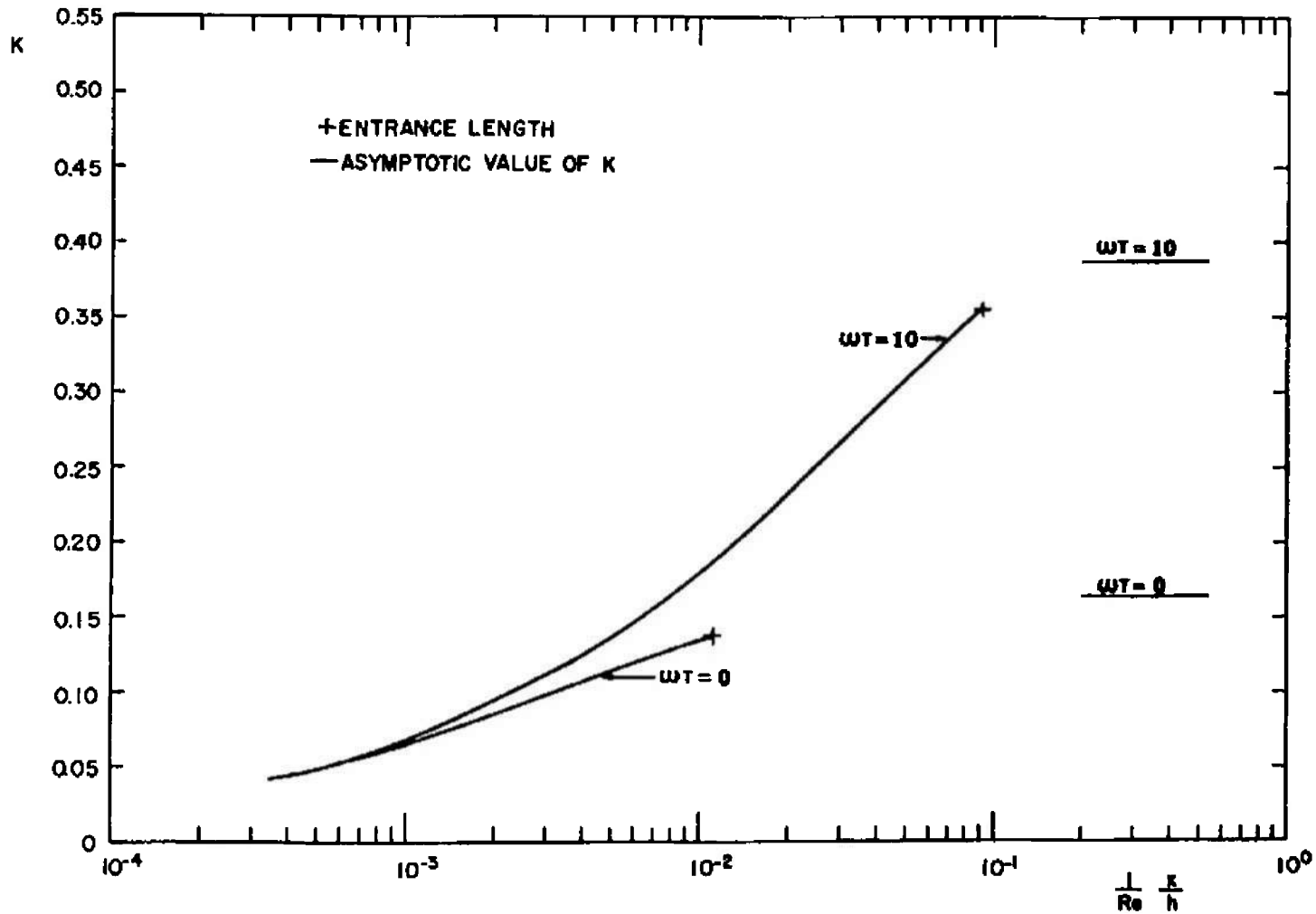

Fig. 14 Entrance Region Pressure Correction for Ha = 6

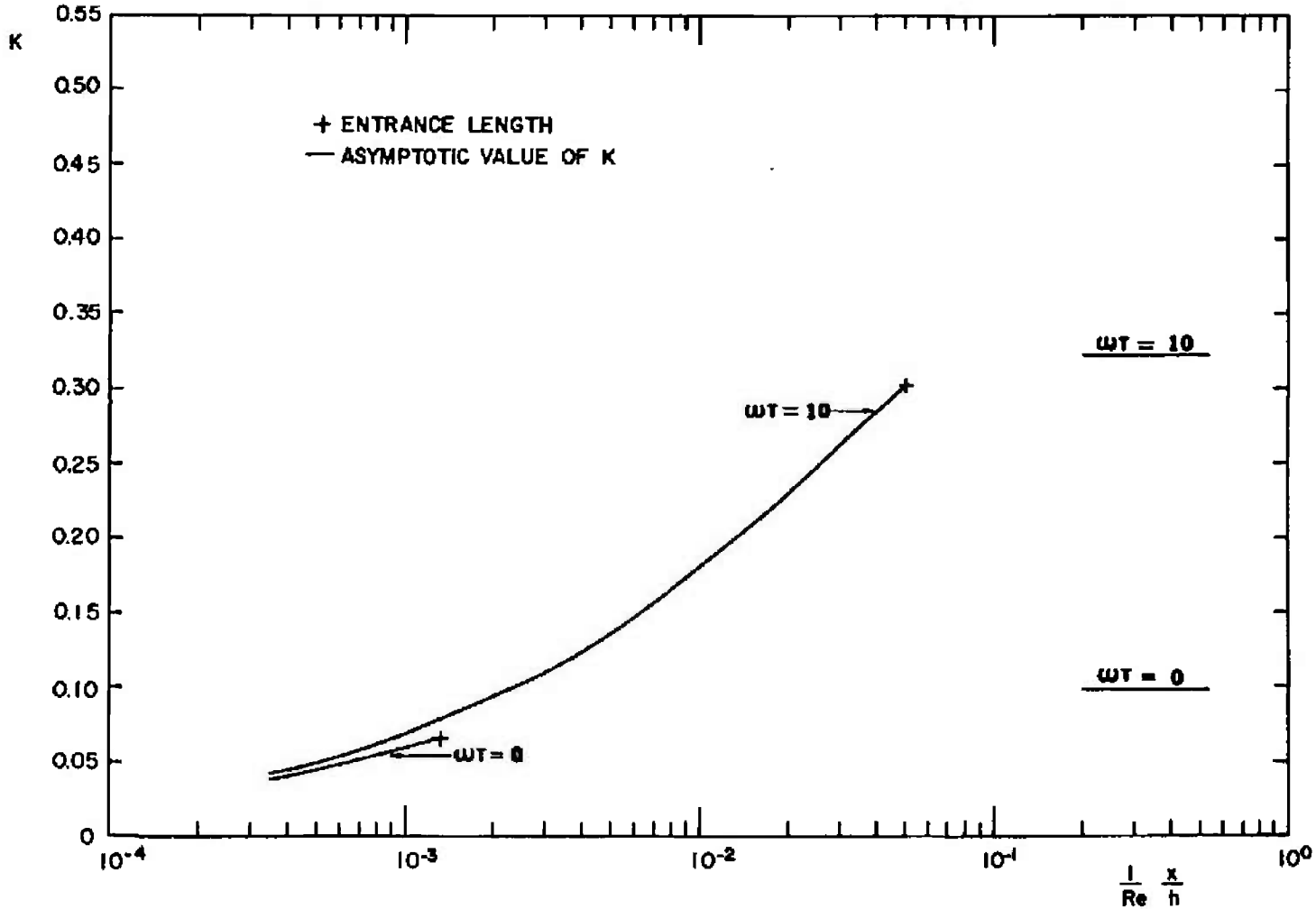

Fig. 15 Entrance Region Pressure Correction for Ha = 10

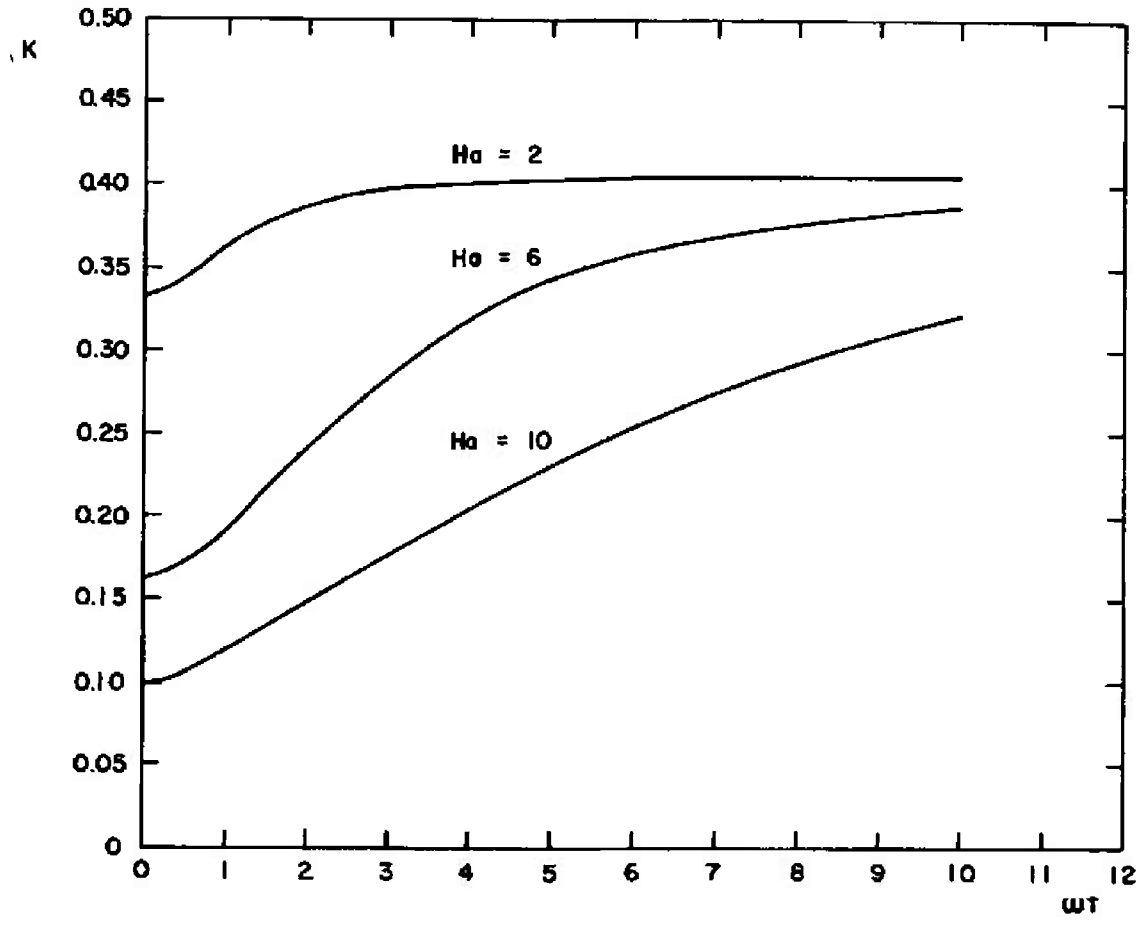

Fig. 16 Asymptotic Values of K

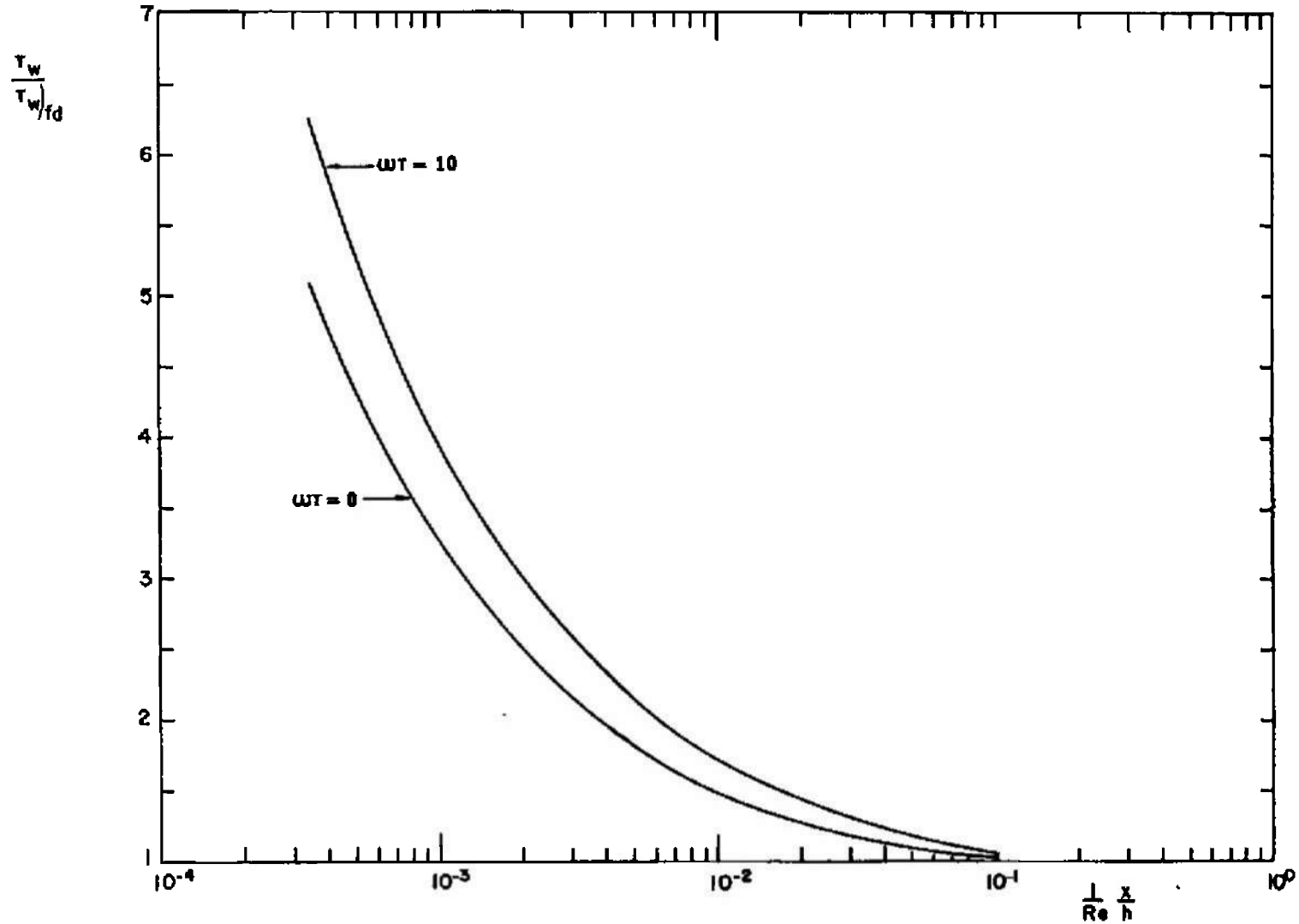

Fig. 17 Entrance Region Wall Shear Stress Distribution for Ha = 2

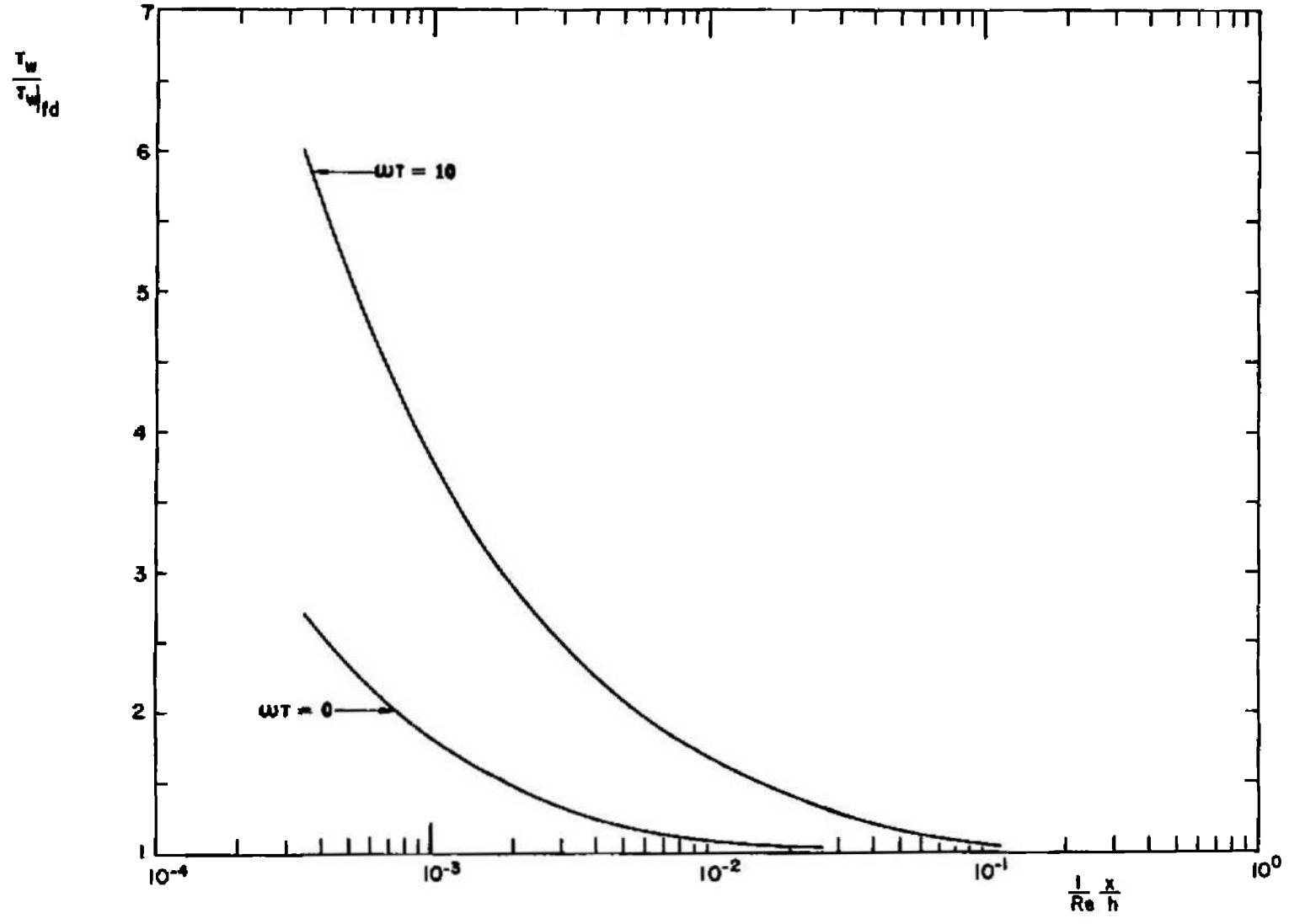

Fig. 18 Entrance Region Wall Shear Stress Distribution for Ha = 6

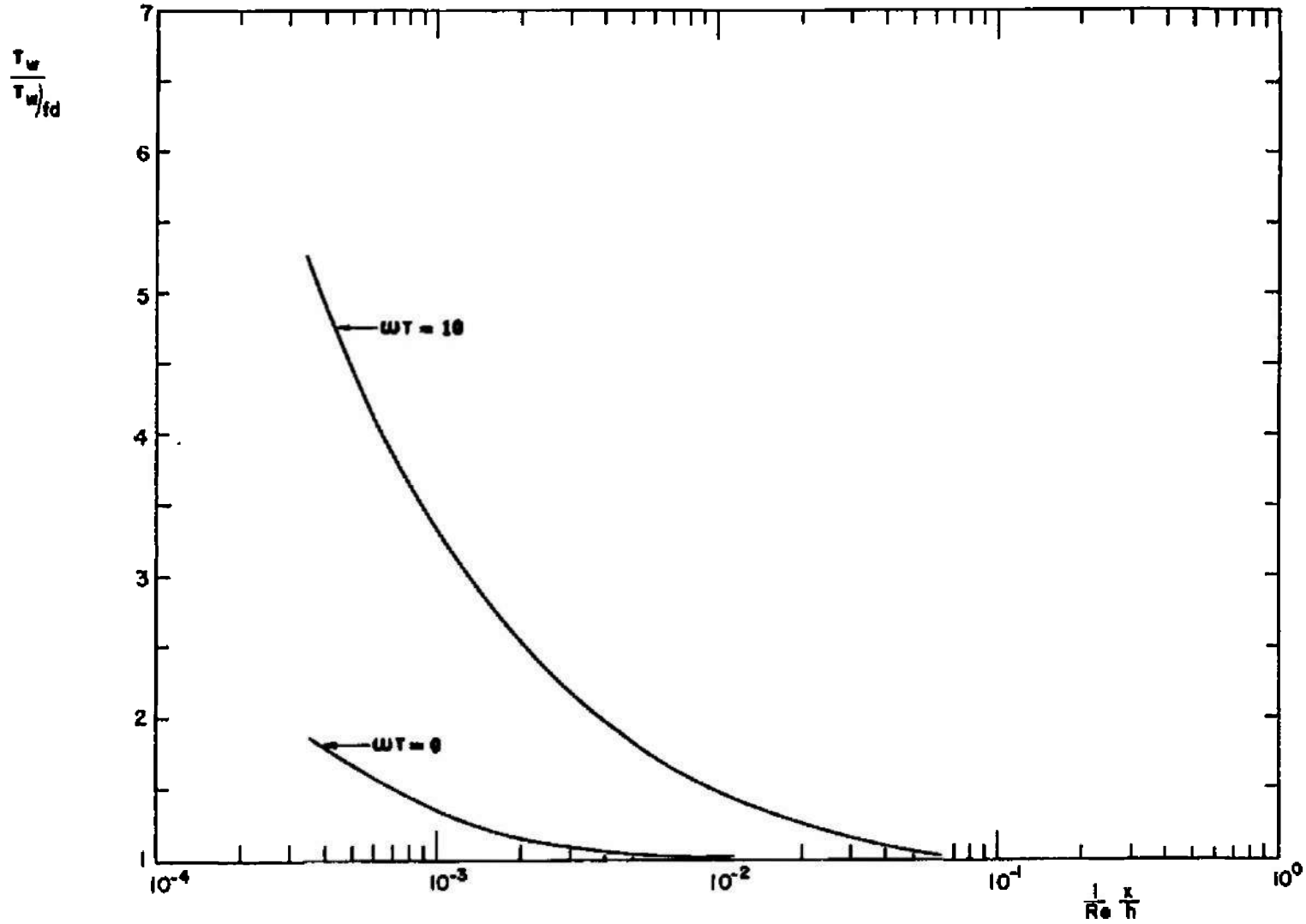

Fig. 19 Entrance Region Wall Shear Stress Distribution for Ha = 10

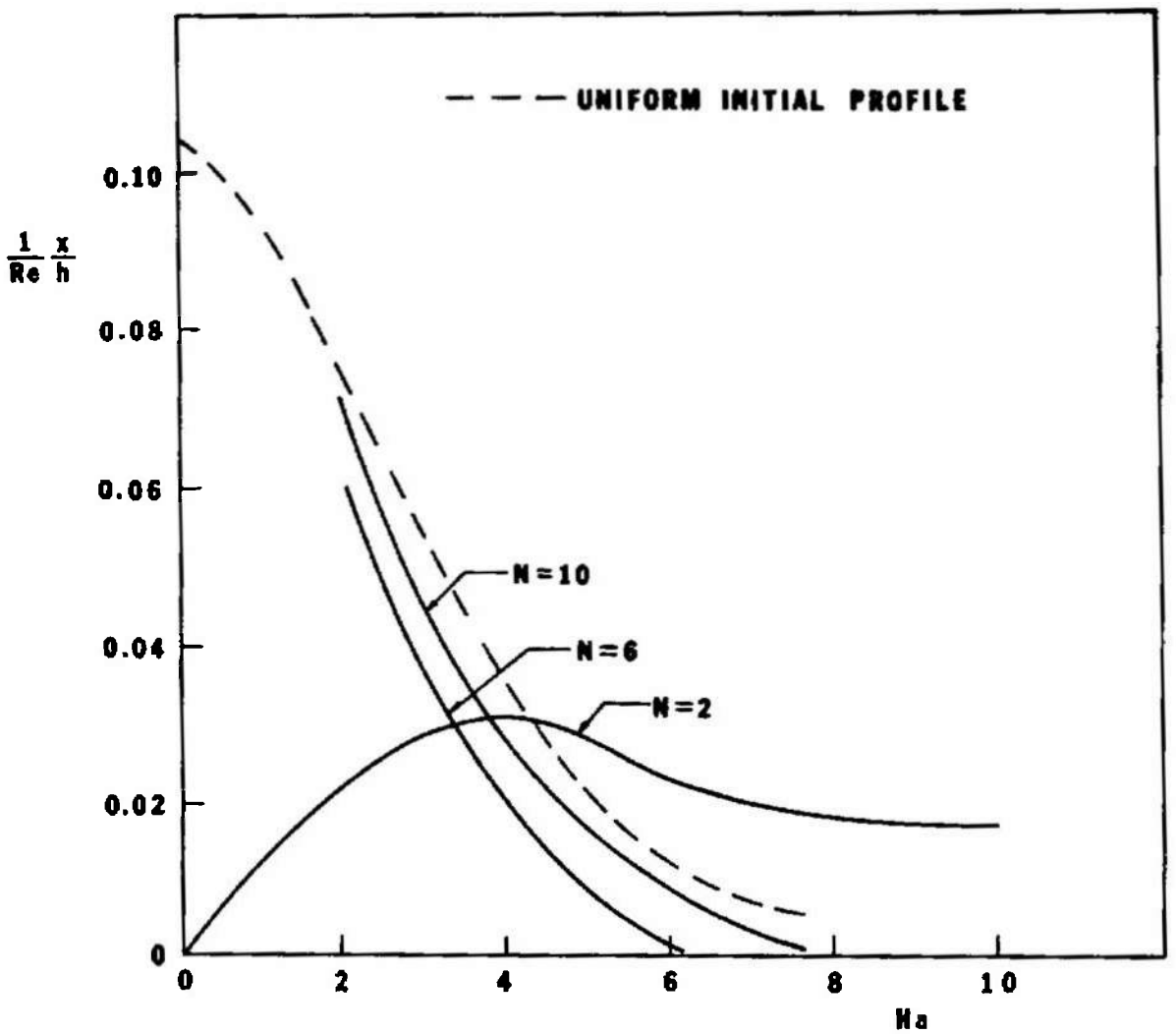

Fig. 20 Entrance Length for $\omega\tau = 0$ and N = 2, 6, 10

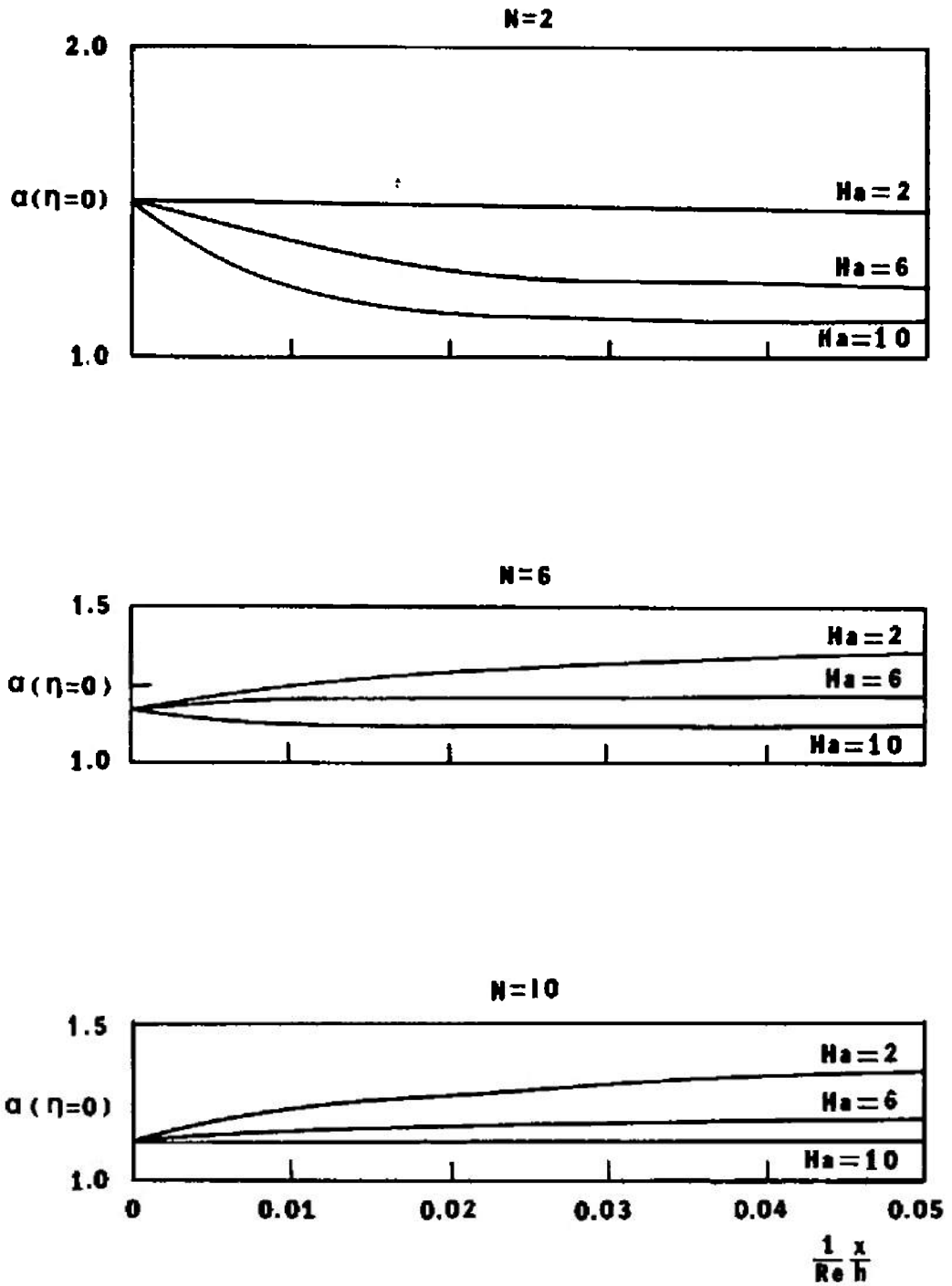

Fig. 21 Longitudinal Variation of Entrance Region Centerline Velocity

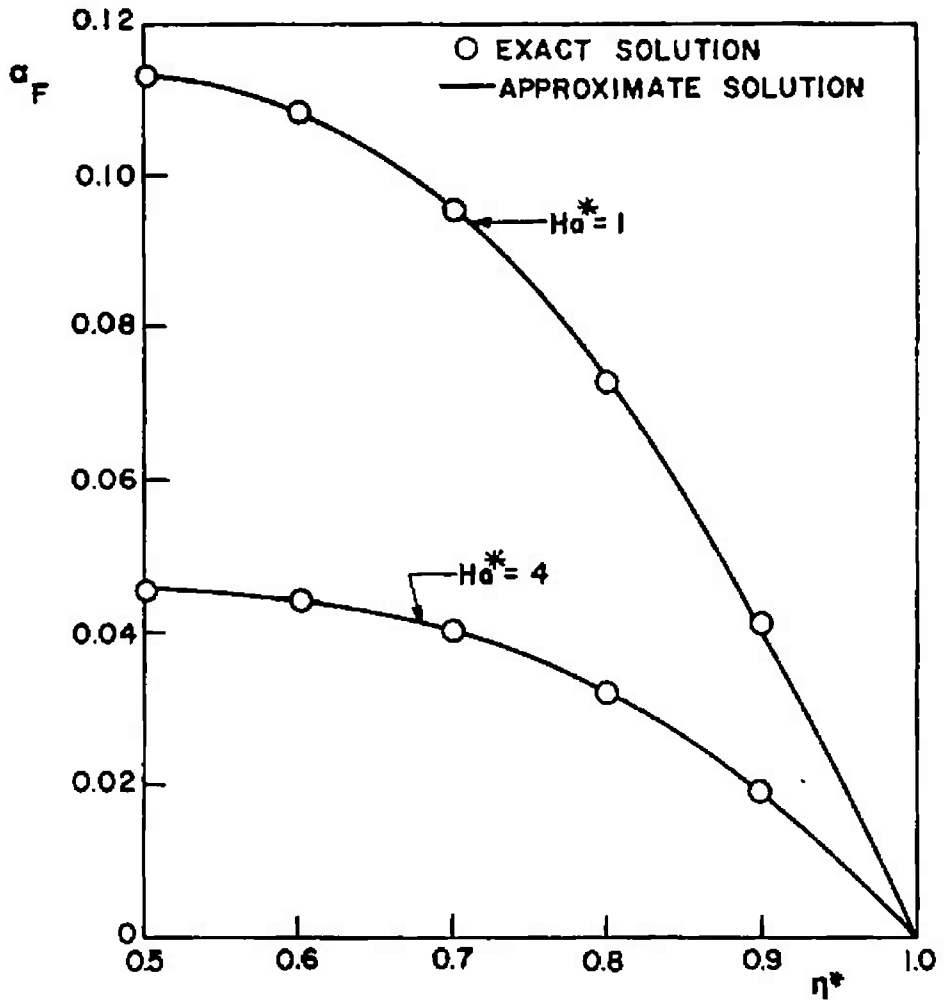

Fig. 22 Velocity Profiles for Case I with $M = 3$, $\Phi_y^* = 0$ Using Fredholm Integral Equation Formulation

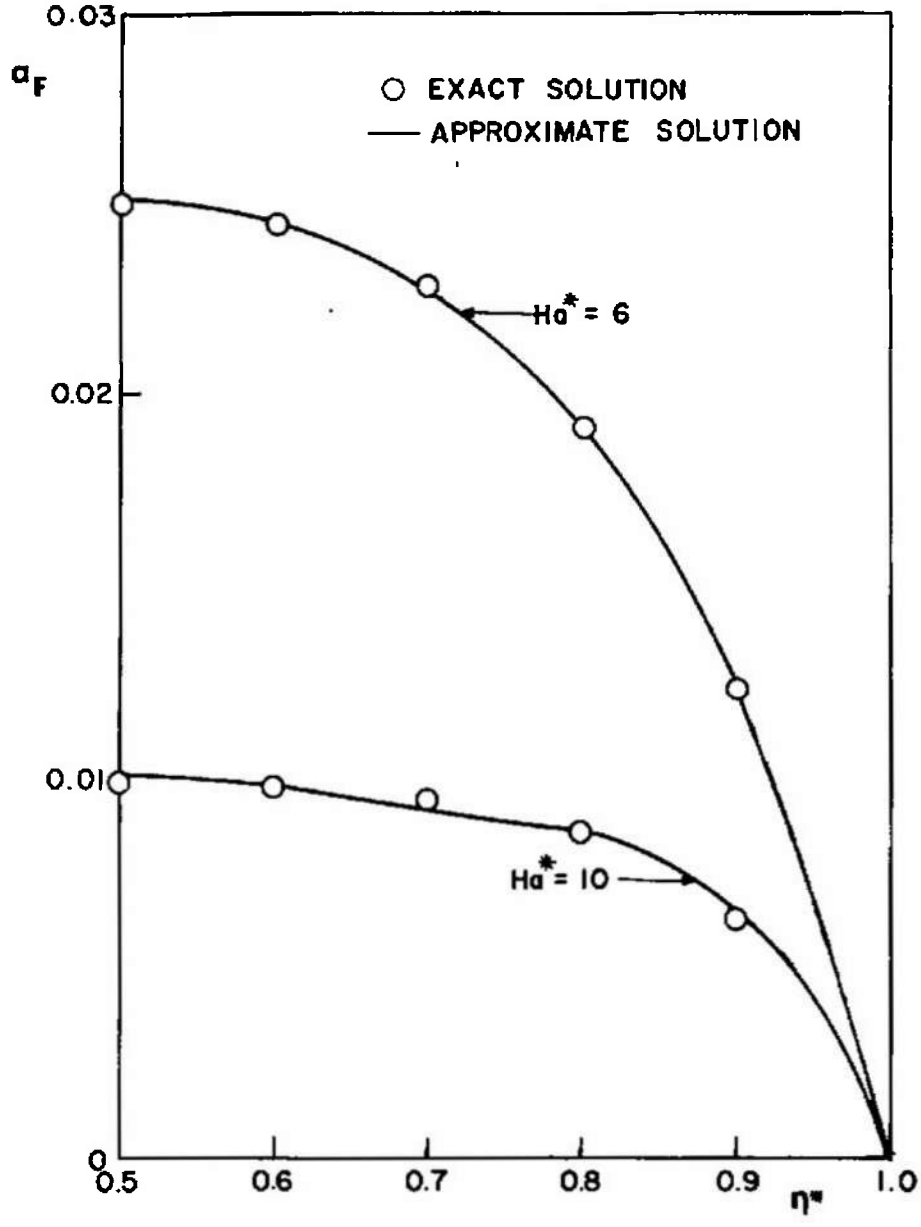

Fig. 23 Velocity Profiles for Case II with M = 3, $\Phi_y^* = 0$
Using Fredholm Integral Equation Formulation

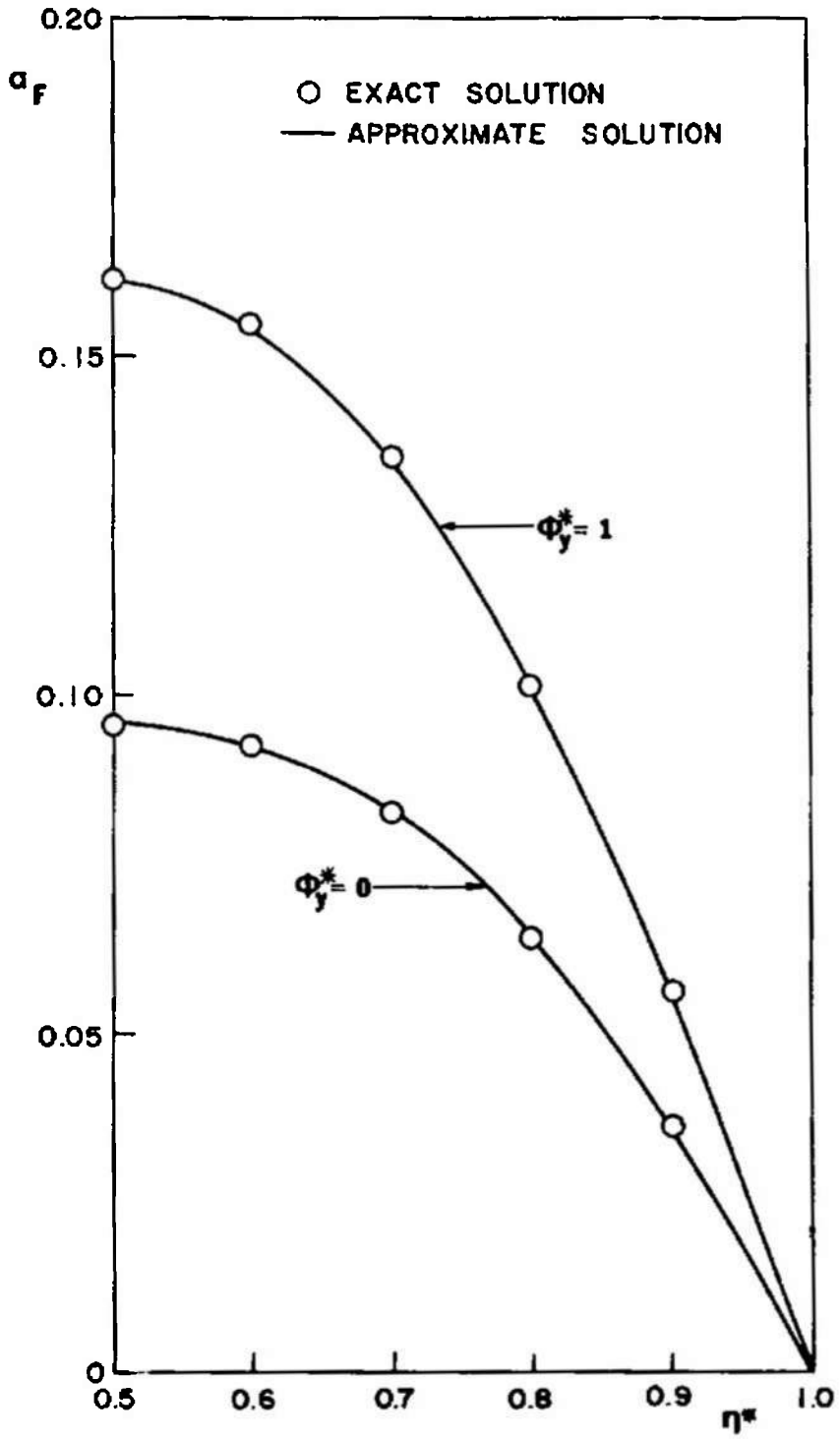

Fig. 24 Velocity Profiles for Case II with M = 3, Ha* = 2 Using Fredholm Integral Equation Formulation

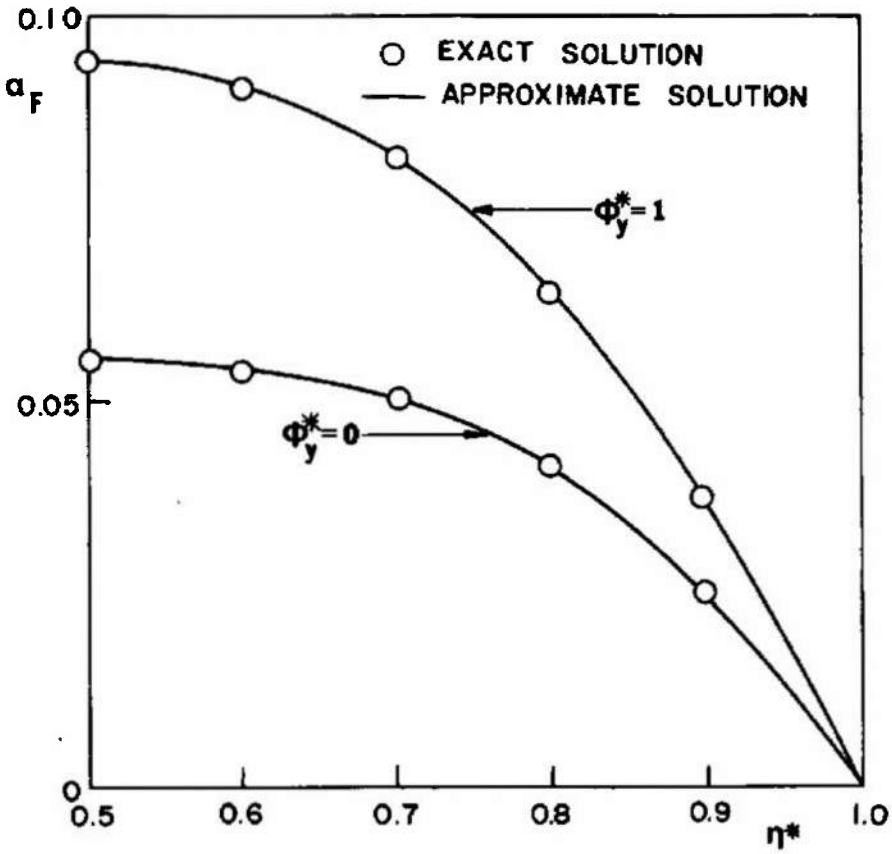

Fig. 25 Velocity Profiles for Case II with M = 3, Ha* = 4
Using Fredholm Integral Equation Formulation

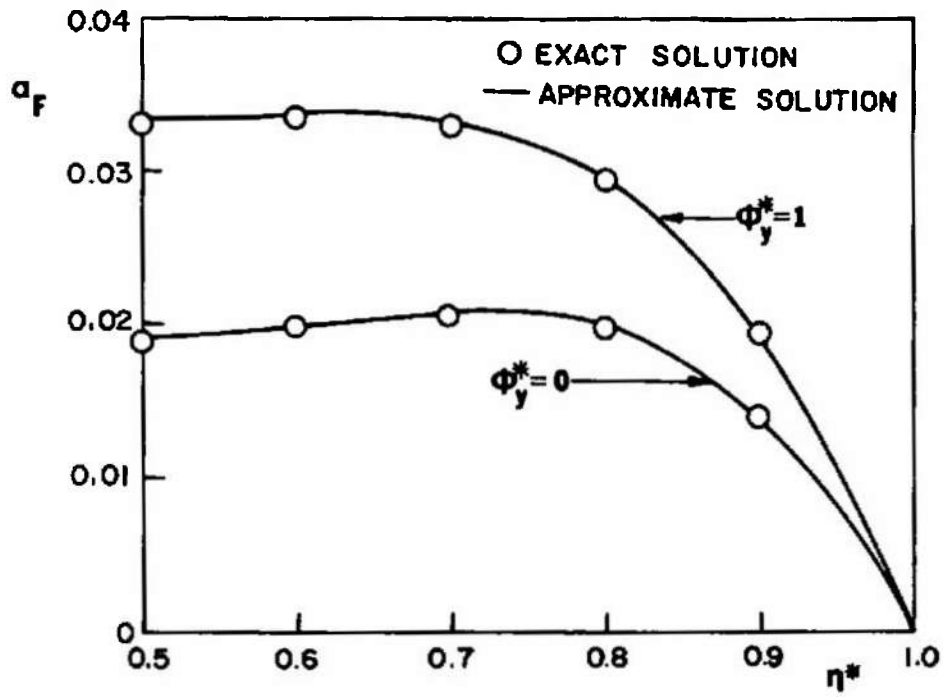

Fig. 26 Velocity Profiles for Case II with M = 3, Ha* = 8
Using Fredholm Integral Equation Formulation

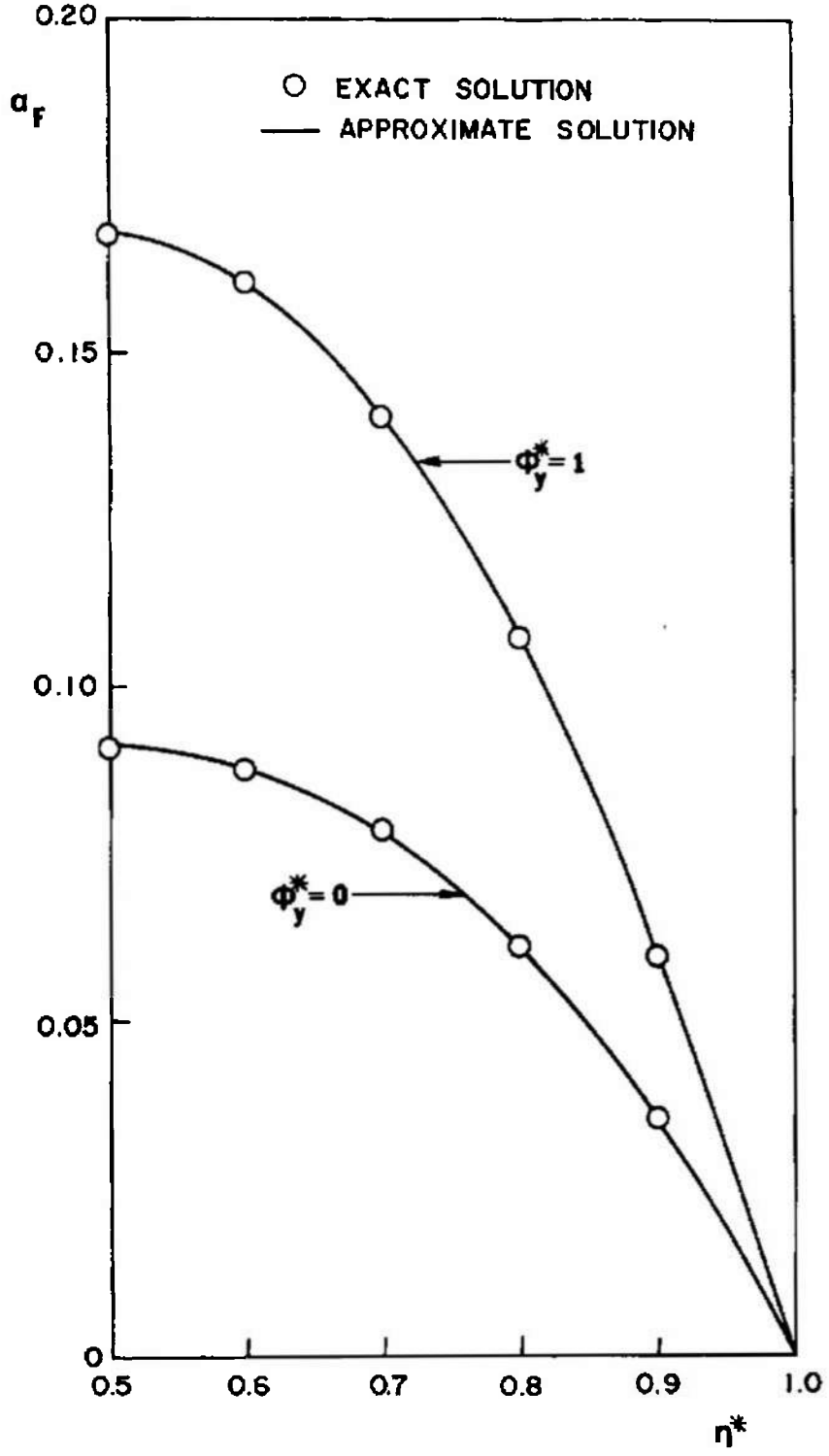

Fig. 27 Velocity Profiles for Case III with M = 3, Ha* = 2 Using Fredholm Integral Equation Formulation

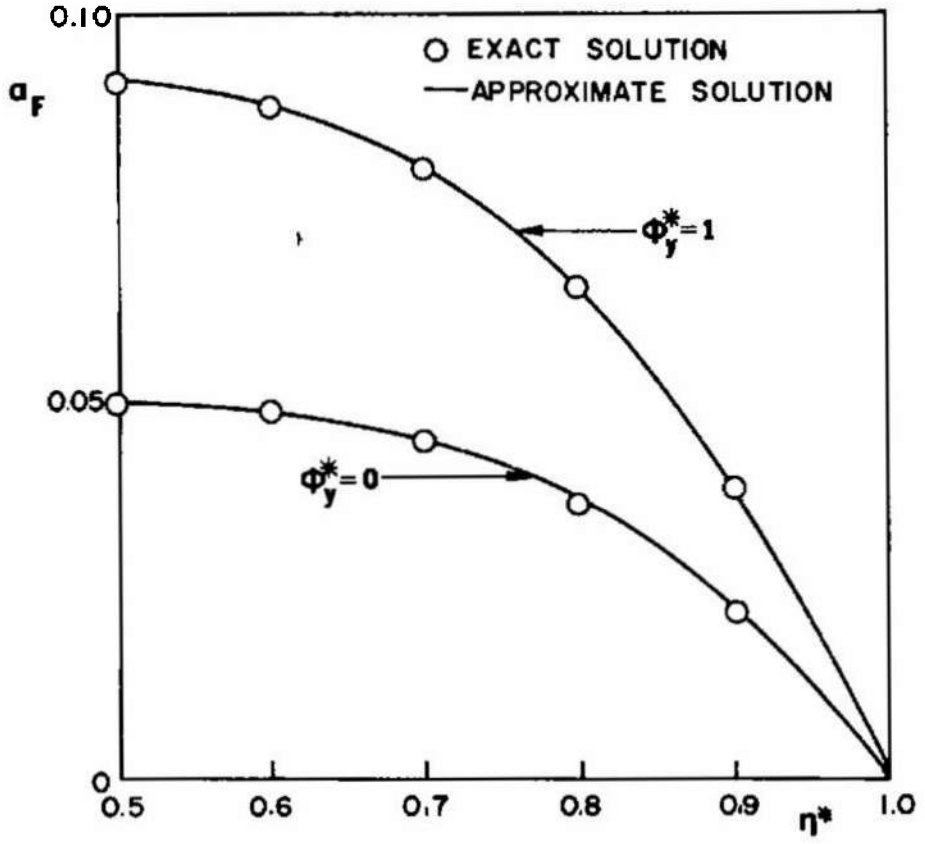

Fig. 28 Velocity Profiles for Case III with M = 3, Ha* = 4 Using Fredholm Integral Equation Formulation

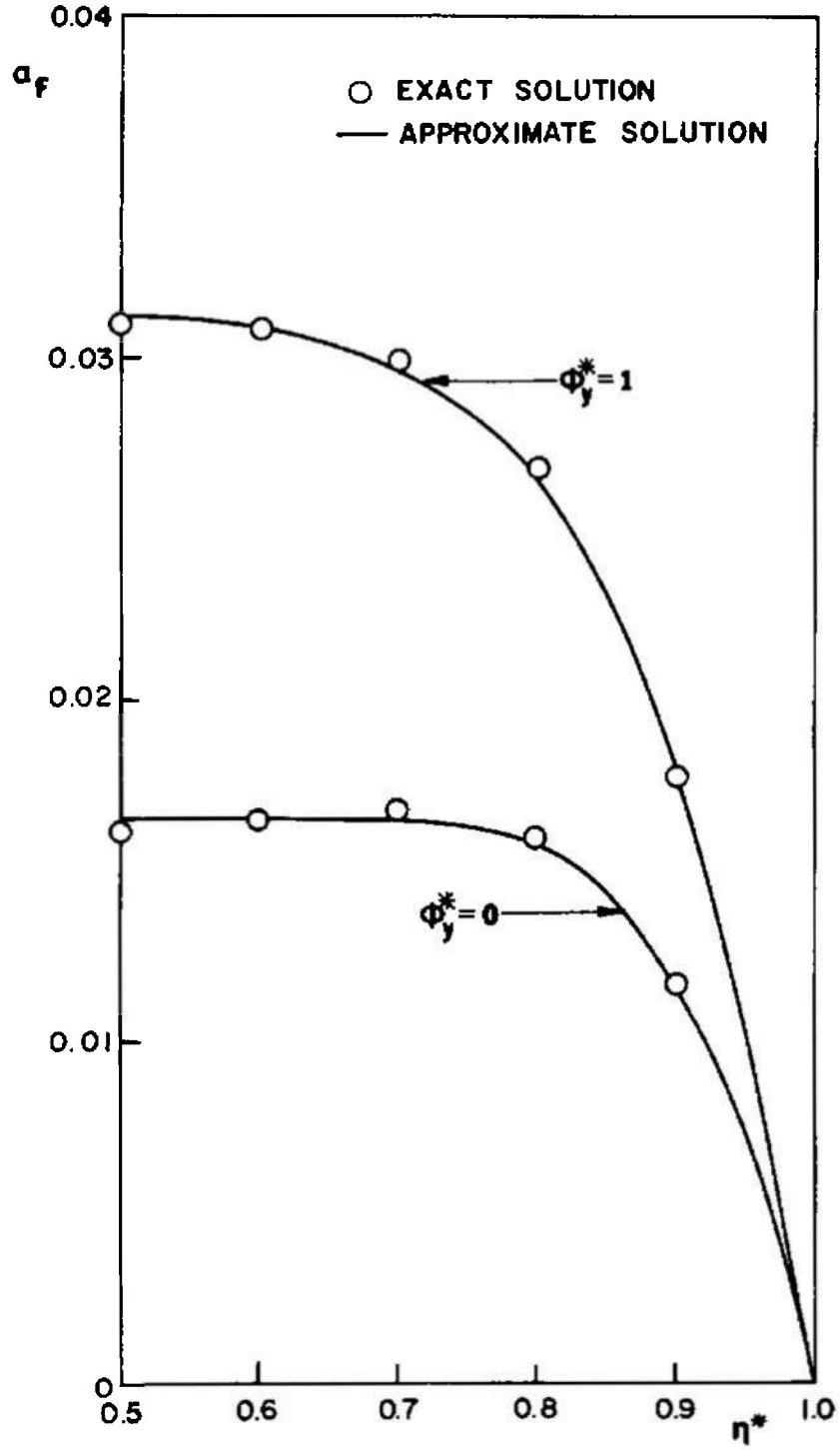

Fig. 29 Velocity Profiles for Case III with M = 3, Ha* = 8 Using Fredholm Integral Equation Formulation

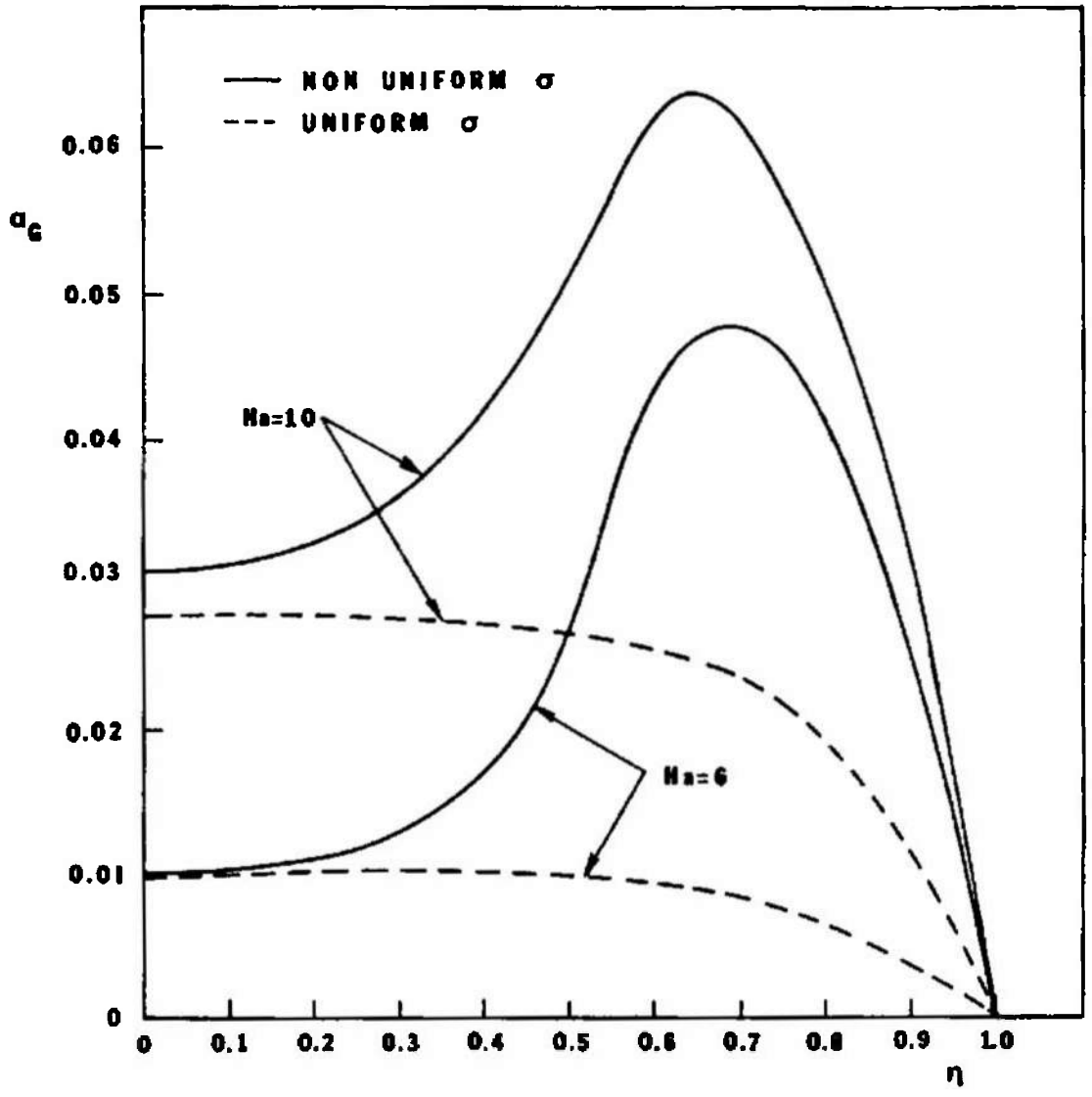

Fig. 30 Short Circuit Velocity Profiles for Case IV by the B.G. Galerkin Method

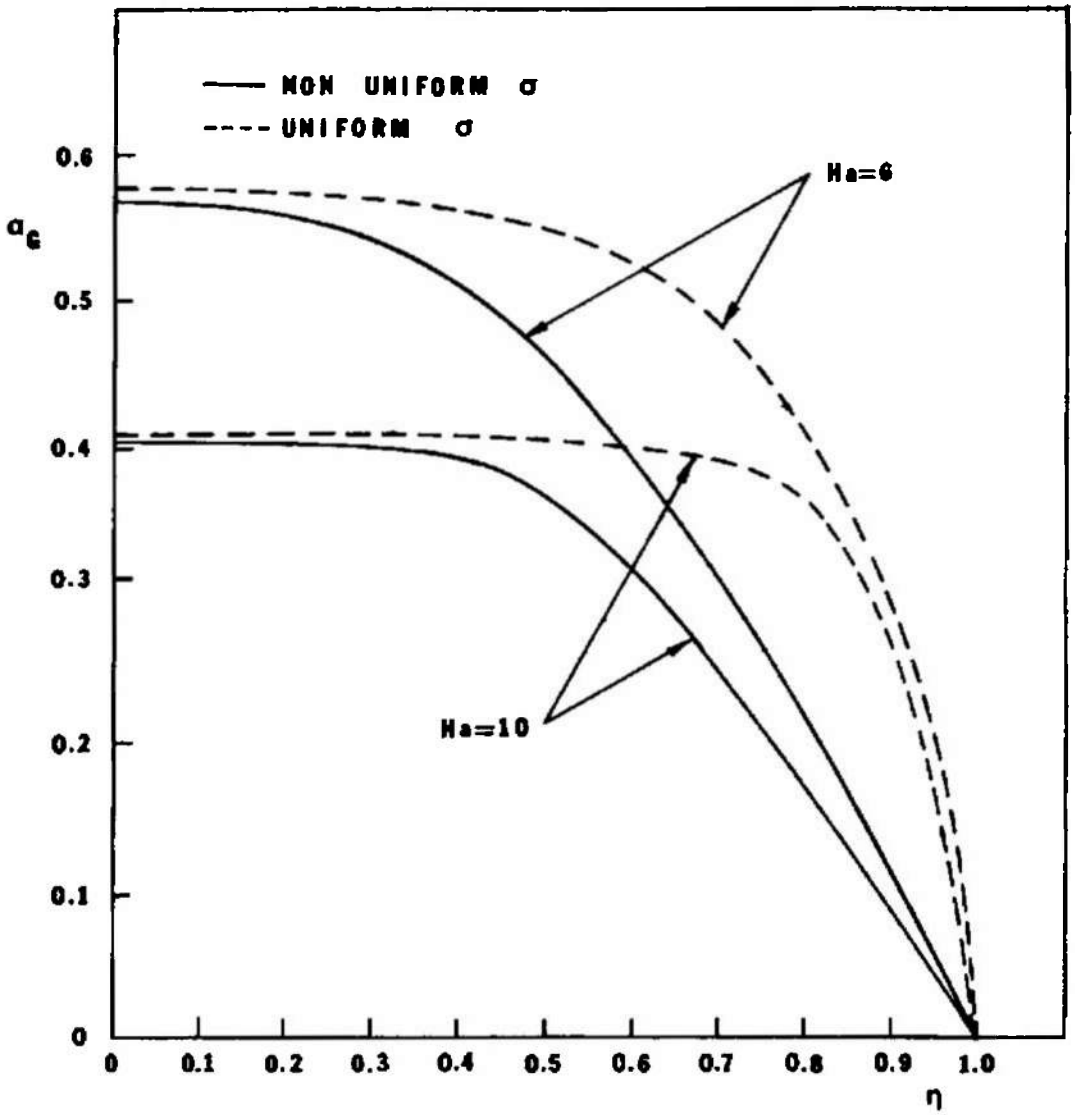

Fig. 31 Open Circuit Velocity Profiles for Case IV by the B. G. Galerkin Method

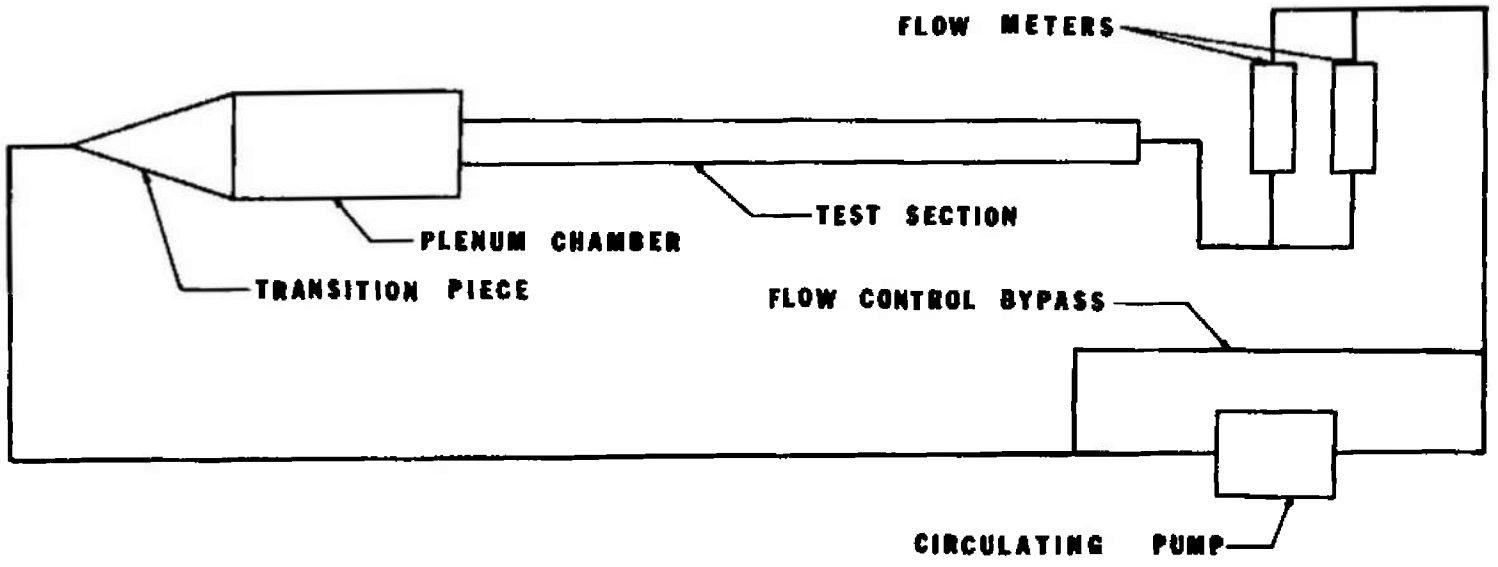

Fig. 32 Schematic Drawing of MHD Flow Loop

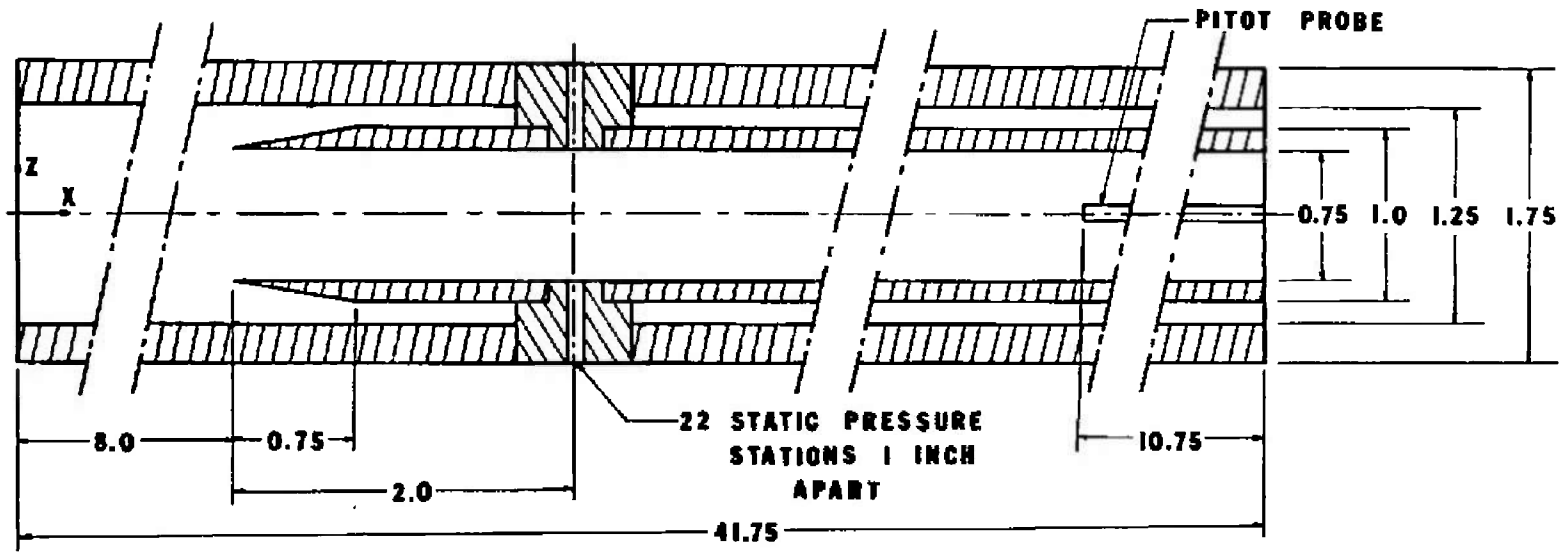

Fig. 33 MHD Flow Loop Test Section

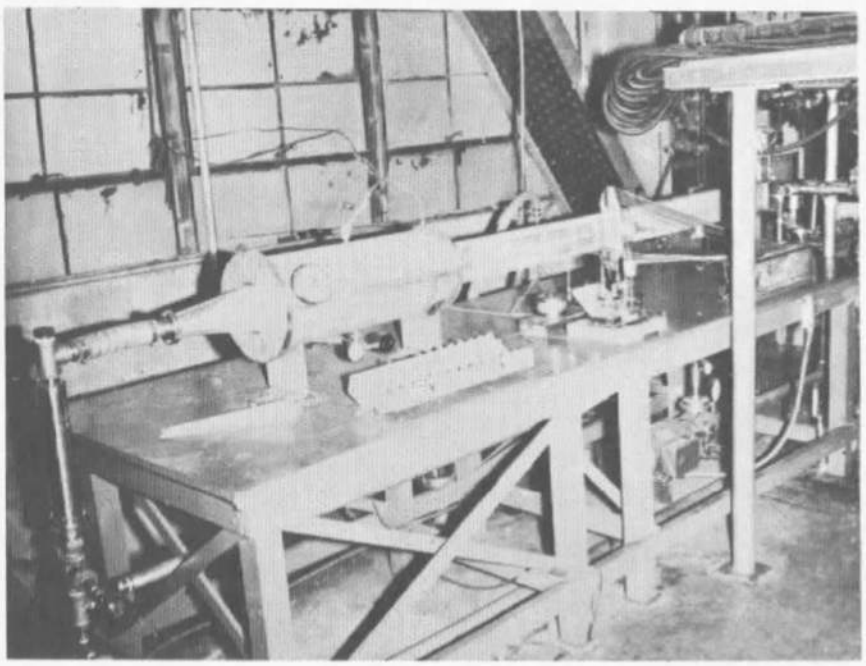

Fig. 34 Photograph of MHD Flow Loop and Test Section

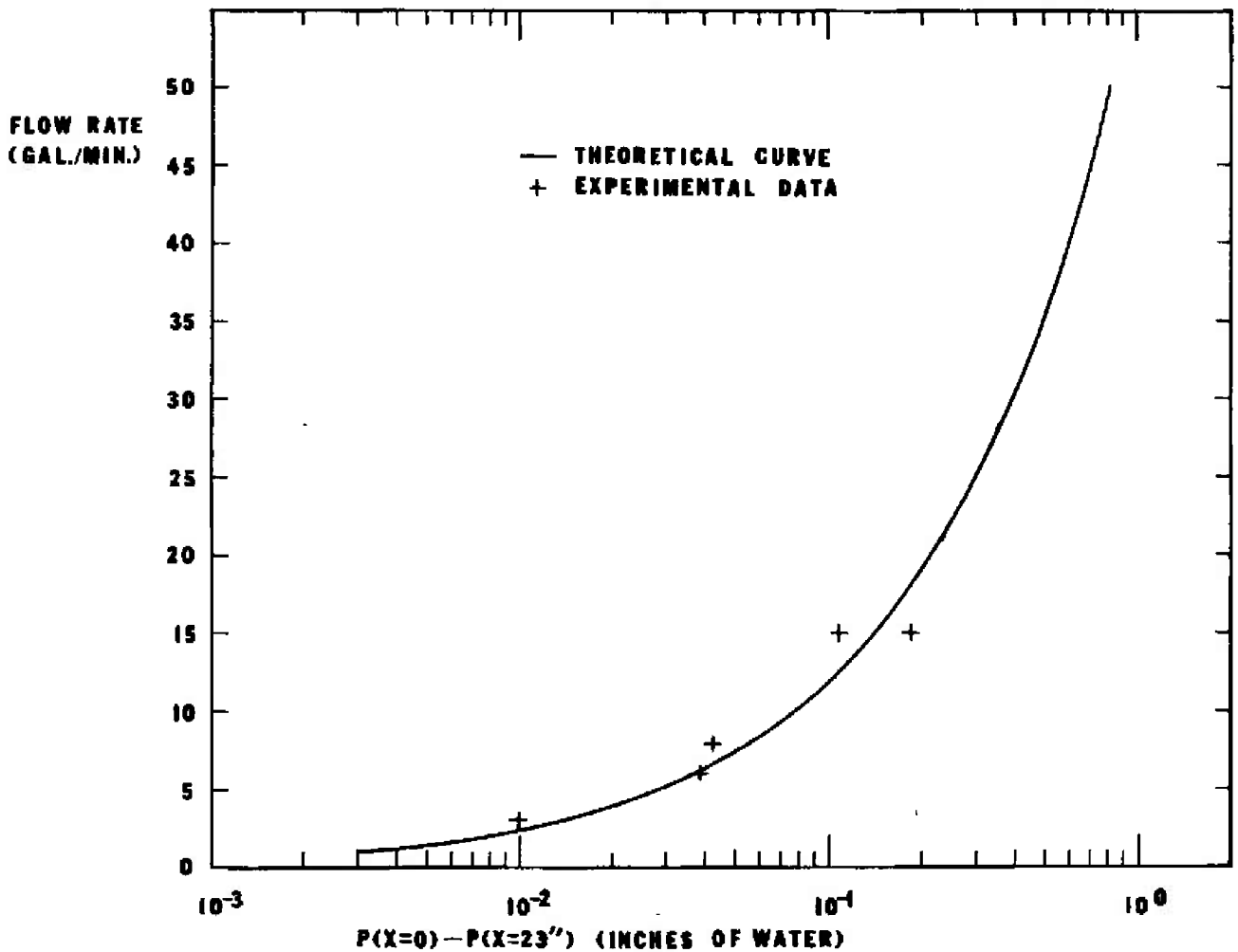

Fig. 35 Experimental Entrance Region Pressure Drop for Ha = 0

TABLE 1
EIGENVALUES OF $\tan \gamma_n = \gamma_n$

n	γ_n	n	γ_n	n	γ_n
1	4.4934127	33	105.23392	66	208.91127
2	7.7252596	34	108.37579	67	212.05293
3	10.904133	35	111.51764	68	215.19459
4	14.066202	36	114.65947	69	218.33625
5	17.220769	37	117.80130	70	221.47790
6	20.371314	38	120.94311	71	224.61956
7	23.519473	39	124.08491	72	227.76121
8	26.666072	40	127.22676	73	230.90286
9	29.811615	41	130.36854	74	234.04451
10	32.956418	42	133.51031	75	237.18616
11	36.100648	43	136.65207	76	240.32781
12	39.244457	44	139.79383	77	243.46945
13	42.387936	45	142.93557	78	246.61109
14	45.531176	46	146.07731	79	249.75286
15	48.674183	47	149.21905	80	252.89450
16	51.817019	48	152.36077	81	256.03613
17	54.959713	49	155.50250	82	259.17777
18	58.102287	50	158.64422	83	262.31941
19	61.244761	51	161.78593	84	265.46104
20	64.387179	52	164.92764	85	268.60268
21	67.529490	53	168.06935	86	271.74431
22	70.671740	54	171.21104	87	274.88594
23	73.813931	55	174.35274	88	278.02757
24	76.956076	56	177.49453	89	281.16920
25	80.098176	57	180.63621	90	284.31083
26	83.240237	58	183.77789	91	287.45246
27	86.382265	59	186.91958	92	290.59408
28	89.524307	60	190.06126	93	293.73571
29	92.666274	61	193.20293	94	296.87734
30	95.808220	62	196.34460	95	300.01897
31	98.950141	63	199.48627	96	303.16059
32	102.09204	64	202.62794	97	306.30222
		65	205.76961	98	309.44384

TABLE 2

EFFECT OF THE DEGREE OF THE POLYNOMIAL VELOCITY PROFILE ON THE ENTRANCE LENGTH

N	Ha - 1	Ha = 6	Ha - 10	Ha = 20	Ha = 100
4	0.09588	not reached	not reached	not reached	0.000026
8	0.09212	not reached	not reached	0.00118	0.000026
16	0.08985	not reached	not reached	0.00110	0.000026
40	0.08835	0.03348	0.00875	0.00106	0.000026
60	0.08801	0.03307	0.00865	0.00105	0.000026

TABLE 3
VALUES OF OPEN CIRCUIT ϕ_y FOR CASE IV

Ha	$\Phi_y)_{oc}$
2	1.3712
4	1.3588
6	1.3492
8	1.3388
10	1.3281

Security Classification

DOCUMENT CONTROL DATA - R&D

(Security classification of title, body of abstract and indexing annotation must be entered when the overall report is classified)

1 ORIGINATING ACTIVITY (Corporate author)	2a REPORT SECURITY CLASSIFICATION
The University of Tennessee Space Institute Tullahoma, Tennessee	UNCLASSIFIED
	2b GROUP N/A

3 REPORT TITLE

THE INFLUENCE OF HALL EFFECT AND INITIAL VELOCITY PROFILE ON MHD FLOW IN THE ENTRANCE REGION OF A PARALLEL PLATE CHANNEL

4 DESCRIPTIVE NOTES *(Type of report and inclusive dates)*

N/A

5 AUTHOR(S) *(Last name, first name, initial)*

Snyder, William T. and Eraslan, Arsev H.

6 REPORT DATE	7a TOTAL NO OF PAGES	7b NO OF REFS
April 1967	98	26

8a CONTRACT OR GRANT NO.	9a ORIGINATOR'S REPORT NUMBER(S)
AF 40(600)-1113 b PROJECT NO 8950 c Program Element 62405334 d Task 895001	AEDC-TR-67-79
	9b OTHER REPORT NO(S) *(Any other numbers that may be assigned this report)* N/A

10 AVAILABILITY/LIMITATION NOTICES

Distribution of this document is unlimited.

11 SUPPLEMENTARY NOTES	12 SPONSORING MILITARY ACTIVITY
Available in DDC	Arnold Engineering Development Center Air Force Systems Command Arnold Air Force Station, Tennessee

13 ABSTRACT

A new method is presented for the analysis of MHD flow in the entrance region of a parallel plate channel including the Hall effect. The method involves a linearization of the inertia terms and the introduction of a stretched axial coordinate. A solution is obtained for the velocity distribution in an incompressible fluid which is valid from the duct inlet to the fully developed region. In practice, flows in which the Hall effect is significant will be compressible. Since the primary objective of the present analysis is to develop the analytical technique for extending the linearization scheme to MHD flows with Hall effect, the constant density assumption is justifiable as a first approximation. From this solution numerical results are obtained for the entrance region for various values of the Hartmann number and the Hall parameter. Two different methods of analysis of fully developed MHD channel flow with variable conductivity are presented. Calculated velocity profiles are presented by the two methods for several conductivity variations across the channel. A new experimental MHD channel flow facility designed to use potassium chloride (KCl) as the working fluid is described. Experimental data for the inlet region pressure distribution in this facility without a magnetic field are presented, and a comparison between the experimental data and analytical prediction is made. The agreement between the experimentally measured entrance region pressure drop and the theoretical curve is considered as satisfactory verification of the theoretical model employed in the present investigation.

DD FORM 1 JAN 64 1473

Security Classification

Security Classification

14 KEY WORDS	LINK A		LINK B		LINK C	
	ROLE	WT	ROLE	WT	ROLE	WT
1 MHD flow velocity 2 Hall effect 5 fluids density potassium chloride 3						

15-20

4 MHD channel flow
5 Parallel plate channels
6. MHD channel flow facility

INSTRUCTIONS

1. ORIGINATING ACTIVITY: Enter the name and address of the contractor, subcontractor, grantee, Department of Defense activity or other organization *(corporate author)* issuing the report.

2a. REPORT SECURITY CLASSIFICATION: Enter the overall security classification of the report. Indicate whether "Restricted Data" is included. Marking is to be in accordance with appropriate security regulations.

2b. GROUP: Automatic downgrading is specified in DoD Directive 5200.10 and Armed Forces Industrial Manual. Enter the group number. Also, when applicable, show that optional markings have been used for Group 3 and Group 4 as authorized.

3. REPORT TITLE: Enter the complete report title in all capital letters. Titles in all cases should be unclassified. If a meaningful title cannot be selected without classification, show title classification in all capitals in parenthesis immediately following the title.

4. DESCRIPTIVE NOTES: If appropriate, enter the type of report, e.g., interim, progress, summary, annual, or final. Give the inclusive dates when a specific reporting period is covered.

5. AUTHOR(S): Enter the name(s) of author(s) as shown on or in the report. Enter last name, first name, middle initial. If military, show rank and branch of service. The name of the principal author is an absolute minimum requirement.

6. REPORT DATE: Enter the date of the report as day, month, year, or month, year. If more than one date appears on the report, use date of publication.

7a. TOTAL NUMBER OF PAGES: The total page count should follow normal pagination procedures, i.e., enter the number of pages containing information.

7b. NUMBER OF REFERENCES: Enter the total number of references cited in the report.

8a. CONTRACT OR GRANT NUMBER: If appropriate, enter the applicable number of the contract or grant under which the report was written.

8b, 8c, & 8d. PROJECT NUMBER: Enter the appropriate military department identification, such as project number, subproject number, system numbers, task number, etc.

9a. ORIGINATOR'S REPORT NUMBER(S). Enter the official report number by which the document will be identified and controlled by the originating activity. This number must be unique to this report.

9b. OTHER REPORT NUMBER(S): If the report has been assigned any other report numbers *(either by the originator or by the sponsor)*, also enter this number(s).

10. AVAILABILITY/LIMITATION NOTICES: Enter any limitations on further dissemination of the report, other than those imposed by security classification, using standard statements such as:

(1) "Qualified requesters may obtain copies of this report from DDC."

(2) "Foreign announcement and dissemination of this report by DDC is not authorized."

(3) "U. S. Government agencies may obtain copies of this report directly from DDC. Other qualified DDC users shall request through _____."

(4) "U. S. military agencies may obtain copies of this report directly from DDC. Other qualified users shall request through _____."

(5) "All distribution of this report is controlled. Qualified DDC users shall request through _____."

If the report has been furnished to the Office of Technical Services, Department of Commerce, for sale to the public, indicate this fact and enter the price, if known.

11. SUPPLEMENTARY NOTES: Use for additional explanatory notes.

12. SPONSORING MILITARY ACTIVITY: Enter the name of the departmental project office or laboratory sponsoring *(paying for)* the research and development. Include address.

13 ABSTRACT: Enter an abstract giving a brief and factual summary of the document indicative of the report, even though it may also appear elsewhere in the body of the technical report. If additional space is required, a continuation sheet shall be attached.

It is highly desirable that the abstract of classified reports be unclassified. Each paragraph of the abstract shall end with an indication of the military security classification of the information in the paragraph, represented as *(TS)*, *(S)*, *(C)*, or *(U)*

There is no limitation on the length of the abstract. However, the suggested length is from 150 to 225 words.

14. KEY WORDS: Key words are technically meaningful terms or short phrases that characterize a report and may be used as index entries for cataloging the report. Key words must be selected so that no security classification is required. Identifiers, such as equipment model designation, trade name, military project code name, geographic location, may be used as key words but will be followed by an indication of technical context. The assignment of links, rules, and weights is optional.

Security Classification